Judith Barbara Moody
Department of Geological Sciences
Ph. D., 1974

Short Title:

SERPENTINIZATION OF IRON-BEARING OLIVINES

SERPENTINIZATION OF IRON-BEARING OLIVINES: AN EXPERIMENTAL STUDY

by

Judith Barbara Moody

A dissertation submitted to the
Faculty of Graduate Studies and Research
in partial fulfillment of the requirements
for the Degree of Doctor of Philosophy

Department of Geological Sciences
McGill University
Montreal
1974

© Judith Barbara Moody 1975

"And yet it seems ludicrous to think that Marie Curie, to whom humanity owes such a huge debt, did not have the right to vote."

Solange Chaput-Roland
The Second Conquest
Reflections II

To my Mother, with love, admiration and gratitude

To my sister Linda, for her indomitable personal courage and determination

and

To my sister Joan, for her devotion

ABSTRACT

The reaction that defines the maximum thermal stability of olivine (Fo_{93})+H_2O at an oxygen fugacity defined by the iron-magnetite (IM) buffer,

$$\underset{\text{olivine}}{10(Mg_{1.86}Fe_{0.14})SiO_4} + 14.2H_2O = \underset{\text{lizardite, clinochrysotile}}{5Mg_3Si_2O_5(OH)_4} + \underset{\text{brucite}}{3.8Mg_{0.95}Fe_{0.05}(OH)_2}$$

$$+ \underset{\text{magnetite}}{0.4\ Fe_3O_4} + 0.4H_2$$

has been bracketed with reversed experiments at: 0.5 kbar, 335°C (± 5°C), 1.0 kbar, 348°C, and 2.0 kbar, 366°C. X-ray and SEM data indicate that lizardite and chrysotile form a stable assemblage within the duration of the experiments. Temperature and pressure of formation had no effect on unit cell dimensions or habit of serpentine minerals, with the possible exception that lizardite laths were observed only at temperatures greater than 315°C. With increased temperature, the iron content of brucite decreases and the amount of magnetite increases.

The calculations of f_{O_2}, f_{H_2}, and f_{H_2O} for the IM and magnetite-awaruite (M-A) assemblages yield extremely high values for f_{H_2}. The ubiquitous assemblage M-A in natural serpentinites provides a definite indicator of a locally, extremely reducing environment, quite different from what is considered to be the normal crustal f_{O_2} environment.

RÉSUMÉ

La réaction qui définit la stabilité thermique maximum de l'olivine (Fo_{93}) + H_2O pour une fugacité d'oxygène determinée par le tampon de fer-magnétite (IM),

$$10(Mg_{1.86}Fe_{0.14})SiO_4 + 14.2H_2O = 5Mg_3Si_2O_5(OH)_4 + 3.8Mg_{0.95}Fe_{0.05}(OH)_2$$

olivine — lizardite, clinochrysotile — brucite

$$+ 0.4Fe_3O_4 + 0.4H_2$$

magnétite

a été cernée par des expériences inverses à: 0.5 kbar, 335°C (±5°C), 1.0 kbar 348°C, et 2.0 kbar, 366°C.

Des mesures aux Rayons-X et au microscope électronique à balayage indiquent que la lizardite et le chrysotile forment un assemblage stable au cours des expériences. Ni la température, ni la pression de formation n'a eu d'effet sur les dimensions de la maille ou la morphologie des serpentines, sauf peut-être pour les plaquettes de lizardite qui n'ont été observées qu'à des températures supérieures à 315°C. Lorsque la température augmente, le contenu en fer de la brucite diminue et la quantité de magnétite augmente.

Les calculs de fugacité de O_2, de H_2 et de H_2O pour le IM et l'assemblage magnétite-awaruite (M-A) donnent des valeurs extrêmement élevées pour la fugacité de H_2. L'assemblage M-A, omniprésent dans les serpentinites, constitue un indicateur certain d'un environment local, extrêmement réducteur, fort différent de ce qui constitue un environnement normal de fugacité de O_2 dans la croûte.

ACKNOWLEDGEMENTS

This work has benefited from the support of many and in the following acknowledgements it is hoped that no one's contribution was overlooked.

Financial support for the research was given by National Research Council of Canada Grant A-7719 to W.H. MacLean. Additional financial support was received from the Faculty of Graduate Studies and Research, McGill University, in scientific equipment grants to R.F. Martin and H. Helmstaedt, and a Sigma Xi Grant-in-Aid to Research to the author. A National Research Council of Canada Research Assistanceship from Grant A-7719 (1970-71), the J.P. Lynch Fellowship (1971-72) and a National Research Council of Canada Post-Graduate Scholarship (1972-74) provided personal financial support to the author.

F.J. Wicks of the Royal Ontario Museum supplied mineral standards and through many discussions and interest in this work provided invaluable insight into serpentine mineralogy and serpentinization. G.W. Fisher, Johns Hopkins University, G. Plant, Geological Survey of Canada, F. Aumento, Dalhousie University, and R.G. Coleman, U.S. Geological Survey, kindly supplied some of the synthetic and natural olivines that were used as standards and starting materials in the experimental work. R.G. Hargraves and N. Dorety, Princeton University, generously performed the magnetic susceptibility measurements of some of the run products. I. Barnes, U.S. Geological Survey, showed the author the classic spring localities in serpentinites of California and provided stimulating

discussions in the field. H. Helgeson and W. Nesbitt, University of California, Berkeley, gave of their time in discussion and elucidation of the high-temperature solution problems and provided copies of computer programs. H.R. Shaw, U.S. Geological Survey, provided important discussion on the problems relating to thermochemical data and the hydrogen buffer. D.R. Wones, U.S. Geological Survey, consistently showed interest in this work by discussion, sent the author calculations bearing on the iron-magnetite buffer and provided much encouragement with difficult experimental problems. J.V. Chernosky, University of Maine, kindly sent preprints on his important work on the aluminum-bearing serpentines. The kind co-operation and discussion on problems of mutual interest with O.R. Eckstrand, Geological Survey of Canada, is greatly appreciated. K. Iishi, Yamaguchi University, provided a preprint of his paper with M. Saito and communicated his interesting but unpublished results on chrysotile. J.R. O'Neil, U.S. Geological Survey, took the time and interest to answer difficult questions concerning the isotope studies related to serpentinization.

At McGill University, E. McKyes and A. Seethie, Department of Civil Engineering, instructed the author in the use of the Scanning Electron Microscope and provided the necessary help and co-operation in completing that study. M. Cooper made available the Pulp and Paper Institute's microdensitometer and helped the author in its use. M.D. Croucher, Department of Chemistry, spent much time in discussion of thermodynamic problems and aided the author invaluably in the tedious checking of many

of the calculations. G.R. Webber and S.J. Horska made available all the equipment and facilities of the geochemical laboratory, without which this study could not have been done. H. Helmstaedt introduced the author to phase contrast microscopy and with A.J. Pearce provided much stimulating discussion on various aspects of this work. A.J. Pearce also gave generously of his time with various computing problems, as well as providing copies of his own programs. R.F. Martin allowed the author full use of his laboratory's facilities and provided valuable help in hydrothermal techniques. W.M. MacLean, my thesis advisor, is thanked for his support of this work.

The manuscript was greatly improved by the critical reading of W.H. MacLean, R.F. Martin, and H. Helmstaedt. Preparation of the text was aided by the expert work of the following people: S. Doughty, typing, D. Nutter, drafting, and A. Graham, photography. The author greatly appreciates the care that they took in editing and in the preparation of the typescript, figures and plates. Y. Le Page and S. Fortier translated the abstract into French.

The author's deep gratitude for the continuous personal support and encouragement of S.J. Horska and M.D. Croucher cannot adequately be put into words.

TABLE OF CONTENTS

	Page
ACKNOWLEDGEMENTS	i
LIST OF TABLES	viii
LIST OF ILLUSTRATIONS	xi
LIST OF APPENDICES	xiv
LIST OF SYMBOLS	xv
INTRODUCTION	1
General Statement	1
Serpentine Mineralogy	1
Previous Experimental Work	4
$MgO-SiO_2-H_2O$	4
$MgO-SiO_2-Fe-H_2O-H_2$	11
$Na_2O-MgO-SiO_2-Fe-H_2O-H_2-HCl$	12
Observations on Serpentinization from Natural Occurrences	14
Serpentinized Ultramafic Rocks	14
Fluids Involved in Serpentinization	18
Stable Isotopes	19
Statement of the Problem	21
Contributions of This Study	23

Page

EXPERIMENTAL METHODS 26

Hydrothermal Runs 26

Starting Materials 26

Charge Preparation 28

Pressure-Temperature Control 30

Analysis of the Products 31

Charge Unloading 31

X-ray Analysis 32

Petrography 33

Scanning Electron Microscopy 33

Magnetic Measurements 35

Fluid Analysis 35

Chemical Analyses 36

pH Measurement 38

EXPERIMENTAL RESULTS 39

Iron-Magnetite Buffer 39

Evaluation of Buffer Effectiveness 39

Possible Hydrogen Leakage 43

Calculation of Fugacity of Oxygen, Hydrogen and Water 45

Hydrothermal Runs on the Reaction of Synthetic and Natural Olivines with an Aqueous Fluid 51

Experiments Involving Pure Water 51

Experiments Involving Fluids of Variable Composition ... 64

Page

Reversed Experiments on the Reaction Boundary for Olivine (Fo_{93}) + H_2O. 72

Dehydration Reactions 84

Reactions Involving Brucite 89

Fluid Analysis 90

pH Measurement 90

Chemical Analyses 93

DISCUSSION OF RESULTS 107

Oxygen Fugacity 107

Serpentine Mineralogy 112

X-ray Results 113

Habit 122

Temperature, Pressure and Compositional Effects on Formation of Serpentine Minerals 124

Brucite and Magnetite 126

Iron Content of Brucite 126

Stability of $Fe(OH)_2$ 131

Further Observations on Magnetite Occurrence 136

The Bracketing Experiments - Equilibrium Determination 137

Evaluation of Influence of Iron on Lower Thermal Stability of Olivine 137

Tentative Thermodynamic Data Derived from the Equilibrium Curve 142

Rate of Reaction 146

Reaction of Olivine with Fluids Other than Water 147

Composition of Serpentinizing Fluids 149

Page

Application of Experimental Results 154

Evidence on Serpentinization from Equilibrium Determinations and Mineralogy of Phases 154

Evidence on the Nature of the Fluid Phase 157

SUMMARY 161

Oxygen Fugacity 161

Serpentine Mineralogy 162

Brucite and Magnetite 164

Determination of Reaction Boundary for Olivine (Fo_{93}) + H_2O 166

Fluids Involved in Serpentinization 167

REFERENCES CITED 169

APPENDICES 179

LIST OF TABLES

Table		Page
1.	Previous experimental work on alleged equilibrium determinations of reactions (1) and (2) in the $MgO-SiO_2-H_2O$ system.	5
2.	Evidence for constant chemical composition and constant volume serpentinization.	17
3.	Runs in which weight loss at end of run was greater than 1 mg for a 2 g capsule and in which there was no macroscopically observable leak.	44
4.	Comparison of experiments that showed a weight loss of the Au capsule at end of run with those in which there was no weight change.	46
5.	References for data used in calculation of fugacities of oxygen, hydrogen, and water for the IM buffer.	48
6.	Cell parameters and calculated compositions of olivine and brucite starting materials used in the experimental work.	52
7.	Comparison of different olivines for effect of run duration and initial composition on the rate of reaction.	55
8.	Selected olivine cell parameters and calculated compositions from the hydration experiments with pure water.	56
9.	Cell edge and volumes refined for lizardite and chrysotile produced from hydration reaction with water.	58
10.	Summary of SEM results on the distribution of serpentine habit for lizardite and chrysotile produced from hydration of olivine with pure water.	61
11.	Cell edges refined for selected brucites produced during reaction of olivine with pure water.	63
12.	Magnetic measurements of starting material and run products from hydration of a synthetic and natural olivine.	65

Table		Page

13. Selected refined olivine and brucite cell parameters and compositions from the hydration experiments with fluids of varying compositions. 67

14. Selected cell parameters for lizardite and chrysotile produced from the reaction of olivine with fluids of varying composition. 69

15. SEM results for a few serpentine samples formed from the reaction of olivine with fluids other than pure water. 71

16. The microdensitometer intensity measurements and SEM results for the bracketing experiments. 73

17. Criteria for distinguishing the mineral stability fields from morphology of the phases as observed by SEM. 75

18. Summary of SEM results on the distribution of serpentine habit within the serpentine stability field defined by the bracketing experiments. 76

19. Cell parameters for lizardite within stability field of serpentine defined by the bracketing experiments..... 78

20. Cell edge refinements and compositions of brucite in reversed runs in stability field of serpentine-brucite-magnetite. 79

21. Refined cell parameters and compositions of olivines present at completion of the bracketing experiments..... 81

22. Amounts of magnetite observed in bracketing experiments as estimated optically and determined directly from magnetic measurements. 83

23. Refined cell parameters and compositions for olivine, brucite, and serpentine formed in dehydration reactions. 85

24. SEM results on serpentine habit for the dehydration experiments. 88

25. X-ray and SEM results for serpentine formed from reaction of brucite with sodium metasilicate solutions.. 91

26. Quench pH measurements of fluids after reaction of olivine with water. 92

Table		Page

27. Effect of fluid composition and solid product assemblage on the molar ratio of Mg/Si in solution during the hydration experiments with a synthetic olivine (Fo_{95}). 96

28. Possible variation in measured amounts of Mg and Si in final fluid as a function of solid assemblage, temperature, pressure and run duration. 98

29. X-ray and composition data on naturally occurring lizardites. 115

30. X-ray and cell edge data on some iron-bearing members of the serpentine group. 117

31. Comparison of some observed a and b cell parameters and some calculated values taken as the average for ideal tetrahedral and octahedral sheets. 118

32. Habit of natural lizardite and chrysotile observed from both transmission electron and transmitted light microscopy, as compiled from the literature. 123

33. Summary of the iron content of brucite in serpentinites as determined from X-ray and electron microprobe analysis. 127

34. Correlation of iron content of olivine and brucite with magnetite production in the bracketing and hydration experiments. 129

35. Equilibrium temperatures and pressures determined from reversed experiments for reactions involving serpentine... 138

36. Results of calculations based on a large extrapolation of the equation of state for hydrogen-water mixtures..... 144

37. Measured molality of fluids co-existing with natural and synthetic serpentine and olivine at a variety of temperatures and pressures. 150

LIST OF ILLUSTRATIONS

Figure		Page
1.	Capsule configuration used in this study.	29
2.	Plot of percent magnetite in buffer vs time for the reaction of iron sponge + water.	41
3.	Log f_{H_2}/f_{H_2O} vs temperature at P_{total} equal to 500 bars for IM buffer	50
4.	Reaction curve for $10(Mg_{1.86}Fe_{0.14})SiO_4 + 14.2H_2O = 5Mg_3Si_2O_5(OH)_4 + 3.8Mg_{0.95}Fe_{0.05}(OH)_2 + 0.4\ Fe_3O_4 + 0.4H_2$.	77
5. A.	Mg and Si molalities vs temperature at 1.0 kbar P_t for hydration experiments with a synthetic olivine and NaCl as a fluid phase.	
B.	Mg molality vs temperature at 1.0 kbar P_t for hydration experiments with a synthetic olivine and bracketing experiments with pure water.	94
6.	The molar ratio of Mg/Si in solution vs temperature for the experimental fluid compositions.	95
7.	Log f_{H_2}/f_{H_2O} vs temperature for the assemblage IM and magnetite-awaruite for P_t = 500 and 2000 bars.....	109
8.	The Fe-Ni system from Shunk (1969).	111
9.	Compilation of the synthesis and phase equilibrium data on the serpentine minerals as a function of temperature and pressure.	125

Plate		Page
1.	Scanning Electron Microphotographs.	99
	A. Anhedral olivine grains (GSC olivine, Fo_{93}).	
	B. GSC olivine.	
	C. Euhedral lizardite plate (3-1).	
	D. Lizardite (3-1).	
2.	Scanning Electron Microphotographs.	100
	A. Thick brucite platelet surrounded by chrysotile fibers (3-76).	
	B. Chrysotile and lizardite (3-12).	
	C. Thin brucite platelet and chrysotile (3-76).	
	D. Large aggregate of brucite platelets (3-76).	
3.	Scanning Electron Microphotographs.	101
	A. Euhedral, stubby lizardite crystals and chrysotile (3-76).	
	B. Euhedral lizardite (3-76).	
	C. Large euhedral lizardite plate (3-75).	
	D. Lizardite laths (3-99).	
4.	Scanning Electron Microphotographs.	102
	A. Very short chrysotile fibers (3-75).	
	B. Lizardite lath, chrysotile fibers, and brucite platelets (3-71).	
	C. Lengthening of chrysotile fibers (3-76).	
	D. Maximum development of chrysotile into fiber bundles (3-76).	

Plate			Page
5.		Scanning Electron Microphotographs	103
	A.	Mat of interwoven chrysotile fibers (3-99).	
	B.	Aggregation of chrysotile fibers to form bundles (3-99).	
	C.	Shortened chrysotile fibers on an olivine substrate (3-100).	
	D.	Shortened chrysotile fibers (3-100).	
6.		Scanning Electron Microphotographs	104
	A.	Etch and solution pits in lizardite (3-100).	
	B.	Development of euhedral olivine crystals (3-101).	
	C.	Euhedral olivine crystals (3-101).	
	D.	Small euhedral olivine crystals (3-101).	
7.	A.	Fine "dusty" magnetite outlining brucite platelets in a serpentine-brucite-magnetite aggregate (3-85).....	105
	B.	A magnetite + brucite + serpentine aggregate (3-84).	
	C.	"Dusty" magnetite in irregular patches in serpentine (3-84).	
	D.	A magnetite + brucite + serpentine aggregate (3-61).	
8.	A.	Large magnetite aggregate in serpentine (3-105).....	106
	B.	Magnetite-serpentine aggregate (3-105).	
	C.	Magnetite (3-105).	
	D.	Chrysotile growing on a larger mass of lizardite (3-69).	

LIST OF APPENDICES

	Page
Appendix 1a	180
Appendix 1b	186
Appendix 1c	187
Appendix 2	188
Appendix 3	197
Appendix 4	202
Appendix 5	207

LIST OF SYMBOLS

O	-	olivine, $(Mg,Fe)_2SiO_4$
Fo	-	forsterite, Mg_2SiO_4
Fa	-	fayalite, Fe_2SiO_4
L	-	lizardite, $Mg_6Si_4O_{10}(OH)_8$
C	-	chrysotile
An	-	antigorite
B	-	brucite, $Mg(OH)_2$
A	-	awaruite, $(FeNi_3)$
IM	-	iron-magnetite oxygen fugacity buffer $(Fe-Fe_3O_4)$
QFM	-	quartz-fayalite-magnetite oxygen fugacity buffer $(SiO_2-Fe_2SiO_4-Fe_3O_4)$
HM	-	hematite-magnetite oxygen fugacity buffer $(Fe_2O_3-Fe_3O_4)$
NNO	-	nickel-nickel oxide oxygen fugacity buffer (Ni-NiO)
T, T_e	-	temperature in kelvin (^oK) or centigrade (^oC), equilibrium temperature
P, P_e, P_t	-	pressure in bars, atmospheres (atm) or kilobars (kbar), equilibrium pressure, total pressure
ΔV_s	-	sum of total molar volumes of solid products minus sum of total molar volumes of solid reactants; subscript s refers to solid phases
V	-	gram formula volume, calories/bar
a_i	-	activity of component i
x_i	-	mole fraction of component i in a mixture
f_i^o	-	fugacity of component i in a unary gas phase

f_i	-	fugacity of component i in a mixture
γ_i	-	fugacity coefficient of component i
$K_w(T)$	-	equilibrium constant of water at T
K_{12}	-	equilibrium constant for equation 12
Ψ	-	parameter having dimensions of volume used to measure departure of a gas mixture from ideality
Y	-	a parameter defined by $Y = K_w f^o_{H_2} (f_{O_2})^{1/2}/f^o_w$
gfw	-	gram-formula weight
$\Delta G^o_f, \Delta H^o_f, \Delta S^o_f$	-	standard gram-formula Gibbs free energy, enthalpy, entropy of formation of a phase from the elements
ΔG^o_r (T,P)	-	standard gram-formula Gibbs free energy of reaction at temperature and pressure
δ values	-	deviation in per mil of the O^{18}/O^{16} ratio or D/H ratio of the sample from SMOW standard
J_s	-	saturated magnetic moment, emu/g
a, b, c	-	unit-cell edge lengths, A
α, β, γ	-	unit cell interaxial angles
d	-	interplanar spacing, A
SEM	-	Scanning Electron Microscope
μm	-	micrometer, 10^{-6} meter
nm	-	nanometer, 10^{-9} meter
μg	-	microgram, 10^{-6} gram
μl	-	microliter, 10^{-6} liter
A	-	angstrom, 10^{-10} meter
hrs	-	hours
esd	-	estimated standard deviation

wt. %	-	weight percent
ppm	-	parts per million
n.d.	-	not detected

INTRODUCTION

General Statement

Most ultramafic rocks are hydrated to form partially or completely serpentinized rock. It becomes important to understand serpentinization in order: (1) to determine the anhydrous equivalent or parent rock composition, (2) to specify the temperature, pressure conditions under which the hydration takes place to define whether serpentinization occurs in the crust or mantle or both, (3) to evaluate the possible source and composition of the fluid phase necessary for hydration, and (4) to obtain knowledge of the fluid composition after alteration has taken place. The physical properties such as seismic velocity, magnetic susceptibility and ductility of peridotite differ markedly from those of serpentinite (Raleigh) and Paterson, 1965; Christensen, 1970; Coleman, 1971; Aumento and Loubat, 1971) adding importance to the question of where and how the ultramafic rock becomes hydrated with respect to emplacement in the crust. This work will describe an experimental study of the reaction of olivine (Fo_{80}-Fo_{95}) with water and other fluids to produce serpentine, brucite, and magnetite.

Serpentine Mineralogy

The term serpentine will be used in this study as the family name of the three major minerals (lizardite, chrysotile, antigorite) or as a

general term when the individual mineralogy is not known or specified. The following classification of the serpentine minerals has been developed by Whittaker and Zussman (1956, 1971) and Wicks (1969) based on composition and structure and will be used in this work:

- serpentine — $Mg_3Si_2O_5(OH)_4$
  - chrysotile
    - orthochrysotile
    - clinochrysotile
    - parachrysotile
  - lizardite
  - antigorite

6-layer orthoserpentine - $Mg_3Si_2O_5(OH)_4$

Al serpentines	-	substitution of Al for Si and Mg up to the composition of amesite ($Mg_2Al(SiAl)O_5(OH)_4$, intermediate compositions between end member amesite and serpentine are called septechlorites
Ni serpentines	-	those with variable magnesium and nickel compositions $(Mg, Ni)_3Si_2O_5(OH)_4$ are called garnierite; the end member $Ni_3Si_2O_5(OH)_4$ is pecoraite
Fe serpentines	-	end member (ferrous) is greenalite ($Fe_6Si_2O_5(OH)_4$) and end member (ferrous/ferric) is cronstedtite - $Fe_2Fe_2SiO_5(OH)_4$.

Detailed reviews of the chemical composition of lizardite, chrysotile and antigorite (Page, 1968; Whittaker and Wicks, 1970) have shown that the minerals are not polymorphs; there are small but distinct compositional variations among them.

Whittaker and Wicks (1970) concluded from their comparison of the serpentine minerals that:

(1) antigorite has a relatively high wt. % SiO_2 and a relatively low wt. % MgO and H_2O

(2) chrysotile has a relatively low Al_2O_3 content

(3) lizardite has a large ratio of Fe_2O_3 to FeO and is relatively low in FeO.

Chrysotile and lizardite contain H_2O^+ in excess of the ideal formula; antigorite has the highest $FeO/(FeO + Fe_2O_3 + Al_2O_3)$ content, and lizardite the lowest. The extent of substitution of Fe and Al tends to be in the order 6-layer orthoserpentine > lizardite > chrysotile, though substitutions in antigorite extend over the range of all the other minerals.

The serpentine minerals belong to the kaolinite-serpentine group of phyllosilicates. They have a 1:1 layer structure: one octahedral sheet ($Mg(OH)_2$ layer) is coupled to one tetrahedral sheet (SiO_4 layer). As with most layered minerals various regular and disordered stacking arrangements occur, giving rise to different polytypes, especially with the platy mineral, lizardite. Detailed descriptions of the structures and polytypism exhibited by these minerals can be found in Wicks (1969) and Whittaker and Zussman (1971). The elegant electron microscope work of Yada (1967, 1971) has added tremendously to the detailed understanding of the chrysotile structure; however, lizardite has not been as well characterized due to the lack of sufficiently large, well formed crystals suitable for single crystal X-ray work or electron microscopy.

Previous Experimental Work

The experimental work pertaining to serpentinization can be placed in four categories: (1) equilibrium determinations of reactions of interest that define the upper stability limit of serpentine + water and the lower stability limit of olivine + water under specified P,T conditions; (2) synthesis of the serpentine minerals from oxide mixes and gels + water; (3) reaction of olivine with fluids of varying composition; and (4) kinetic studies of the reaction of olivine + water to form serpentine + brucite. Each type of experiment will be discussed within the chemical system defined by the constituents required to describe the pertinent reactions.

$MgO-SiO_2-H_2O$

Table 1 summarizes the experiments in the literature that allege to be equilibrium determinations of stability fields of the assemblages represented by the following reactions:

$$\underset{\text{serpentine}}{Mg_3Si_2O_5(OH)_4} + \underset{\text{brucite}}{Mg(OH)_2} = \underset{\text{forsterite}}{2Mg_2SiO_4} + \underset{\text{water}}{3H_2O} \qquad (1)$$

$$\underset{\text{serpentine}}{5Mg_3Si_2O_5(OH)_4} = \underset{\text{talc}}{Mg_3Si_4O_{10}(OH)_2} + \underset{\text{forsterite}}{6Mg_2SiO_4} + \underset{\text{water}}{9H_2O} \qquad (2)$$

Johannes (1968) demonstrated that all studies previous to his essentially

TABLE 1

Previous experimental work on alleged equilibrium determinations of reactions (1) and (2) in the $MgO-SiO_2-H_2O$ system.

Reaction (1): $Mg_3Si_2O_5(OH)_4 + Mg(OH)_2 = 2Mg_2SiO_4 + 3H_2O$

Investigators	Apparatus	Starting Materials	Pressure kbar	Temperature °C	Run Duration Hrs.	Results
Bowen & Tuttle (1949)	cold-seal bombs	oxide mixes, syn. serpentine + ex. water	0.04-2.72	295-460	6-336	min. stability of forsterite at 450°C, 2 kbar
Pistorius (1963)	piston-anvil	oxide mixes + min. water	5-50	415-500	1-3	curve shifted 30°C lower than Bowen & Tuttle
Kitahara et al. (1966)	piston-cylinder	oxide mixes, syn. phases + water	6-30	450-600	2.5-67	curve coincided with Bowen & Tuttle when extrapolated to lower pressures
Scarfe & Wyllie (1967)	cold-seal bombs	syn. forsterite + ex. water	0.5-3.0	300-330	504	curve 100°C lower than Bowen & Tuttle, studied in one direction only
Johannes (1968)	cold-seal bombs	equal weight mixture of syn. prods. & react. + ex. water	0.5-7.0	330-440	576-3480	curve shifted 60°C from Bowen & Tuttle's synthesis boundary, reversed, equilibrium determination

Table 1 cont'd.

Reaction (2): $5Mg_3Si_2O_5(OH)_4 = Mg_3Si_4O_{10}(OH)_2 + 6Mg_2SiO_4 + 9H_2O$

Investigators	Apparatus	Starting Materials	Pressure kbar	Temperature °C	Run Duration hrs.	Results
Bowen & Tuttle (1949)	cold-seal bombs	oxide mixes, syn. serpentine + ex. water	0.14-2.04	485-535	5-72	max. stability of serpentine 500°C 2 kbar, serpentine "magma" discredited
Pistorius (1963)	piston-anvil	oxide mixes + min. water	5-50	495-625	1-62	curve shifted 30°C lower than Bowen & Tuttle
Kitahara et al. (1966)	piston-cylinder	oxide mixes, syn. phases + water	6-30	550-620	3-45	curve coincided with Bowen & Tuttle when extrapolated to lower pressures
Yoder (1967)	cold-seal bomb	periclase + silica + H_2O	1-10	400-560	*	curve not reversed, located between curve of Pistorius and Kitahara et al.
Scarfe & Wyllie (1967)	cold-seal bomb	mix of syn. prods. & reacts. + water	1-3	410-470	200-600	reversed reaction, direction of reaction determined by topotactic crystallization
Dietrich & Peters (1971)	cold-seal bomb	nat. C, nat. C+An, with H_2O & mixtures of H_2O+CO_2	1.0-2.6	250-606	600-6480	one direction determination with C at 480°C, 2 kbar with 0-10.8 wt.% H_2O, CO_2 results similar to Johannes (1969)

*run duration was not specified

Table 1 cont'd.

Investigators	Apparatus	Starting Materials	Pressure kbar	Temperature °C	Run Duration hrs.	Results
Chernosky (1973)	cold-seal bomb	mix of syn. prods. & reacts. + water	0.5-7.0	387-598	237-3960	equilibrium determination, reversed direction of reaction determined by change in X-ray intensities, 20°C lower than Scarfe and Wyllie

syn. = synthetic
hrs. = hours
ex. = excess
prods. = products
reacts. = reactants
min. = minimum
max. = maximum
nat. = natural

represented the determination of synthesis boundaries[a] for reaction (1). The same criticism holds for the work done on reaction (2) before the studies of Scarfe and Wyllie (1967) and Chernosky (1973). Approximately 20°C separate Scarfe and Wyllie's curve from that of Chernosky, the discrepancy being due to the difficulty in determining the reaction direction for these very sluggish reactions at low temperatures. The upper limit of the assemblage chrysotile + talc + forsterite + water has been defined by Chernosky as 440°C at 2 kbar in a reversed set of experiments. The lower stability limit of forsterite + water + chrysotile + brucite is taken to be 380°C at 2 kbar (Johannes, 1968).

The serpentine minerals have been synthesized by Yang (1960, 1961), Speakman (1970), Jasmund and Sylla (1971, 1972), and Iishi and Saito (1973). Yang (1960) studied the phases in the system $MgO-SiO_2-H_2O$ between 100 and 300°C, 1 bar to 1.36 kbar. For run durations of 2 hours to 3 weeks and with excess water in the charge, chrysotile and talc were formed with a MgO/SiO_2 ratio between 0.25-1.33, for $MgO/SiO_2 = 1.5$ only serpentine was synthesized and for $MgO/SiO_2 > 1.50$ serpentine + brucite was formed. In the temperature range 100-160°C for $MgO/SiO_2 = 1.5$, Yang (1960) reported a "crumpled foil" serpentine phase (lizardite?) from electron micrographs of the product; however, only chrysotile was demonstrated at temperatures

---

(a) A "synthesis boundary" indicates conditions for formation of a particular mineral or mineral paragenesis where those conditions do not coincide with the equilibrium curve because (1) within the length of the time of experimental run, nucleation and growth of phases in the neighborhood of the equilibrium curve was not achieved or (2) within the given amount of time one or more phases formed metastably (Johannes, 1968).

greater than 160°C. Yang (1961) stated that the optimum conditions for chrysotile formation in the T-P range investigated were 300-350°C, 0.08-0.12 kbar, 5-10 days, pH = 10.3-10.7 with 1-2 weight % of 0.01M NH_4F added to the oxide mix that had MgO/SiO_2 ratio = 1.5, and water/solid ratio of 10. Trace amounts of lizardite were found with the chrysotile. Jasmund and Sylla (1971, 1972) formed 6-layer orthoserpentine from $MgCl_2$, sodium silicate and NaOH, at pH = 12, 320-350°C, 0.2-0.25 kbar in 170 hours. Well crystallized hexagonal platelets formed with a small amount of fibrous chrysotile.

Speakman (1970) studied the compositions $3MgO:2SiO_2$ and $2MgO:SiO_2$ with gels as well as forsterite ± quartz as starting materials in presence of excess water between 100-350°C, 10 bars to 2.0 kbar total pressure and run durations of 6 to 90 days. The gel composition $3MgO:2SiO_2$ produced serpentine only, but the forsterite + quartz starting material first produced talc, which subsequently reacted slowly with the forsterite to produce serpentine. The gel composition $2MgO:SiO_2$ formed serpentine + brucite, but forsterite persisted as the major phase in runs up to 90 days at 180°C, 10 bars. The temperature and pressure were raised to 300°C, 86 bars, resulting in the complete disappearance of the forsterite within 90 days. The serpentine phase formed in Speakman's experiments was chrysotile of various states of crystallinity. Sluggishness of reaction was noted, particularly in the case of well-crystallized starting materials (forsterite ± quartz).

Iishi and Saito (1973) synthesized lizardite, chrysotile and antigorite from gels with the molecular ratio of $MgO:SiO_2:H_2O$ from 4.99:4.0:2.52 to 6.16:4.0:23.60 between 300-550°C, 0.5 to 1.7 kbar pressure; note that ideally, serpentine contains these constituents in the ratio of 6:4:4. This study was the first reported synthesis of antigorite, and Iishi and Saito found that the formation of antigorite depended on the molecular ratio of MgO to SiO_2 and to a certain extent on the amount of water present during the reaction.

Martin and Fyfe (1970) measured the rate of hydration of synthetic forsterite as defined by reaction (1). A natural olivine (Fo_{85}) and an olivine basalt were also studied. The rate of reaction was determined in terms of the weight increase of products compared to the starting material and was corroborated by X-ray intensity measurements of the product phases. The amount of water used was slightly greater or less than the amount needed for total conversion of the olivine to the hydrated products. At 1.36 kbar and 260°C, more than 60% of the olivine was converted to serpentine + brucite after 6 days. The rate of conversion was increased with addition of more than the stiochiometric amount of water defined by reaction (1). Rates of reaction are very fast in the geologic time scale for the P,T region of maximum conversion as determined by Martin and Fyfe.

$MgO-SiO_2-Fe-H_2O-H_2$

Bowen and Tuttle (1949) reported some unbuffered experimental runs with a natural olivine (Fo_{90}) and concluded that the position of the curve for the assemblage Fo_{90} + water + serpentine + brucite + magnetite was lowered 80°C from the curve defined for reaction (1). Using oxygen buffer techniques developed by Eugster (1957, 1959) and Eugster and Wones (1962), Page (1966) synthesized an iron-bearing lizardite from oxide mixes of SiO_2, MgO, and $Fe_2C_2O_4$ plus water in molar proportions of 5.6MgO:0.01FeO: $4SiO_2$ to 4MgO:2FeO:$4SiO_2$ at temperatures from 363 to 476°C and pressures from 1 to 2 kbar. Page also tried to synthesize a serpentine of theoretical composition $Mg_{5.4}Fe_{0.6}Si_4O_{10}(OH)_8$ with a starting material of olivine (Fo_{90}) and SiO_2 (as quartz or amorphous silica) and obtained as products talc, olivine and an occasional iron mineral for the same P,T range stated above. Page (1966) was not completely successful in these syntheses of iron-bearing serpentines for the following reasons: (1) the starting material of olivine + quartz had sufficient silica to form talc rather than serpentine (talc being the more silica-rich phase of the two); (2) $Fe_2C_2O_4$, a component of the oxide starting mixture breaks down at elevated T and P to FeO + CO_2, and Johannes (1969) has shown that serpentine is not stable with respect to talc under these conditions except in very CO_2-poor fluids (< 0.06 mole fraction CO_2); (3) the temperatures chosen for the syntheses were rather high for the optimum conditions for formation of serpentine as shown by Yang (1961) and Martin and Fyfe (1970);

furthermore, a majority of the runs were actually outside the field of serpentine stability at 427°C for 1 kbar and 441°C for 2 kbar according to the results of Chernosky (1973); and (4) there are additional problems of equilibration of oxygen buffers especially at temperatures below 500°C (Huebner, 1971).

Martin and Fyfe (1970) studied the hydration of a natural olivine (Fo_{85}) with similar results to those for synthetic forsterite except that reaction times were 2-3 times longer. No magnetite could be detected optically in the hydration product of Fo_{85}. Martin and Fyfe reported from X-ray evidence that iron had entered the brucite structure. Experiments with grain size of the natural olivine as a variable indicated a very rapid decrease in the rate of reaction with increasing grain size. An increase in grain size from 50 μm to 150 μm produced a drop in percent conversion of olivine at 250°C, 1.3 kbar, in 3 weeks, from 25% conversion to barely discernable reaction.

Na_2O-MgO-SiO_2-Fe-H_2O-HCl-H_2

Several Russian researchers have investigated the hydration of a natural olivine (Fo_{85}) with a variety of fluid compositions, chiefly solutions of HCl, NaOH, and Na metasilicate. The experimental apparatus described by Korytkova and Fedoseev (1969) is comparable to a Morey bomb. All reported experiments were unbuffered with respect to oxygen fugacity.

Korytkova and Makarova (1971) and Korytkova et al. (1972) produced antigorite + chrysotile + magnetite by reaction of 0.1-0.75 M NaOH solution with olivine (Fo_{85}) at 250-300°C, 0.5 to 0.9 kbar with run durations ranging from 3 to 30 days. Product identification techniques included optical, X-ray, and transmission electron microscope data. Antigorite grew in form of hexagonal platelets, and chrysotile grew in its typical fibrous habit. Reaction of olivine with silica-bearing alkaline fluids led to more rapid breakdown of olivine than with the silica-free solutions at the same temperature and pressure, and run duration. After 30 days, 250°C, 0.5 kbar, in silica-bearing 0.1-0.2 M NaOH solution, a product of approximately 80% antigorite and 20% chrysotile is formed from the breakdown of olivine. The concentration of silica in solution was not specified. Pure water and acidic solutions (0.001-0.00001 M HCl) were not as reactive in the same P,T range and run duration as the alkaline solutions and formed lizardite + chrysotile with some olivine remaining at the end of the run. Korytkova and Makarova (1972) extended the work on the alteration of olivine with alkaline solutions (± silica) from 100°C, 0.3 kbar to 600°C and 0.5 kbar. No breakdown of olivine was observed in the interval 100-250°C, 0.3-0.5 kbar in alkaline solutions (± silica) after one week. At 350°C and 0.3 kbar, the product from a 1.5% NaOH silica solution is 60% olivine, 30% antigorite, and 10% Mg-arfvedsonite. With an increase in temperature the amount of amphibole increased, until at 500°C, 0.7 kbar in a silica-bearing 0.8% NaOH fluid, only a trace of olivine remained and no serpentine formed.

Observation on Serpentinization from Natural Occurrences

Serpentinized Ultramafic Rocks

Serpentinization processes in naturally occurring ultramafic rocks have been exhaustively discussed in recent literature. The main points of the recent prolific discussion are: (1) the differences between the reaction of dunite and pyroxenite with a fluid phase; (2) the temperature-pressure of the regime of hydration; (3) the mineral assemblages produced during serpentinization; (4) the problem of whether serpentinization takes place at constant volume or constant composition, or combination of both conditions; (5) the influence of fluid composition on hydration and mineralogy of serpentinite; and (6) the origin of the serpentinizing fluids.

Ultramafic complexes are made up of dunite, harzburgite and lherzolite (Wyllie, 1967; Coleman, 1971; Moores, 1973). The major minerals are olivine, orthopyroxene, clinopyroxene, and chromite. Wicks' (1969) detailed textural studies of a variety of serpentinized ultramafic rocks illustrated that the rate of alteration is: olivine > orthopyroxene > clinopyroxene. Wicks (1969) and Coleman and Keith (1971) have shown that the common hydrated equivalents of ultramafic rocks produce the assemblage: lizardite > chrysotile, brucite and magnetite. Small amounts of awaruite, native metals and low-sulfur sulfides are common. Brucite is often missed in thin section studies of serpentinized rocks because it is fine-grained and intimately intergrown with serpentine, but brucite is readily identified

in a whole-rock X-ray diffraction pattern. Hostetler et al. (1966) demonstrated the importance of brucite; its presence defines a lower temperature of serpentinization (reaction (1)) than the presence of serpentine alone (reaction (2)). Thayer (1966) suggested that brucite may be only a transitory phase, disappearing as serpentinization proceeds.

Iron in olivine (or pyroxene) may re-distribute during serpentinization, entering the structure of the serpentine minerals or brucite, or forming a separate oxide phase, magnetite. Mumpton and Thompson (1966), Hostetler et al. (1966), Page (1967a) and Wicks (1969) have documented the iron substitution for magnesium in brucite during serpentinization - from 6 to 72 mole percent $Fe(OH)_2$ has been recorded. Coleman and Keith (1971) have shown the same amount of magnetite produced from dunite and harzburgite from magnetic susceptibility measurements, but Page (1966) and Wicks (1969) stated from petrologic observations that magnetite is produced in only trace amounts from the serpentinization of pyroxenes.

In comparison to lizardite and chrysotile, antigorite predominates in alpine-type ultramafic rocks that have undergone regional metamorphism (Wicks, 1969; Coleman, 1971). Antigorite does occur with brucite (Jahns, 1967; Trommsdorff and Evans, 1972). Serpentinites consisting predominately of antigorite also have higher modal abundances of magnetite on the average than lizardite-chrysotile serpentinites (Wenner and Taylor, 1971).

The major chemical problem of serpentinization is the necessity for the existence of an interacting, aqueous fluid phase: where does it come from, does it leach constituents from the primary rock, and what are its original and secondary chemical characteristics (pH, f_{O_2}, dissolved

constituents)? Therefore, serpentinization requires introduction of water into an anhydrous rock, which causes a decrease in the density of the rock and a concomitant increase in volume of the rock mass unless material is removed in solution. The constant volume-constant chemical composition evidence for serpentinization is presented in Table 2; detailed equations to demonstrate the two points of view can be found in Hostetler et al. (1966) and Thayer (1966). The difference in opinion between Thayer (1966, 1967) and Hostetler et al. (1966) and Page (1967b) comes from the difficulty in obtaining good chemical composition data on both the ultramafic rock and its serpentinized equivalent and obtaining unequivocal geological criteria for volume constancy or change. Bogolepov (1969) has used a large number of chemical analyses of these rocks to show that chemical composition does remain constant during serpentinization of the Alpine-type ultramafic rock with the volume increase taking place by "mosaic type of displacement of individual tectonic blocks in vertical directions". Wicks (1969) is essentially in agreement with Bogolepov from his detailed mineralogical data and analysis of the replacement of olivine by serpentine-brucite. Bogolepov also shows that local serpentinization (i.e. chrysotile vein formation) occurs with change in chemical composition, thus making an important distinction in the type of serpentine being formed and demonstrating that both constant chemical composition and constant volume serpentinization most probably take place. Good chemical data from two recent studies provide additional evidence that both processes occur: (1) constant chemical composition at Burro Mountain (Coleman and Keith, 1971) and (2) constant volume and change in chemical composition at

TABLE 2

Evidence for constant chemical composition and constant volume serpentinization.

Constant Chemical Composition[1], [2]	Constant Volume[3]
1. no indication of Si or Mg metasomatism in surrounding country rocks	1. perfect pseudomorphic replacement of euhedral olivine by serpentine
2. chemical composition of hydrated and anhydrous parent material are the same except for addition of water	2. density decreased and porosity increased of serpentinite compared to the parent ultramafic body
3. faulted contacts, internal fractures, slickensided and highly sheared border zones indicate volume increase	3. a portion of the Mg, Ca, and Si removed during serpentinization may be deposited far from the source.*

[1] Hostetler et al. (1966)

[2] Page (1967)

[3] Thayer (1966, 1967)

*Barnes et al. (1972) infer from the precipitation of brucite at the orifice of Complexion Spring that fluid flow may allow reaction products to be deposited at a distance from point of dissolution; in the case of Complexion Spring, magnesium was precipitated within the limits of the ultramafic complex

Webster-Addie ultramafic intrusion with loss in Fe, Mg and addition of Si and Na (Condie and Madison, 1969).

Fluids Involved in Serpentinization

Barnes and O'Neil (1969) and Barnes et al. (1972) have shown that serpentinization can occur under conditions existing at the earth's surface. They have classified the fluids related to serpentinization into three types on the basis of their chemistry and isotopic compositions. The waters are characterized by a high pH (> 10), low Mg concentration and they may also have a high chloride content. Thermodynamic calculations, from 25°C, 1 atm thermochemical data for relevant phase-solution equilibria, indicate that these waters are undersaturated with respect to olivine, orthopyroxene, and supersaturated with respect to chrysotile, diopside, tremolite and brucite (except for one water that is undersaturated with respect to brucite).

Faust et al. (1956) and Varlakov and Zhuzhgova (1964) have shown that the boron content of continental ultramafic rocks is greater in the serpentinite than in the parent rock. Thompson and Melson (1970) demonstrated boron enrichment in serpentinites collected from the Atlantic Ocean at 43° and 11°N (5-10 ppm boron in unserpentinized rocks and 70-100 ppm B in serpentinized peridotite). The boron enrichment in serpentinized portions of ultramafic rocks from oceanic ridge systems was further confirmed by the results of Seitz and Hart (1973). Barnes et al. (1972) analyzed gels precipitating from chloride-rich waters (Aqua de Ney, Siskiyou Co., Calif. and TC-2, Trinity Co., Calif., Complexion Spring, Lake Co., Calif.); the gels contained considerable boron in concentrations of 700

to 5000 ppm B. The boron concentrations, coupled with B isotopic data, may be a critical test of a possible sea-water provenance of boron; sea water is enriched in B^{11} compared to boron found in terrestrial rocks. High-temperature reactions (600°C) of basalt and sea water have shown that boron from sea water is preferentially partitioned into the fluid phase, whereas basaltic rocks exposed on the sea floor undergoing low-temperature weathering by ocean water become enriched in boron (Thompson and Melson, 1970, Table 2). By analogy with basalts, the boron concentrations of serpentinites may also give a clue to the temperature of serpentinization: at temperatures less than 200°C, boron in the fluid would partition into serpentine, possibly in structural sites.

Stable Isotopes

Stable isotope geochemistry has been used to deduce temperatures of serpentinization and to provide evidence on the origin of serpentinizing fluids. Barnes et al. (1972) measured the δO^{18} and δD compositions of three serpentinizing fluids and compared the spring water composition to their locally derived meteoric waters (LDMW):

	δO^{18}	δD
Creek at Lazton Mine (LDMW)	-6.45	-40.6
Cazadero A	-6.45	-40.6
Barrel Spring (LDMW)	-8.78	-62.3
Complexion Spring	+2.22	+ 6.2
Soda Spring (LDMW)	-10.3	-83.2
Aqua de Ney	+6.02	-15.6
TC-2	-2.18	-48.6

Cazadero A spring water has the same isotopic composition as its locally derived meteoric water. Complexion Spring, Aqua de Ney, TC-2 waters have very different isotopic compositions from their locally derived meteoric waters. This difference involves further considerations of the depletion and enrichment of the stable isotopes in comparison to the source of the water and its interaction with the ultramafic rock.

Wenner and Taylor (1971) studied the $0^{18}/0^{16}$ ratio between co-existing magnetite and serpentine (lizardite, chrysotile serpentinites from California, Guatemala, Dominican Republic, Mid-Atlantic Ridge and antigorite serpentinites from Vermont and Pennsylvania). The normal lizardite, chrysotile serpentinites, which had homogeneous magnetite distributions, had a Δ value (difference between $\delta 0^{18}$ of serpentine and magnetite) between 10.0 and 15.1. The Δ values for the antigorite serpentinites were between 4.8 and 8.6. Assuming isotopic equilibrium, the difference between the Δ values for lizardite, chrysotile and antigorite serpentinites were explained as due to the difference in temperature of formation. Wenner and Taylor then derived an approximate serpentine-magnetite geothermometer by: (1) extrapolation of $\delta 0^{18}$ fractionations between co-existing chlorites and Fe-Ti oxides in low grade pelitic schists whose isotopic equilibration temperatures are known from the quartz-muscovite 0^{18} geothermometer, and (2) estimates of 0^{18} fractionation factor between chlorite and serpentine, assumed to be equal to one. The geothermometer yields the following temperatures from the measured Δ values: continental

lizardite, chrysotile, 85-115°C, oceanic lizardite and chrysotile, 130 and 185°C respectively, oceanic antigorite, 235°C, continental antigorites 220-460°C. With the large number of assumptions that were necessary to derive the serpentine-magnetite geothermometer, the unusually low temperature estimates for the formation of the serpentine minerals may be too low by as much as 100°C (Bottinga and Javoy, 1973), though the isotope data strongly indicate that antigorite forms at higher temperatures than lizardite or chrysotile. The δO^{18} and δD measurements together indicate that lizardite, chrysotile serpentinites probably formed at temperatures not greater than 200°C (J.R. O'Neil, pers. comm., 1974). Wenner and Taylor's (1973) comparisons of δO^{18} and δD of mid-oceanic ridge serpentinites and continental serpentinites that have been classified as ophiolitic complexes, show distinctly different δD and δO^{18} distributions. Wenner and Taylor conclude that the difference in isotopic composition indicates that different waters were involved in the serpentinization of the two types of ultramafic body, and that if ophiolite complexes truly represent exposures of the oceanic crust and mantle, they were probably largely unserpentinized prior to their continental emplacement.

Statement of Problem

In light of the information presented in the previous sections, several definite statements can be made on the serpentinization process:

(a) the dominant minerals produced are lizardite, chrysotile, brucite, $\pm$ magnetite, such that reaction (1) generally describes the hydration of most dunites with respect to condensed phases; (b) the presence of brucite as specified in reaction (1) means that this mineral assemblage represents a lower P,T limit of serpentinization when compared to reaction (2); (c) the iron component of olivine is partitioned between serpentine or brucite, or forms a separate phase - magnetite; (d) the fluid involved in hydration more than likely has a complex origin: it becomes alkaline, is CO_2 poor, low in Mg and may have a high chloride content; (e) the presence of silica-bearing, alkaline fluids changes the serpentine mineralogy and the serpentinization process as defined by reaction (1), again emphasizing the importance of fluid-mineral interaction; and (f) serpentinization takes place over a wide range of T,P conditions, from earth surface conditions to at least the T,P regime for reaction (1) as determined by Johannes (1968).

Olivine in dunites typically varies between Fo_{80} to Fo_{95} with an average of Fo_{90} (Miyashiro, 1966). With the development of oxygen buffer techniques (Eugster, 1957, 1959; Eugster and Wones, 1962) it has become possible to consider the effect of adding iron to the system $MgO-SiO_2-H_2O$. Such experiments obviously provide a closer simulation to the natural systems. The present work was undertaken: (I) to determine the effect of iron on the equilibrium curve defined by Johannes (1968) for the lower temperature reaction involving brucite; (2) to evaluate the chemical parameters that affect the mobility of iron during the reaction, i.e., its partition among serpentine or brucite or the formation of magnetite; (3) to determine by

careful mineralogical analysis which factors influence the formation of the different serpentine minerals; and (4) to measure the effect of changing fluid composition on the breakdown of olivine.

Contributions of This Study

The efficiency of the iron-magnetite buffer has been demonstrated to temperatures as low as 300°C at 0.5 kbar total pressure. Thermodynamic calculations show that the vapor phase defined by this buffer is extremely hydrogen-rich. Neither the ideal mixing model of Eugster and Wones (1962) nor mixing model of Shaw (1963, 1967) extrapolated by Zen (1973) adequately define the vapor phase.

The equilibrium curve for the phase assemblage olivine (Fo_{93}) + water + lizardite + clinochrysotile + brucite + magnetite has been determined and was shifted 15°C from the curve defined by Johannes (1968) for the assemblage forsterite + brucite + clinochrysotile + water. The Scanning Electron Microscope was an invaluable tool in defining the dissociation boundary.

Iron-bearing brucite and magnetite were present as products of the experimental runs. The iron content of brucite is a function of temperature: as temperature is increased the amount of iron in brucite decreases and the amount of magnetite increases. The brucite solid solution breaks down by the following reaction:

$$3Fe(OH)_2 = Fe_3O_4 + 2H_2O + H_2$$

where $x_{Fe(OH)_2}$ is the mole fraction of $Fe(OH)_2$ in the solid solution. The iron content of the brucite is most probably also a function of iron content of the primary olivine and oxygen fugacity as well as temperature.

Lizardite plates, laths and euhedral (hexagonal) crystals, as well as chrysotile fibers, laths, and fiber bundles are clearly observable by the SEM studies of the run products. All the crystal forms have been observed in natural specimens of the minerals with the exception of the well-crystallized hexagonal crystals of lizardite. Temperature and pressure of formation do not affect habit except in the case of lizardite laths, which were observed only at temperatures greater than 315°C. The unit cell parameters of lizardite show the same variation as has been observed in natural samples, and could not be related to temperature or pressure of formation. The variation in the cell dimensions is attributed to structural effects, but the possible effect of iron for magnesium substitution on the structure of lizardite must await further detailed work on synthetic iron-bearing lizardite. The iron content of the lizardite produced in the experimental runs is small but was not determined due to analytical difficulties.

The amounts of dissolved Mg and Si averaged 4.8 ppm Mg and 10.4 ppm Si in pure water experiments, with Si the same and Mg increased to 11.0 ppm in NaCl, NaOH, and alkaline chloride fluids. The NaCl solutions do not lead to appreciable formation of serpentine within the duration of experiments; however, with NaOH and alkaline chloride solutions olivine reacts

efficiently to form the assemblage of serpentine, brucite, and magnetite.

Applications of the experimental results to natural assemblages are discussed.

EXPERIMENTAL METHODS

Charges were loaded into noble-metal capsules with a fluid phase as described by Huebner (1971), welded shut, placed in cold-seal pressure vessels (Tuttle, 1949), and subjected to a temperature-pressure regime for a given period of time. Then, after the run was quenched, the resulting solids and fluid phase were examined by a variety of techniques to establish the nature of their mineralogical and chemical compositions. Fisher ACS reagent grade chemicals and distilled, deionized water were used in all experimental and analytical work.

Hydrothermal Runs

Starting Materials

A variety of synthetic olivines (and some natural olivines) were used in this study. Synthetic olivines were prepared hydrothermally from a mixture of MgO, SiO_2, and native iron according to the method of Fisher and Medaris (1969). The MgO was dried 48 hours at 115°C in a drying oven and stored in a vacuum dessicator. The SiO_2 was obtained as pure silica glass tubing (99.9%), crushed to 150 mesh, washed in weak hydrochloric acid and then several times with water. Then, the silica was fired to

600°C and stored at room temperature and pressure. Before using after storage, the silica was dried in the same manner as the MgO and put in a vacuum dessicator. Native iron was added in the form of iron fillings (Johnson, Matthey, & Mallory, Ltd., 99.999% purity) or as sponge (Johnson, Matthey, & Mallory, Ltd., 99.99% purity). A polished section of the iron sponge showed a small amount of magnetite (< 5%).

Synthetic olivines were obtained from G.W. Fisher (OP 194 and OP 54) and G. Plant (GSC olivine). Two natural olivines were supplied by R.G. Coleman (2-BU-77) and F.J. Wicks (M7863).

In the hydration experiments, the starting material was an olivine (synthetic or natural) plus a fluid phase (water, NaCl solution, etc.). The equilibrium runs (i.e. reversed or bracketing experiments) had an equal weight mixture of reactants and products plus water as the starting material. The equilibrium mix was made by reacting a synthetic olivine with water to give the products and then combining an equal weight of these products with the same olivine. This method differs from that used by Johannes (1968) and Chernosky (1973) who synthesized all phases of the reaction separately, then put them together in an equal weight mixture. A few dehydration experiments were done in which the starting material consisted of the product phases (serpentine, brucite, magnetite, trace olivine) plus water placed in the pressure-temperature stability field of olivine + water.

Charge Preparation

Figure 1 illustrates the capsule configuration used. The Au and Ag tubing was unoxidized when used and was pre-treated only by rinsing with acetone and dried. The Au tubing was 30 mm x 4 mm with a wall thickness of 0.25 mm and the Ag was 20 mm x 2 mm with a wall thickness of 0.13 mm. The loading procedure was:

(1) the Ag tubing was cut, washed, dried, and crimped at one end, the Au was prepared in the same manner except that it was welded shut at one end

(2) both capsules were weighed

(3) the starting material was loaded into Ag capsule with a small funnel and weighed; average charges weighed 5-10 mg

(4) the fluid was added to Ag capsule with a microsyringe (5-10 mg), the capsule crimped shut and weighed (capsule handled with disposable gloves and tweezers)

(5) the buffer charge (approximately 20-30 mg) was loaded with a small funnel into the Au capsule and weighed

(6) the loaded Ag capsule was put into the Au capsule, and water added with the syringe (50-100 mg)

(7) the Au capsule was crimped shut and welded, with the capsule immersed in an ice bath to minimize fluid loss

(8) after welding and allowing to reach room temperature, the Au capsule was wiped with acetone and weighed.

All weighing was done on a Mettler balance, sensitivity to $\pm$ 0.05 mg. The completely loaded and welded capsule was then placed in a drying oven (115°C) for 20 minutes to an hour to check for gas leakage. If there was no weight change, the capsule was considered ready for the hydrothermal run.

Figure 1: Capsule configuration used in this study.

The inner Ag capsule was crimped closed.

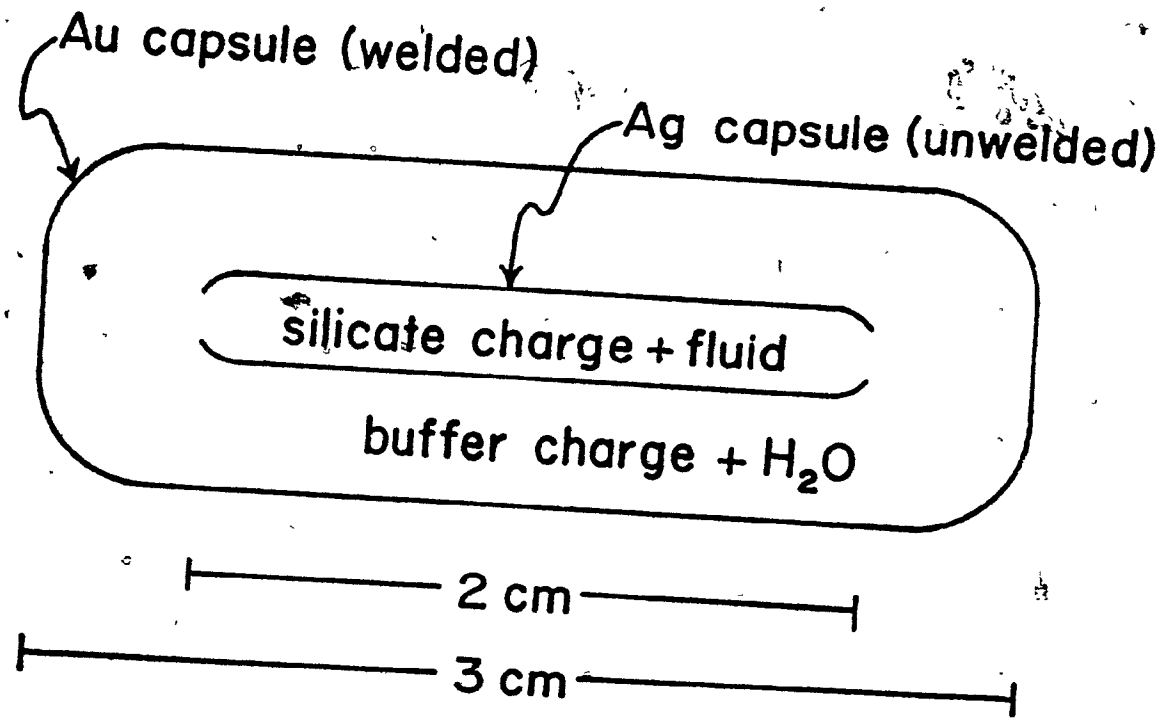
Au capsule (welded)
Ag capsule (unwelded)
silicate charge + fluid
buffer charge + H_2O
2 cm
3 cm

The capsule was placed in a cold-seal bomb, a steel rod was inserted, the bomb filled with water, the head-nut assembly was screwed on and the bomb was attached to the pressure line. A bare chromel-alumel thermocouple protected by 99.7% Al_2O_3 was inserted into the thermocouple well and held in place with wire or by ceramic cement. The bomb was brought to the run pressure and held there for 10-15 minutes to check for leaks in the line. Then, the bomb was placed in a tubular horizontal furnace and brought to run temperature, adjusting the pressure continually by bleeding. At the completion of a run the bomb was quenched in water, again holding pressure constant during the quench.

Pressure-Temperature Control

Temperatures were maintained constant with McGill-built and Thermoelectric temperature controllers. Constancy of temperature during the run was followed by continuous recording on a potentiometric strip chart recorder. However, temperatures were also measured daily with an ice bath reference junction and precise potentiometer with a null indicator reading to ± 0.005 mv ($\pm$ 0.13°C). The entire measuring circuit was calibrated against the melting points of Zn (419.5°C) and Bi (271°C); the metals were sealed in evacuated silica glass tubes. The quoted run temperatures (Appendix 2) are an average of 20 to 30 individual measurements, and in all cases the temperature variation during the run was less than 2°C. The maximum error in the stated temperatures is well within $\pm$ 5°C, considering the temperature calibration ($\pm$ 2°C), temperature variation

during the run ($\pm$ 2°C) and thermal gradient ($\pm$ 1°C) (Huebner, 1971).

Water pressures were generated with a hand-driven piston cylinder pump. Pressures were monitored with a 6" Bourdon gauge which was calibrated against a 12" Heise gauge. The pressure was checked every one to two days, the recorded pressure (Appendix 2) being an average of 15 to 25 readings. The recorded pressures varied less than 30 bars and are considered accurate to $\pm$ 50 bars.

Analysis of Products

Charge Unloading

After the run was quenched, the Au capsule was removed from the bomb, and observed for gross morphology, i.e., degree of "puffiness". Only one capsule could be run per bomb because of the large degree of "puffiness" which developed during most of the runs. The capsule was wiped with acetone and weighed. It was necessary to puncture the capsule carefully with a syringe tip, allowing the gas to escape. The fluid was removed with a disposable syringe or a Hamilton 200 μl syringe and put into a weighed amount of water. The Au capsule was opened completely and the buffer charge examined. The Au + Ag capsules were placed in a drying oven (115°C) for about 12 hours. After drying, both buffer and silicate charge were placed in separate vials and stored in a vacuum dessicator.

X-ray Analysis

A Guinier-Hagg powder pattern was obtained on all starting materials and products with NaCl as an internal standard. The powder camera (Incentive Research Development - AB, X-ray Diffraction Guinier XDC-700) was used with a fine-focus Cu tube (35 Kv, 20 mA) yielding CuKα_1 monochromatic radiation (1.54051 A). The X-ray patterns were read on a manual film reader to 0.01 mm. A computer program was written to correct all lines to the internal standard (calculated 2θ for NaCl used were 27.36, 31.70, 45.44, 56.47, 66.22 and 75.29) and give a listing of the corrected two theta and corresponding d-spacings. The average standard error associated with a reading of a given diffraction line is $\pm$ 0.01° 2θ, which corresponds to less than 0.002 A for most of the d range of concern. Least squares refinement was done using both Burnham (1962) (olivine, brucite) and Evans et al. (1963) (serpentine) programs.

Careful X-ray intensity measurements were attempted for determination of reaction change in the reversed experiments. The films were measured by means of a double-beam recording microdensitometer (Joyce, Loeble & Co., Ltd., Model MK IIICS). The intensity of the peaks for the products was then compared to intensity of the peaks for the starting material to determine whether there was change in the amount of olivine before and after the run. A 20% increase or decrease in intensity of the peaks was observed before change (+ or -) was noted.

Petrography

A polished section of the buffer charge was made following the method of Kullerud (1971) and examined in reflecting light using a Zeiss research photomicroscope. Grain mounts were made of the silicate products and examined with a combination of transmitted and reflected light micrography. Phase contrast microscopy was useful in detecting small amounts of olivine and/or brucite. Optical observation of the charge was essential in the identification of magnetite. Photography was routinely used as a permanent record and was helpful in comparison of grain mounts of products, especially between widely spaced runs.

Scanning Electron Microscopy

The Scanning Electron Microscope (SEM) was found to be very useful and in some cases essential in the documentation of run products. An excellent review of the use of the SEM and sample preparation is found in Hearle et al. (1972) and the following discussion is meant to illustrate those problems particular to the study of synthetic assemblages. The sample preparation for the SEM work consisted of:

(1) a small glass cover slip (8 mm square) was glued to the sample holder

(2) a small amount of the sample was transferred to the cover slip with a clean microspatula

(3) one to two drops of water were added to the powder to act as a dispersant

(4) after the water evaporated, samples were stored in a closed, dust-free container until coating

(5) two vacuum evaporation coating[a] procedures were used:

(a) 10 cm of AuPd (20%Pd) wire placed approximately 7 cm from sample, evaporated

(b) 5 cm of AuPd wire and an equal amount of Carbon, the C coating evaporated on first followed by the AuPd.

Note: the sample was rotated while the metals were being evaporated.

At first a clean mica flake was used as a supporter for the sample rather than the glass cover slip. Mica proved to be unsatisfactory because: (1) its platy habit and irregular surface features sometimes made the mica difficult to distinguish from the sample itself; and (2) the mica had a tendency to exfoliate under vacuum.

The Cambridge Stereoscan 600 SEM was used under the following operating conditions:

25 Kv beam voltage
10 mm working distance
0.5 sec scanning speed (photograph at 50 sec)
5th spot size (out of 6 possible)

The sample stage permitted rotation and tilting of the sample, which proved to have considerable advantage in studies of these multi-phase samples.

Charging is defined as a reversible effect of the electron beam on the specimen which causes the image to deteriorate (Hearle et al., 1972).

---

[a] Coating is the application of a conducting layer of C or metal in order to suppress charging and increase electron emission. The purpose of coating is to put on a uniform layer of conductive material, so that the surface coating is, as nearly as possible, an exact positive replica of the surface of the underlying material.

The processes that cause the deterioration are not well understood but charging has been found to be controlled by changing the beam energy (usually by lowering it) or by making a good conduction path to earth from all parts of the sample surface. The double-coating procedure was much more effective in decreasing the amount of charging of the sample, chiefly because of the greater penetrative power of carbon compared to AuPd alone. The problem of sample charging appeared also to be related to the samples themselves in the sense that the better crystallized samples charged less. Using a lower beam voltage did not decrease the charging.

Magnetic Measurements

R.B. Hargraves performed magnetic measurements on several starting materials and products to determine the net amount of magnetite produced during the reaction. The magnetic moment of a weighed sample was measured as a function of field strength on a Frantz translation balance. From calibration of the instrument and knowledge of the magnitude of the saturated magnetic moment of magnetite, the magnetic moment of the sample can be related to the amount of magnetite present in the sample.

Fluid Analysis

On puncturing the run capsule, a gas phase escaped, and the maximum amount of recoverable fluid was transferred by syringe to a weighed plastic

vial of water (4 ml). The vial was again weighed after addition of fluid, covered with parafilm, and stored in a closed drawer until analysis. At the time of analysis the vial was re-weighed. The weight loss was attributed to water evaporation and subtracted from the total amount of water used in the dilution. In a final set of samples, the 4 ml of water was acidified with a drop of concentrated HCl. Before acidification iron was not detected by AA analysis of the solutions, though it was detected in the diluted acid solutions.

Chemical Analyses

The solutions were analyzed for Mg and Fe by atomic absorption and Si spectrophotometrically as the molybdate blue complex. Standard solutions were made from Fisher certified Atomic Absorption Standard Reference Solutions, which were diluted with water and, in the appropriate samples, sufficient concentrated HCl was added to give the same concentration of HCl in the standard solutions as in the sample solutions. Fresh standards were diluted from the reference solutions for each batch of samples.

The Mg and Fe analyses were performed with a Perkin Elmer Model 403 Atomic Absorption unit with a 4" burner, air-acetylene flame, and single-element hollow cathode lamps. The standard instrument settings and procedures as outlined in Perkin Elmer Analytical Methods for AA Spectrophotometry (1971) were followed. The AA unit was calibrated directly in ppm after periodic

checking of absorbance of standards. Normally three standards were prepared in the anticipated concentration range. Routinely, 5-10 readings on the standard were taken, 5 samples read, the standard read again, another 5 samples, etc. Due to the small sample volume, only 3 to 5 (10 average) individual readings could be taken. Blank corrections were necessary for iron. The standard error in the analyses was calculated from the readings of the standard solutions. The 0.2 ppm Mg standard contained 0.198 ppm with a computed standard error of 0.009 ppm, based on 83 degrees of freedom[b] applying the Student's t test for 95% confidence limits. The 1.0 ppm Fe standard averaged 0.987 $\pm$ 0.059 at 95% confidence limit with 11 degrees of freedom; the 10 ppm Fe standard was 9.944 $\pm$ 0.146 ppm at 95% confidence limits with 4 degrees of freedom. Kahn (1968) defines the detection limit as the concentration of the element in a solution which gives a signal twice the size of the peak-to-peak variability of the background. By this definition the detection limit for Mg was 0.006 ppm and Fe was 0.032 ppm.

The procedure of Rainwater and Thatcher (1960) was used for Si determinations. Standards were diluted with water or acidified as described above. The absorbance measurements utilized a Bausch and Lomb Spectronic 88 Spectrophotometer at 700 nm with 10 cm cells. Use of the 10 cm cells combined with the expanded mode on the spectrophotometer allowed detection of 0.1 micrograms of Si. A standard curve of absorbance vs μg of Si was

---

[b] The degrees of freedom = N -1, where N = number of individual measurements.

prepared with 8 standards, a minimum of 2 standards run with each batch of samples. The standard error in the samples was computed from the regression line of the standard absorbance curve. The standard error in the regression line calculated for the Si analysis was $Y = 0.015 (\pm 0.036) + 6.167 X$ (± 0.256) at 95% confidence limits.

pH Measurement

The pH measurement was made immediately after quenching (within 5-10 minutes) by placing 2-3 drops of the fluid on a glass slide and touching the pH electrode to the fluid making sure that the bulb and glass frit were covered with sample solution. Measurement was made with a miniature combination pH electrode (Microelectrode, Inc.) attached to an Orion Research Specific Ion Meter (Model 407) with an internal temperature compensator. The mV expanded scale of the meter was used with the electrode calibrated against pH buffers (Fisher certified buffer solutions of 7.00, 8.00, 9.18 and 10.40). A standard curve was prepared of mV vs pH, i.e., the measurement was made in mV and converted to pH units. Before measurement, the meter was calibrated with buffers 9.18 and 10.40.

Unfortunately, difficulties with the new model electrode did not permit more than a few measurements. Considering the small sample size and the difficulty in measurement, the measured values are believed to be accurate to within ± 0.1 pH units.

EXPERIMENTAL RESULTS

Iron-Magnetite Buffer

Evaluation of Buffer Effectiveness

In the temperature-pressure range of the experimental work (300-400°C, 0.5-2.0 kbar), the rate at which oxygen buffers equilibrate has not been systematically evaluated. Eugster and Wones (1962) stated that in buffered experiments in which hydrogen transfer is not restricted by diffusion through metal, i.e., where an open inner capsule is used, the buffer may be effectively reactive at temperatures less than 400°C. Shaw (1967) reported that the rate of diffusion of hydrogen through platinum and silver-palladium ($Ag_{70}Pd_{30}$) decreases rapidly at temperatures below 700°C. Huebner (1971) stated that with hydrogen diffusion through metal, the hydrogen-rich buffers will equilibrate at temperatures below 500°C and perhaps as low as 400°C. Wise and Eugster (1964) report using the IM buffer to 350°C, 2 kbar. In view of the uncertainty involved in the effectiveness of the oxygen buffers at these low temperatures, it was decided:

(1) to use an open inner capsule to insure gas transport from the buffer charge to inner silicate charge, and

(2) to evaluate the kinetics of the IM buffer reaction in the T,P range of interest.

The buffering action can be described by two equivalent reactions:

$$3Fe + 2O_2 = Fe_3O_4 \quad (3)$$

$$3Fe + 4H_2O = Fe_3O_4 + 4H_2 \quad (4)$$

Equation (4) describes the reaction more realistically because hydrogen production can be observed macroscopically in the "puffiness" of the capsule and gas escape on opening the charge. Magnetite production can be confirmed in a polished section of the buffer material.

The buffer charge for the rate study was native iron plus water. Initially, only Fe filings were used but the filings proved to be relatively unreactive, apparently due to large grain size and therefore small surface area. The sluggish reactivity was gauged by the small amount of magnetite and gas produced at the end of the experiment. Subsequently, Fe sponge (approximately 10-40 μm size) proved to react far more rapidly. Figure 2 shows that the iron sponge produced effective buffering action within a few hours of placing the charge within a particular T,P regime. The buffer charge for the majority of the runs was a mixture of Fe sponge and Fe filings. The sponge was used to insure rapid buffering and the filings were added in case the sponge became exhausted during the longer runs.

The experimental criteria developed for the judgement of effectiveness of the IM buffer at run completion are:

(1) "puffiness" of the capsule, indicating hydrogen production, and gas escape on puncturing the capsule

(2) no weight loss of the capsule (suggested by Huebner (1971) to be less than 1 mg for a 2 g capsule)

Figure 2: Plot of percent magnetite in buffer vs time for the reaction of iron sponge + water. The percent magnetite was estimated from a polished section of the buffer material (Runs 3-6a, 3-6b, and 3-6c). Note that this experiment was done to determine the rate of reaction and the buffer charge for the normal experimental runs was a mixture of iron sponge + filings; the sponge was used to insure rapid buffering and the filings were added in case the sponge became exhausted during the longer runs.

IRON SPONGE

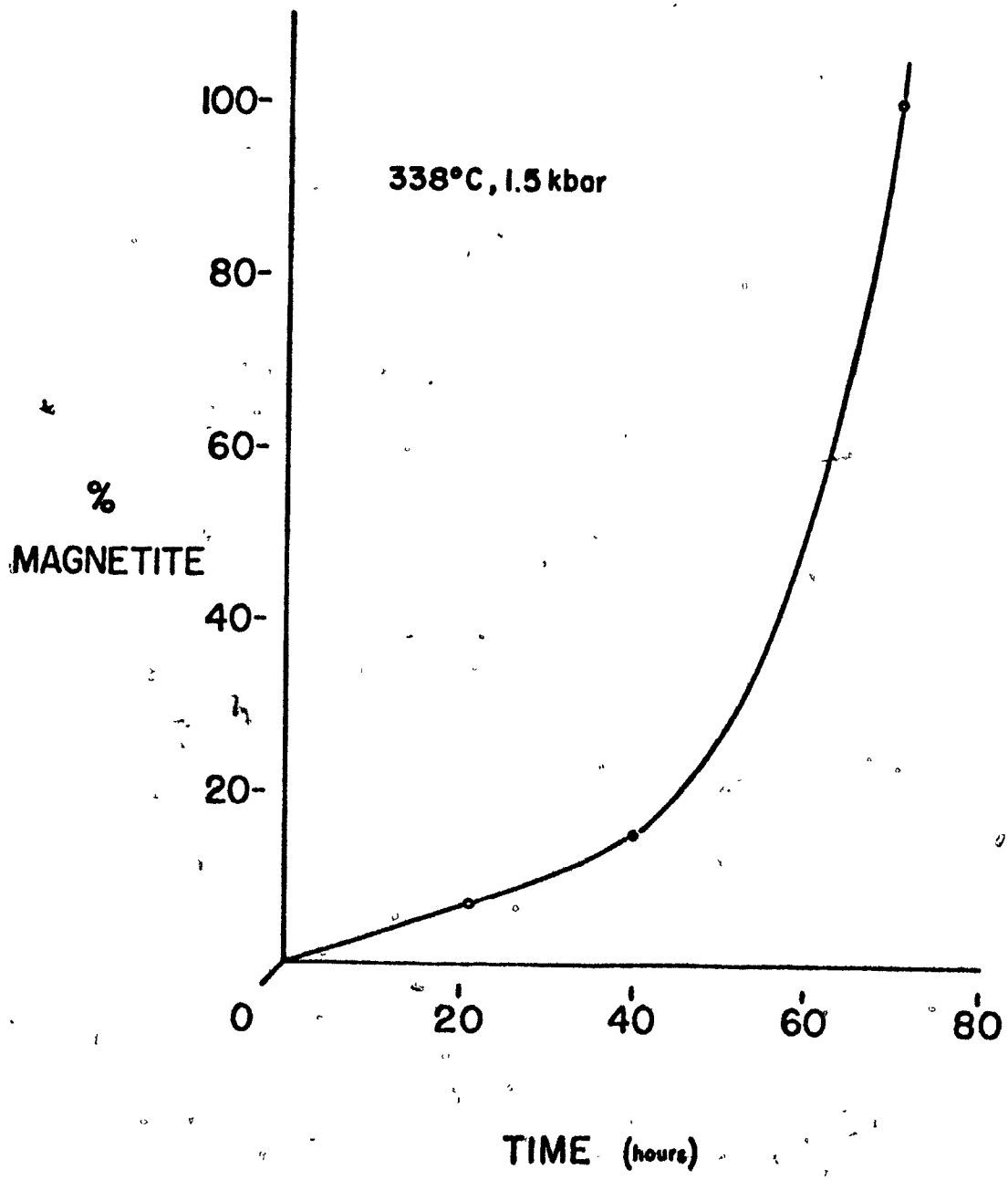

(3) water still present when the capsule is opened

(4) detection of co-existing magnetite and native iron in the residual buffer charge.

Appendix 1a presents the observations on the buffer effectiveness for each of the experimental runs. The most difficult experimental problem with the IM buffer was encountered on the quench. If the pressure was not maintained in the line during quench, the capsule often leaked because of the pressure differential. For those capsules which had leaked detectably on removal from the bomb, it was assumed that the leak occurred on quench if there was no oxidation of the buffer charge.

Some iron from the buffer charge can dissolve into the fluid phase. The resulting precipitation on quench was first noticed in examination of the buffer in polished section as an orange aggregate of material around some of the magnetite grains. However, when examined under a binocular microscope immediately upon opening the capsule, the buffer did not contain any orange precipitate. As the charge is placed in a drying oven, evaporation of the fluid remaining on the buffer charge caused oxidation and precipitation of $Fe(OH)_3$ (most probably). The process was studied under a binocular microscope with a freshly opened charge placed close to a 150 watt bulb; the precipitation of an orange material was immediately observed during evaporation of the fluid. All subsequent runs were checked before being placed in the drying oven for any orange precipitate. It can be concluded that at run T,P the buffer charge was not oxidized, but some iron did dissolve. Upon quenching to room T,P and oxidation of the fluid,

the iron precipitated out of the solution. Chemical analysis of the acidified diluted fluids collected from some of the experimental runs, showed some iron in solution (see Appendix 5). The acidification of the diluted fluid was necessary to prevent the adsorption and fine, colloidal precipitation of the ferric hydroxide.

As the inner capsule was open to the outer capsule, an attempt was made to evaluate possible iron transfer from the outer to the inner capsule via the fluid phase. Run 2-67 produced a pure brucite (identified by cell edge determination) from a mixture of MgO and H_2O at 300°C and 1.5 kbar in the presence of the IM buffer. Optical examination of the buffer and silicate charge in experimental runs revealed no evidence suggestive of iron transport from the outer to inner capsule. Some transfer of iron probably does occur, but to such a small extent that it does not appear to affect the reactions studied.

Possible Hydrogen Leakage

The IM buffer is highly reducing as it involves a large production of hydrogen. Therefore, hydrogen may slowly diffuse through gold because the fugacity of hydrogen is much higher in the charge than in water pressure medium. Hydrogen diffusion through gold is a function of temperature and the container thickness. The method of determining hydrogen loss is by weight change of the capsule after the run (Huebner, 1971).

Table 3 presents the results from evaluation of those runs in which a weight change was observed. Runs 3-102, 3-93, 3-92, 3-50 and 3-23 had

TABLE 3

Runs in which weight loss at end of run was greater than 1 mg for a 2 g capsule (Huebner, 1971) and in which there was no macroscopically observable leak.

Run	Gas Escape On Opening	Wt.Loss,mg	Buffer mg*	H_2O mg*	Fluid Remaining	mg H_2 **
+3-102	no	7.88	18.53	115.99	yes	12.98
+3-93	yes, minor	31.79	19.29	117.92	yes, >50%	13.19
+3-92	no	48.10	21.85	121.56	yes, 50%	13.60
3-76a	yes, major	2.19	22.72	91.66	yes, <10%	10.25
3-74	yes	6.06	29.42	107.77	yes, >10%	12.06
3-70	yes, major	2.93	27.47	79.14	yes, >10%	8.85
3-51	yes, major	0.47	27.44	96.45	yes, 25%	10.79
+3-50	no	2.88	32.80	71.63	yes, >10%	8.02
3-43	yes, major	9.07	26.02	99.96	yes, 33%	11.19
3-42	yes, major	1.11	38.03	101.56	yes, 10%	11.36
3-32	yes, major	0.69	36.32	173.76	yes, 33%	19.44
+3-23	yes, minor	7.91	32.38	134.19	yes, 50%	15.02
3-8	yes	1.86	43.17	118.20	yes	13.26

*initial amount present

**amount of hydrogen produced by complete dissociation of the initial water in buffer charge

+possible leak on quench because there was no gas escape upon opening or only minor gas escape

no gas or minor gas escape on puncturing the capsule, indicating possible leakage on quench. For Runs 3-93 and 3-92 the weight loss was too great to be attributed to loss of hydrogen, there must have been loss of water as well. The remaining runs perhaps are consistent with a loss of hydrogen through the gold capsule. The weight loss ranges from 0.69 to 9.07 mg. Those runs that did show a weight loss are compared with experiments at the same T,P and run duration which did not show any weight loss in Table 4. This comparison does not support the conclusion that the weight loss was due to hydrogen diffusion through the gold because there was no consistent explanation why one capsule would diffuse hydrogen and another held at the same T,P and run duration would not. It is possible that leakage that occurred on quench was not continued observably when the capsule was removed from the bomb at room T,P. Also, Runs 3-42, 3-43, 3-50, 3-51, 3-92 and 3-93 involved alkaline fluids, which in some cases reacted with the Au capsule, perhaps leading to pin-hole size leaks especially around the welded portion of the capsule.

Calculation of Fugacity of Oxygen, Hydrogen and Water

The oxygen fugacity at temperature and pressure of the experiment can be calculated from thermochemical data. The method of calculation is based on the equation:

$$3/2\ Fe + O_2 = 1/2\ Fe_3O_4 \qquad \text{(equation (3), p. 40)}$$

where

TABLE 4

Comparison of experiments that showed a weight loss of the Au capsule at end of run with those in which there was no weight change.

Run	T, °C	P, kbar	Run Duration hrs.	Wt.loss,mg	Buffer mg*	Wt. % Sponge Fe*	H_2O mg*	Fluid Remaining	f/b**	% M ***
3-70	322	1.00	837	2.93	27.47	47	79.14	>10%	2.9	20
3-104	330	1.00	1035		22.92	74	108.75	33%	4.8	25
3-74	341	1.48	481	6.06	29.42	80	107.70	>10%	3.7	10
3-49	342	1.49	596		33.63	34	85.65	>33%	2.5	20
3-32	307	1.47	911	0.69	36.32	46	173.76	33%	4.8	20
3-48	309	1.48	862		42.39	34	138.30	<10%	3.3	10
3-23	323	0.54	1605	7.91	32.38	30	134.19	50%	4.1	20
3-68	322	0.56	863		32.81	46	84.28	10%	2.6	10
3-43	331	0.99	573	9.07	26.02	54	99.96	33%	3.8	45
3-63	332	1.00	524		23.51	43	77.73	>25%	3.3	25
3-42	306	0.99	573	1.11	38.03	53	101.56	33%	2.7	35
3-54	302	1.00	550		31.08	57	120.37	<10%	3.9	15

*initial amount

**ratio of weight of fluid to weight of buffer (initial)

***approximate percent of magnetite estimated visually from polished section

$$K = \frac{(a_{Fe_3O_4})^{1/2}}{(a_{Fe})^{3/2} \quad (f_{O_2})} \tag{5}$$

Then $\Delta G_r^o (T) = 1/2 \Delta G_{f,M}^o (T)$ (6)

and $\Delta G_r^o (T) = -2.303 \text{ RT log } K$ (7)

and $\log K = -\log f_{O_2}$ (8)

if the activity of the solid phases are unity. Standard states for solids, liquids and gases are as defined by Robie and Waldbaum (1968). The pressure correction to the oxygen fugacity required to bring f_{O_2} to total pressure (Eugster and Wones, 1962) is:

$$- \frac{\Delta V_g (P - 1)}{2.303RT} \tag{9}$$

With the data sources listed in Table 5, the oxygen fugacity is defined by:

$$\log f_{O_2} = - \frac{28880}{T} + 8.240 + \frac{0.0607(P - 1)}{T} \tag{10}$$

where T (^oK) and P (bars) for the temperature range from 298.15 to 1100^oK. Derivation of equation (10) involved obtaining by linear regression from the plot of $1/2\Delta G_{f,M}^o$ vs temperature an equation which describes ΔG_r^o as a function of temperature, dividing by -2.303 RT and equating to $\log f_{O_2}$ and, then, calculation of the pressure term which is added to the first term. If

$$P_{total} = P_{H_2} + P_{H_2O} = f_{H_2}/ \gamma_{H_2} + f_{H_2O}/ \gamma_{H_2O} \tag{11}$$

TABLE 5

References for data used in calculation of fugacities of oxygen, hydrogen and water for the IM buffer.

Data	Reference
$\Delta G^{o}_{f,M}$ (T)	Haas and Robie (1973)
V_M	Robie and Waldbaum (1968)
V_{Fe}	Robie and Waldbaum (1968)
γ_{H_2}	Shaw and Wones (1964)
γ_{H_2O}	Burnham et al. (1969)
K_w	Zen (1973)

and

$$K_w = \frac{f_{H_2O}}{f_{H_2} \; (f_{O_2})^{1/2}} \tag{12}$$

then

$$f_{H_2O} = \frac{(P_t) \; (K_w) \; (f_{O_2})^{1/2} \; \gamma_{H_2} \; \gamma_{H_2O}}{\left[K_w \; (f_{O_2})^{1/2} \; \gamma_{H_2}\right] + \gamma_{H_2O}} \tag{13}$$

and

$$f_{H_2} = \frac{P_t \; \gamma_{H_2} \; \gamma_{H_2O}}{\left[K_w \; (f_{O_2})^{1/2} \; \gamma_{H_2}\right] + \gamma_{H_2O}} \tag{14}$$

The P_{total} equation (11) of Eugster and Wones (1962) assumes ideal mixing of two non-ideal gases, which means that the fugacity coefficient of each gas in the mixture at a given temperature is that of the pure gas at the same temperature and total pressure (Zen, 1973). Appendix 1b lists the calculated values for fugacity of oxygen, hydrogen and water for the temperature and pressure range of interest in this study. Figure 3 illustrates the variation in gas composition as a function of temperature and total pressure. The gas phase is an aqueous fluid rich in hydrogen and depleted in oxygen.

Figure 3: Log f_{H_2}/f_{H_2O} vs temperature at P_{total} equal to 500 and 2000 bars for the IM buffer. Calculations are described in the text.

IRON-MAGNETITE BUFFER

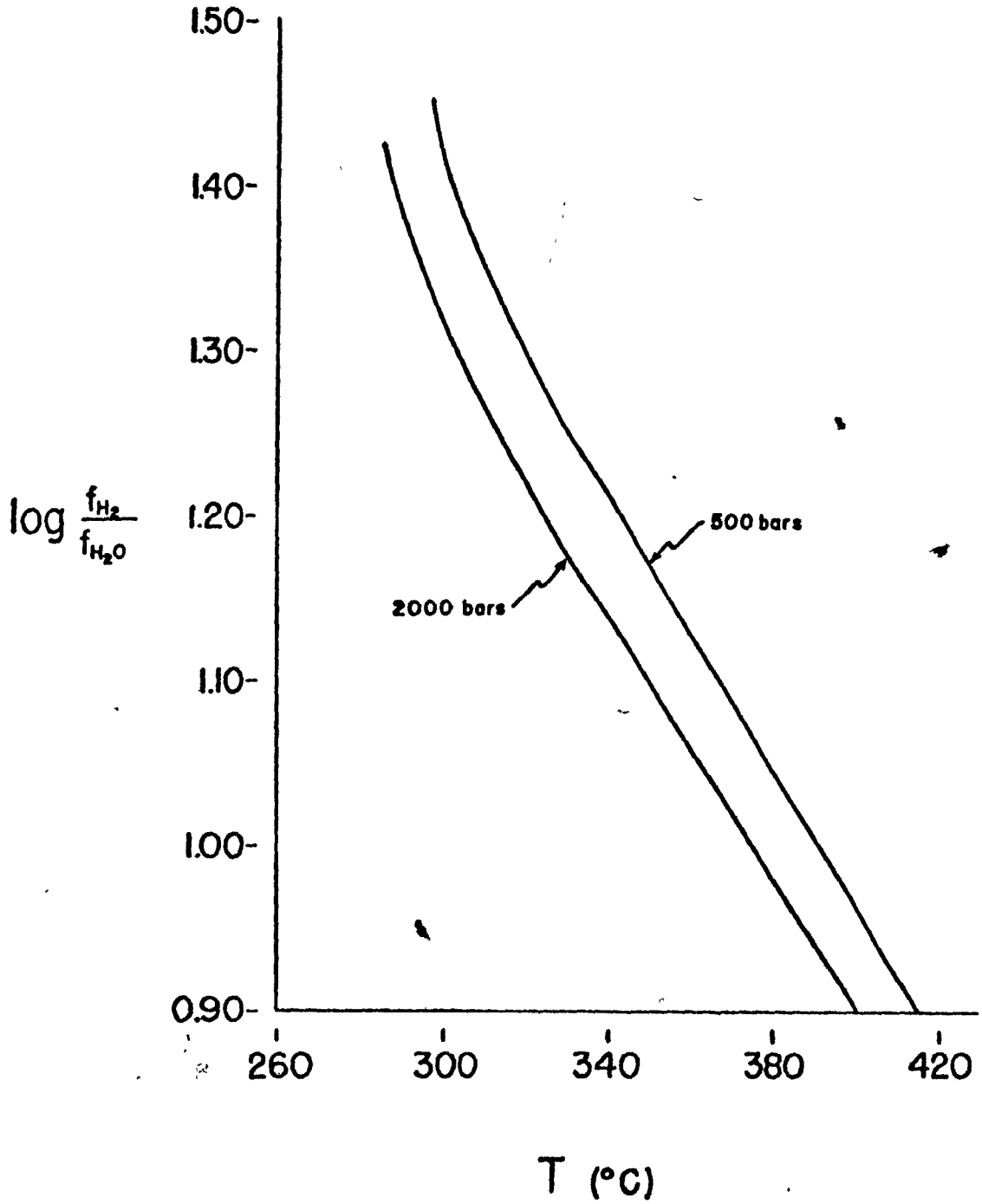

Hydrothermal Runs on the Reaction of Synthetic and Natural Olivines with an Aqueous Fluid

The starting materials (olivine and brucite) were characterized by optical and X-ray study. Unit cell parameters are presented in Table 6. There were small amounts of impurities in some of the synthetic materials. Magnetite was observed optically in olivine 2-17 (< 3%) due to partial oxidation of the charge. Fisher and Medaris (1969) reported trace amounts (< 1%) of impurities including magnetite in OP 194 and OP 54. Both natural olivines appear nearly single-phase from X-ray and optical examination. A trace of periclase was detected optically in brucite 2-67.

Details of the starting material, temperature, pressure, run duration and product phases for the hydrothermal runs are given in Appendix 2. In what follows, each type of experiment investigated will be described together with the results of the optical, X-ray and SEM analysis of the products. The term "hydration" run is used to define a type of reaction that chiefly involves the addition of water (Martin and Fyfe, 1970; Fyfe, 1973) and therefore, a reaction studied in one direction only.

Experiments Involving Pure Water

Johannes (1968) has demonstrated in $MgO-SiO_2-H_2O$ system that synthesis boundaries are obtained from reactions that are studied from one

TABLE 6

Cell parameters and calculated compositions of olivine and brucite starting materials used in the experimental work.

Olivine	a (A)	b (A)	c (A)	V (A^3)	d_{130} (A)	composition mole % Fo*
2-33	4.758(2)	10.242(5)	5.996(3)	292.22(22)	2.7729	88
2-17	4.757(1)	10.213(1)	5.984(1)	290.73(4)	2.7683	95
2-19	4.754(1)	10.205(2)	5.983(1)	291.82(29)	2.7660	100
+GSC Fo_{90}	4.758(1)	10.214(2)	5.989(1)	291.13(11)	2.7695	93
++OP194	4.770(1)	10.258(3)	6.009(2)	292.04(8)	2.7781	80
++OP54	4.813(1)	10.417(2)	6.067(1)	304.18(5)	2.8155	20
°M7863	4.764(1)	10.228(1)	5.994(1)	292.04(8)	2.7730	88
°°2-BU-66	4.759(1)	10.215(1)	5.988(1)	291.08(4)	2.7691	94
Brucite						mole % $Mg(OH)_2$
2-67	3.148(1)		4.775(2)	41.00(3)		100
3-19	3.146(1)		4.774(2)	40.93(3)		100

Parenthesized figures represent the estimated standard deviation (esd) calculated from Burnham's (1962) program in terms of least units cited for the value to their immediate left, thus 4.758(2) indicates an esd of 0.002

Table 6 cont'd

*composition calculated from d(130) with determinative curve of Fisher and Medaris (1969), maximum error is ± 2 mole % Fo

+synthetic olivine of composition 92.9 mole % Fo reported by Jambor and Smith (1964)

++synthetic olivines reported by Fisher and Medaris (1969), OP194 cell refinements were re-determined in this study

°natural olivine, Royal Ontario Museum M7863, Arizona, U.S.A.

°°natural olivine separate, Burro Mt., California, Loney et al. (1971, Table 4) reported 92.5 mole % Fo from a chemical analysis

direction only. Therefore, the hydration experiments will not be discussed in terms of definition of a P,T curve, but the mineralogy of the phase assemblage will be described as a basis for comparison with other experiments and observations on natural serpentinites. The products of the reaction were: lizardite, brucite, magnetite $\pm$ chrysotile.

Table 7 shows a comparison of different olivine starting materials at the same T,P with percent olivine remaining at end of run. There is a correlation of the rate of reaction with initial composition: Fo_{95} (2-17) was more resistant to alteration than the other more iron-rich olivines. These data suggest that grain size and perhaps iron content of olivine influence the rate of alteration (the synthetic olivines have a smaller grain size on the average than the natural olivines). Table 8 gives the unit cell dimensions for some of the olivines and their compositions. Only Run 3-47 showed appreciable change in iron content at the end of the run.

Both lizardite and chrysotile were produced in these experiments. Detection of the first appearance of lizardite was not difficult optically nor in the Guinier X-ray powder pattern. However, detection of chrysotile in a mixture of olivine + lizardite was difficult due to overlapping of diffraction lines and lack of positive optical identification due to fine grain size of serpentine. The SEM was extremely useful in solving this problem and allowed easy detection of chrysotile due to its distinctive fiber habit. For example, in Run 3-30, olivine and lizardite were detected in an X-ray pattern, brucite and magnetite optically and chrysotile by SEM (see Appendix 3).

TABLE 7

Comparison of different olivines for effect of run duration and initial composition on the rate of reaction.

Run	Olivine	T(°C)	P(kbar)	Run Duration hrs.	Composition mole % Fo	% Olivine Remaining
3-30	OP194	331	1.47	764	80	70
3-47	M7863	331	1.00	1127	88	40
3-2	2-17	329	1.00	1637	95	98
2-99	2-33	329	1.47	529	88	tr.

TABLE 8

Selected olivine cell parameters and calculated compositions from the hydration experiments with pure water.

Run	a (A)	b (A)	c (A)	V (A^3)	Composition mole % Fo	Δ, mole % Fo*
3-25	4.756(1)	10.217(2)	5.988(1)	291.01(9)	93	-2
3-15	4.756(1)	10.217(2)	5.986(1)	290.98(6)	94	-1
3-32	4.760(1)	10.218(2)	5.990(1)	291.32(6)	95	+2
3-30	4.764(3)	10.240(9)	6.000(2)	292.72(21)	81	+1
3-47	4.756(1)	10.220(3)	5.988(2)	291.10(11)	96	+8
3-77	4.758(1)	10.210(2)	5.989(2)	290.94(8)	93	-1

Refinement and compositions are obtained as in Table 6

*difference between the starting material and product, minus (-) means a decrease in Fo content and plus (+) indicates an increase in Fo content

Table 9 presents the X-ray results for selected lizardites and chrysotiles. Lizardite was refined on the basis of an orthorhombic cell. Whittaker and Zussman (1956) established that c = 14.6 A for clinochrysotile, though Yada (1967, 1971) has presented evidence from lattice fringe edge dislocations that the repeat unit in the c direction also may be 7.3 A. Zvyagin (1967) has shown that both one-layer (7.3 A) and two-layer (14.3 A) monoclinic structures exist for clinochrysotile, but the distinction between the one- or two-layer structure can only be made from single-crystal photographs of higher-order layer lines or from electron diffraction patterns (Wicks, 1969). When chrysotile makes up greater than 50% of the serpentine, the Guinier powder pattern allowed refinement of both the chrysotile and lizardite cell dimensions. The cell edges and volumes are comparable to natural lizardites and chrysotiles as shown in Table 9. The variation in these parameters for lizardite are:

		range of values			
		minimum		maximum	difference
a (A)	=	5.300	-	5.363	0.063
b (A)	=	9.179	-	9.211	0.032
c (A)	=	7.290	-	7.322	0.032
V (A^3)	=	355.85	-	361.73	5.88

There does not appear to be any systematic variation in cell edge or volume with temperature and pressure of formation or composition of initial starting olivine.

TABLE 9

Cell edge and volumes refined for lizardite and chrysotile produced from hydration reaction with water.

Run	a (A)	b (A)	c (A)	V (A^3)	β	d_{002} (A)+
3-25(L)	5.318(3)*	9.185(4)	7.290(6)	356.11(37)		3.646
3-26(L)	5.309(13)	9.210(4)	7.295(11)	356.72(68)		3.647
3-26(C)	5.288(8)	9.212(8)	14.650(74)	712.72(31)	93° 11'(11')	
3-61(L)	5.326(12)	9.196(5)	7.291(10)	357.14(59)		3.646
3-15(L)	5.316(1)	9.183(1)	7.313(1)	357.05(5)		
2-99(L)	5.363(18)	9.211(3)	7.322(8)	361.73(122)		3.661
3-48(L)	5.300(12)	9.208(4)	7.307(11)	356.63(60)		3.655
3-48(C)	5.277(27)	9.214(7)	14.618(75)	703.80(65)	91° 57'(33')	
3-32(L)	5.319(4)	9.204(4)	7.293(9)	357.10(50)		3.649
3-4 (L)	5.311(9)	9.179(4)	7.298(8)	355.85(46)		3.650
3-1 (L)	5.301(21)	9.197(6)	7.311(18)	356.48(100)		3.655
3-22(L)	5.323(23)	9.197(7)	7.295(20)	357.20(111)		3.643
3-22(C)	5.269(16)	9.210(7)	14.650(74)	712.72(31)	93 11'(11')	

Table 9 cont'd

Run	a (A)	b (A)	c (A)	V (A^3)	β	d_{002} (A)+
3-47(L)	5.317	9.198(6)	7.280(11)	356.11(59)		
3-77(L)	5.302(10)	9.199(3)	7.310(3)	356.63(49)		3.656
**241M(L)	5.312(4)	9.204(17)	7.237(15)	353.81(112)		3.619
**212M(C)	5.306(6)	9.176(12)	14.650(8)	712.13(177)	93° 20'	3.656
°M19804 (L)	5.319(2)	9.223(3)	7.313(6)	358.84(29)		3.661
°°M19142 (L)	5.317(1)	9.208(2)	7.305(4)	357.69(21)		3.653
°°°M8507 (C)	5.320(3)	9.208(4)	14.631(17)	715.72(8)	93° 18'(3')	3.652

+d (002), observed, basal spacing of serpentine minerals, Chernosky (1973) showed maximum variation in Al content to be reflected in d (002) of serpentine, Forbes (1969) illustrated change in iron content of talc with its basal spacing

*figures in parenthesis represent the estimated standard deviation (esd) calculated from the Appleman et al. (1963) program, 5.318(3) indicates an esd of 0.003.

**pure synthetic lizardite and chrysotile (Chernosky, 1973)

°Royal Ontario Museum standard lizardite, Madoc Twp., Ontario

°°Royal Ontario Museum standard lizardite, Dypingdal, Snarum, Norway

°°°Royal Ontario Museum standard clinochrysotile, Montreal Chrome Pit, East Broughton, Quebec

Table 10 summarizes the results of the SEM work, presented in detail in Appendix 3. The habit of the phases as distinguished by SEM is:

olivine - anhedral, massive grains on order of 20-100 μm in width (Plates 1A, 1B)

lizardite - massive, platy, laths and euhedral crystals which exhibit hexagonal symmetry (Plates 1C, 1D, 3A, 3B, 3C, 3D)

chrysotile - fibers (i.e. tubes), and laths, distinguished from lizardite laths by width; chrysotile laths are much narrower, on the order of less than a few μm (Plates 4A, 4B, 4C, 4D)

brucite - hexagonal plates, 4-100 μm (Plates 2A, 2C, 2D)

magnetite - cubes, 1-2 μm.

Magnetite was rarely observed in SEM studies. The most common serpentine habits are lizardite plates and chrysotile fibers. Lizardite laths appear to form at temperatures greater than 315°C, in the pressure range 0.5-1.5 kbar, whereas euhedral, hexagonal forms of lizardite form at low temperatures (< 305°C) or long run duration at both high and low temperatures. Chrysotile laths form at low temperatures (< 310°C) and relatively high pressure with shorter run durations. Lizardite is the first serpentine mineral to appear from the reaction of olivine with water. Chrysotile forms as run duration is increased. Evidence will be presented in a later section to show that lizardite and chrysotile appear to co-exist stably, i.e., chrysotile is not replacing lizardite.

Brucite occurs in all run products in which alteration had proceeded to such an extent that less than 60% of the olivine remained. Run 2-99 is

TABLE 10

Summary of SEM results on the distribution of serpentine habit for lizardite and chrysotile produced from hydration of olivine with pure water.

Run	T(°C)	P(kbar)	Run Duration hrs.	Massive, Platy L	Lath L	Euhedral L	Fibers C	Lath C	Relative Amount*
+3-12	321	1.99	1150	x		x	x		L > C
3-77	307	1.93	999	x			x	x	L > C
3-61	302	1.93	504	x			x	x	L > C
2-94	339	1.47	575	x	x				L
+3-30	331	1.47	765	x			x		L > C
++2-102	317	1.47	504	x	x		x		L >> C
3-48	309	1.48	1773	x			x		L ≅ C
3-4	317	1.01	1492	x	x		x		L > C
3-1	302	1.01	1660	x		x	x		L > C
+3-23	323	0.54	1606	x	x		x		L > C
3-22	304	0.54	1605	x		x	x	x	L ≅ C

*estimated visually from SEM samples and correlated with X-ray results

+no cell refinement possible for lizardite or chrysotile

++least squares cell refinement not attempted

the only one in which brucite was not observed either by X-ray or optical examination though it may have been present in trace amounts which escaped optical detection. Table 11 presents the cell edge refinements and the iron content for those brucites that had sufficient X-ray lines for a least squares refinement. Runs 3-12 and 3-61 at 2.0 kbar and Runs 3-4 and 3-1 at 1.0 kbar show the same trend: more iron enrichment in brucite formed at lower temperature. The variation in the iron content of brucite as a function of temperature will be discussed later. Runs 3-12 and 3-25, conducted at the same T,P with the same olivine starting material, may indicate an increase in the iron content of brucite with run duration.

In most cases magnetite was identified optically in the run products (see Appendix 4). A correlation of grain size with color of the powder was made: a light tan powder indicated that the magnetite was finely disseminated ("dusty") throughout the serpentine (grain size, 1-2 μm). In the grey powders, the magnetite was larger in grain size (4 to 10 μm) and in some cases had begun to aggregate. When the grain size and the amount of the magnetite became large enough it could be identified in the X-ray pattern (Plate 7D). Runs 3-48 and 3-32 at the same T and P allow comparison of magnetite production with run duration; the longer the run the greater the amount of magnetite. The natural olivines appear to produce approximately the same amount and grain size of magnetite as the synthetic olivines within the compositions and run durations investigated.

TABLE 11

Cell edges refined for selected brucites produced during reaction of olivine with pure water.

Run	a (A)	c (A)	mole % $Mg(OH)_2$*
3-25		+4.767(23)	98(2)
3-12		+4.759(19)	93(7)
3-61	3.176(1)	4.734(1)	82(1)
3-48	3.159(3)	4.756(3)	92(1)
3-1	3.156(1)	4.753(3)	90(1)
3-4	3.152(1)	4.762(3)	95(2)
3-22	3.156(1)	4.760(3)	94(2)

Refinement as specified in Table 6

*determined from the d(001) reflection (c cell edge) after Mumpton and Thompson (1966), error calculated from esd in c cell edge refinement; Page (1966) has shown good agreement between iron content of brucite from X-ray cell edge determination and electron-microprobe analysis of brucite

+only c refined due to small number of brucite reflections

Table 12 presents a few magnetic measurements. More magnetite was produced in Run 2-98 than in 2-100. Those runs differ in temperature (2-98, lower) and starting material, but are otherwise identical. Run 2-98 had a synthetic olivine as starting material, 2-100 a natural olivine of which approximately 70% remained at the end of the run. The incompleteness of the reaction for Run 2-100 probably accounts for the lower magnetite production in comparison to Run 2-98. These measurements illustrate the difficulty in an optical assessment of the amount of magnetite produced when it is present in range of 2-10% in the sample.

Experiments Involving Fluids of Variable Composition

The fluids other than water used to study the alteration of olivine were chosen to conform with the natural serpentinizing fluids as studied by Barnes et al. (1969, 1972): 0.1-0.4 M NaCl, 0.01-0.03 M NaOH, 0.05-0.14 M sodium metasilicate ($Na_2SiO_3.9H_2O$) and an alkaline chloride solution (a mixture of NaOH and NaCl). The rate of reaction as a function of fluid composition is:

Na metasilicate > NaOH ≅ alkaline chloride > H_2O > NaCl.

With sodium metasilicate solutions, the four-phase assemblage lizardite, chrysotile, brucite, and magnetite was formed only at the lowest temperature (306°C, 0.99 kbar), whereas lizardite, magnetite, minor olivine ± chrysotile were observed up to 352°C, 1.5 kbar, but without brucite (refer to Appendix 2). The assemblage lizardite, chrysotile, brucite and magnetite was observed for the NaOH and alkaline chloride solutions. Only traces

TABLE 12

Magnetic measurements* of starting material and run products from hydration of a synthetic and natural olivine.

Material	Js, emu/g*	Eq. M, wt. %	Net Increase M, wt. %**
2-98	4.5	4.8	4.8+
M7863 (starting material for Run 2-100)	0.03	0.04	
2-100	0.68	0.70	0.66

*courtesy of R.B. Hargraves, Princeton University

**net increase in amount of magnetite: product magnetite minus the magnetite in starting material

+a magnetic measurement was not made of the starting material; however, magnetite was not observed in starting material with optical and X-ray examination

of serpentine + brucite were observed in reaction of olivine with NaCl solutions.

Table 13 presents the cell edge refinements for some olivines and brucites with their corresponding iron contents. The olivines show no change in composition in three samples and possible iron enrichment in the other five. The brucites are pure $Mg(OH)_2$ in three samples but contains 13 mole % $Fe(OH)_2$ in Run 3-46.

Lizardite is the dominant serpentine mineral in these experiments, though chrysotile is observed in the lower temperature runs with all the fluids except those containing NaCl. However, these runs averaged about 500 hours in duration whereas some of the experiments with pure water were extended for twice that time. The lizardite shows a larger variation in unit cell parameters than those formed in the experiments with pure water, though the d (002) falls consistently between the values of 3.652 and 3.661 ~~(see Table 14)~~:

		range of values			
		minimum		maximum	difference
a (A)	=	5.278	-	5.380	0.102
b (A)	=	9.143	-	9.193	0.050
c (A)	=	7.292	-	7.329	0.037
V (A^3)	=	355.08	-	361.43	5.35

Run 3-64 allowed refinement of the X-ray pattern for chrysotile but not for lizardite; the abundance of chrysotile in the sample is substantiated from

TABLE 13

Selected refined olivine and brucite cell parameters and compositions from the hydration experiments with fluids of varying compositions.

Run	a (A)	b (A)	c (A)	V (A^3)	Composition mole % Fo	Δ, mole % Fo*
Olivine						
3-62	4.757(1)	10.218(2)	5.987(1)	291.01(9)	95	0
3-49	4.758(1)	10.207(3)	5.986(1)	290.70(7)	90	-5
3-46	4.758(2)	10.213(3)	5.987(2)	290.44(11)	96	+1
3-63	4.758(1)	10.214(1)	5.987(1)	290.97(5)	90	-5
3-96	4.759(1)	10.221(1)	5.990(1)	291.40(4)	91	-3
3-95	4.759(1)	10.230(3)	5.986(1)	291.41(11)	95	+1
3-92	4.772(2)	10.223(3)	5.986(1)	292.04(11)	88	-6
3-94	4.762(1)	10.221(2)	5.993(1)	291.70(8)	90	-4
Brucite					mole % $Mg(OH)_2$**	
3-49	3.147(4)		4.767(2)		98(2)	
3-46	3.158(3)		4.747(6)		87(3)	
3-54	3.152(7)		4.753(18)		90(10)	
3-95			+4.771(2)		100	
3-92			+4.771(7)		100	

Table 13 cont'd

Refinement and olivine composition as specified in Table 6.

*difference between the starting material and the product

**determined from the d(001) reflection after Mumpton and Thompson (1966), error calculated from esd in d(001)

+c refined only

TABLE 14

Selected cell parameters for lizardite and chrysotile produced from the reaction of olivine with fluids of varying composition.

Run	a (A)	b (A)	c (A)	V (A^3)	β	d(002) (A)
3-51 (L)	5.380(100)	9.180(44)	7.316(25)	361.43(569)		3.652
3-42 (L)	5.320(5)	9.143(25)	7.320(14)	356.14(125)		3.656
3-42 (C)	5.307(11)	9.213(11)	14.644(100)	715.13(46)	92° 53'(16')	
3-49 (L)	5.315(6)	9.173(9)	7.306(13)	356.30(74)		3.655
3-46 (L)	5.311(8)	9.191(8)	7.292(16)	355.97(87)		3.652
3-54 (L)	5.309(11)	9.194(7)	7.317(20)	357.17(125)		3.655
3-64 (C)	5.305(6)	9.201(6)	14.622(54)	712.97(24)	92° 54'(8')	
3-96 (L)	5.278(13)	9.179(6)	7.329(11)	355.08(68)		3.661
3-95 (L)	5.298(30)	9.193(9)	7.317(25)	356.42(147)		3.661
3-93 (L)	5.300(9)	9.188(4)	7.307(8)	355.91(48)		3.650

Refinement as specified in Table 9

TABLE 15

SEM results for a few serpentine samples formed from the reaction of olivine with fluids other than pure water.

Run	T(°C)	P(kbar)	Run Duration hrs	Fluid	Massive Platy L	Euhedral L	Fibers C	Laths C	Relative amount*
3-42	306	0.99	573	0.06M NaSi+	x	x	x		L ≡ C
3-54	302	1.00	550	0.01M NaOH	x		x	x	L > C
3-64	302	1.00	524	0.33M NaCl 0.02M NaOH	x		x		C > L

*estimated visually from SEM samples

+sodium metasilicate, $Na_2SiO_3 \cdot 9H_2O$

In Run 3-28 gold was detected in the X-ray pattern of the product material. As the solutions were not analyzed for gold, there may have been some dissolution of Au with the NaCl and alkaline chloride fluids as well. There was, however, no discoloration of the fluid nor recrystallization of the Au as reported by Anderson and Burnham (1967). It is not likely that at the lower temperatures and pressures of the runs with the less concentrated fluids used in this study, the solubility of gold was as great as shown by Anderson and Burnham (1967). No evidence for dissolution of silver from the inner capsule container was observed in any of the runs.

Reversed Experiments on the Reaction Boundary for Olivine (Fo_{93}) + H_2O

In order to establish criteria of equilibrium, it was necessary to study the reaction of an iron-bearing olivine with water in both directions, i.e., to conduct bracketing experiments. The reversal was done by reacting GSC olivine (Fo_{93}) with water to form the products of reaction (Run 3-48). The products of Run 3-48 were then mixed with an equal weight of the GSC olivine, and the appearance or disappearance of olivine determined in the mixture.

The microdensitometer intensity measurements of the X-ray films of the run products and the SEM results are presented in Table 16. The X-ray intensity measurements for the reversed experiments were not decisive for Runs 3-98, 3-85, 3-99 and 3-100. These are interpreted to be close to the

TABLE 16

The microdensitometer intensity measurements and SEM° results for the bracketing experiments. These results are also summarized in Figure 4.

0.5 kbar

	3-69	3-68	3-97	3-98
O	- (-)	-	- (-)	* (+)
L	* (*)	*	* (+)	(-)
C	* (+)	*	+ (+)	+ (-)
B	* (+)	*	+ (+)	+ (-)
T (°C)	311	322	336	352
duration (hrs.)	895	863	814	814

1.0 kbar

	3-70	3-71	3-84	3-85	3-87	3-86
O	- (-)	- (-)	- (-)	* (+)	+ (+)	- (+)
L	* (+)	+ (+)	*	* (-)	* (-)	- (-)
C	* (+)?	* (*)	+ (+)	* (-)	* (-)	- (-)
B	* (+)	+ (+)	* (*)	* (-)	* (-)	- (-)
T (°C)	322	330	341	349	361	371
duration (hrs.)	837	792	568	567	568	569

1.5 kbar

	3-72	3-74
O	- (-)	-
L	* (+)	*
C	* (*)	+
B	* (*)	+
T (°C)	332	341
duration (hrs.)	791	481

2.0 kbar

	3-75	3-76	3-99	3-100	3-101
O	- (-)	- (-)	* (-)	* (+)	+ (+)
L	* (*)	* (+)	* (-)	* (-)	- (-)
C	* (*)	+ (+)	+ (+)	* (-)	- (-)
B	* (*)	* (+)	+ (+)	* (-)	- (-)
T (°C)	335	344	361	376	392
duration (hrs.)	480	479	793	794	695

- disappearance of a phase

+ growth of a phase

* no change

°SEM results are in parenthesis

equilibrium curve. The SEM was used to further delineate the direction of the reaction and Table 17 summarizes the criteria developed to distinguish the mineral stability fields developed from the SEM work. Plates 2-6 illustrate these criteria. Table 18 summarizes the serpentine habit for these runs. Figure 4 presents the T,P reaction boundary defined by the X-ray and SEM work for an olivine of composition Fo_{93}. This boundary is shifted to the left i.e. to lower temperatures by 15°C compared to Johannes' (1968) curve for pure forsterite + H_2O.

Table 19 presents the cell edge and volume data for the lizardites in the equilibrium runs within the stability field for serpentine. These lizardites had a smaller variation in cell edge compared to those discussed in previous two sections, consistent with a close approach to equilibrium:

		range of values minimum	maximum	difference
a (A)	=	5.295 -	5.322	0.027
b (A)	=	9.174 -	9.201	0.027
c (A)	=	7.289 -	7.314	0.025
V (A^3)	=	355.18 -	356.97	1.79

Chrysotile refinements attempted for Runs 3-99, 3-84 and 3-97 were not successful.

The cell edge refinements and iron content of the brucites are presented in Table 20. These brucites contain more iron at lower temperatures compared to the starting material than was observed with the pure water

TABLE 17

Criteria for distinguishing the mineral stability fields from habit of the phases as observed by SEM.

Serpentine-Brucite-Magnetite

1. lengthening of chrysotile fibers (Plates 4A, 4C)
2. formation of chrysotile fiber bundles (Plate 4D)
3. increase in average size of brucite plates (Plate 2D)
4. formation of euhedral lizardite crystals (Plates 3A, 3B, 3C)
5. absence of olivine

Olivine

1. decrease in size and amount of other phases (serpentine + brucite) with respect to olivine, e.g., shortening of chrysotile fibers (Plates 5C, 5D)
2. solution and etching of lizardite (Plate 6A)
3. increase in grain size of olivine
4. crystallization of olivine to form euhedral crystals (Plates 6B, 6C, 6D)

TABLE 18

Summary of SEM results on the distribution of serpentine habit within the serpentine stability field defined by the bracketing experiments.

Run	T(°C)	P(kbar)	Run Duration hrs	Massive Platy L	Lath L	Euhedral L	Fibers C	Fiber Bundles	Relative Amount*
3-99	361	2.01	793	x	x		x	+	L ≅ C
3-76	344	1.93	479			x	x	x	C > L
3-75	335	1.93	480	x			x		L > C
3-72	332	1.48	791	x	x		x		L > C
3-84	341	1.01	568			x		x	L ≅ C
3-71	330	1.00	792	x	x	x	x		L > C
3-70	322	1.00	837	x		x	x		L ≅ C
3-97	336	0.54	814		+	x	x	x	L ≅ C
3-69	311	0.56	895	x			x	+	L ≅ C

*estimated visually from SEM samples

+present in minor amounts

Figure 4: The reaction curve for $10(Mg_{1.86}Fe_{0.14})SiO_4 + 14.2H_2O = 5Mg_3Si_2O_5(OH)_4 + 3.8(Mg_{0.95}Fe_{0.05})(OH)_2 + 0.4Fe_3O_4 + 0.4H_2$. The open triangles indicate that olivine disappeared and the other phases grew, the open circles indicate that olivine grew and the other phases disappeared. The filled circles and triangles indicate the same direction of reaction as the open triangle or circles, but imply that the direction of the reaction was determined from SEM results rather than X-ray intensity measurements (see Table 16). The dashed curve was determined by Johannes (1968) for the reaction: $2Mg_2SiO_4 + 3H_2O = Mg_3Si_2O_5(OH)_4 + Mg(OH)_2$. The error bars estimated by the authors are placed on the curves.

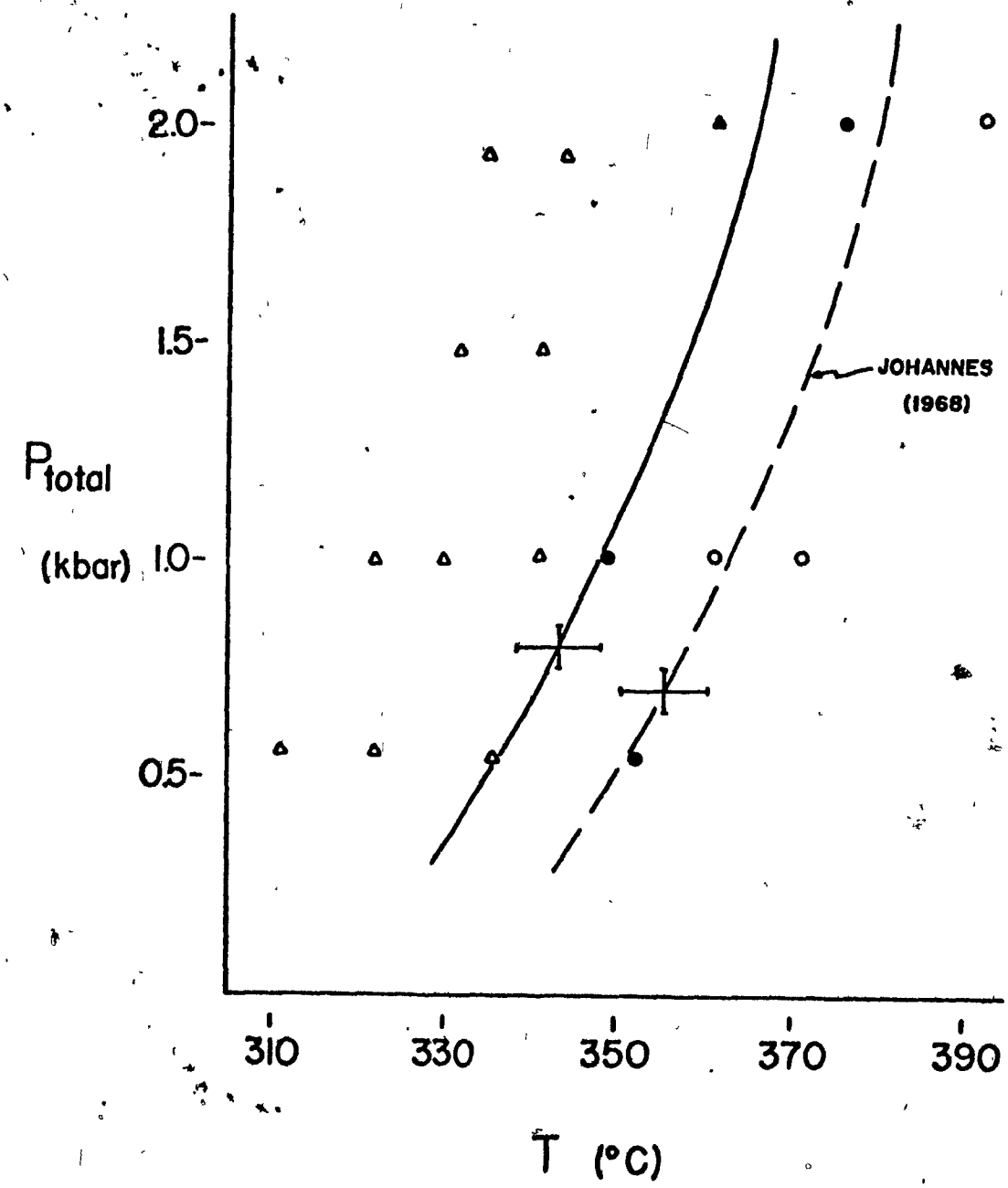
2.0-
1.5-
1.0-
0.5-
P_{total}
(kbar)
JOHANNES
(1968)
310
330
350
370
390
T (°C)

TABLE 19

Cell parameters for lizardite within stability field of serpentine defined by the bracketing experiments.

Run	a (A)	b (A)	c (A)	V (A^3)	d(002) (A)
3-99	5.295(1)	9.174(2)	7.310(1)	355.18(10)	3.655
3-76	5.322(1)	9.196(2)	7.292(3)	356.89(19)	3.649
3-75	5.306(7)	9.201(3)	7.301(6)	356.59(36)	3.652
3-74	5.315(9)	9.190(9)	7.290(19)	356.17(98)	3.656
3-72	5.299(2)	9.187(2)	7.301(2)	355.47(14)	3.650
3-84	5.318(6)	9.194(6)	7.289(12)	356.43(64)	3.646
3-71	5.302(18)	9.199(5)	7.300(15)	356.09(89)	3.649
3-78	5.317(7)	9.187(8)	7.290(15)	356.12(82)	3.651
3-70	5.318(3)	9.190(5)	7.300(7)	356.78(41)	3.653
3-97	5.315(5)	9.199(5)	7.300(11)	356.96(59)	3.655
3-68	5.301(3)	9.176(1)	7.314(3)	355.80(17)	3.656
3-69	5.317(8)	9.195(8)	7.300(16)	356.97(89)	3.656

Refinement as specified in Table 9

TABLE 20

Cell edge refinements and compositions of brucite in reversed runs in stability field of serpentine-brucite-magnetite.

Run	a (A)	c (A)	mole % $Mg(OH)_2$	Δ^*
3-99		+4.760(1)	94(1)	+2
3-76	3.158(1)	4.751(1)	89(1)	-3
3-74	3.149(4)	4.754(16)	91(9)	-1
3-72	3.152(1)	4.752(1)	89(1)	-3
3-84	3.150(5)	4.763(21)	96(4)	+4
3-71		+4.766(19)	98(2)	+6
3-78	3.158(4)	4.744(17)	85(9)	-7
3-70	3.160(1)	4.748(2)	87(1)	-5
3-97		+4.758(3)	93(2)	+1
3-68		+4.772(19)	100	+8

Refinement and composition as specified in Table 11

*change from starting composition of 92 mole % $Mg(OH)_2$

+c refined only

experiments (Table 11), except for the 0.5 kbar runs which are extremely sluggish. Runs 3-99 and 3-97 show no change, but they are very close to the equilibrium curve.

Table 21 presents the cell edge and volume data for the olivines. Most olivines did not change in composition from before to after the run. The definite exceptions are Runs 3-76, 3-85 and 3-84; the 2 kbar runs showing a gain in iron content and the one kbar experiments showing a loss. These runs exhibiting definite change fall into the narrow temperature range of 340-350°C.

Magnetite occurs in the bracketing experiments as very small grains disseminated in the serpentine aggregates as has been described in petrographic investigations of serpentinites as "dusty" magnetite (Thayer, 1966). The dusty magnetite appears to outline grains of brucite (Plate 7A) and forms irregular patches in the serpentine (Plate 7C). Table 22 summarizes the amount of magnetite observed, as obtained from optical examination of the charge and from the magnetic measurements. At 0.5 kbar, all runs lasted 800-900 hours so that the only variable was temperature. Run 3-97 was directly on the equilibrium curve, which may be the explanation for the decrease in the amount of magnetite as compared to 3-68. At 1.0 kbar, Run 3-84, which had the largest amount of magnetite, had also a shorter run duration than the other two runs within its stability field, but was at a higher temperature. Run 3-72 at 1.5 kbar had twice the run time of Run 3-74, but approximately the same amount of magnetite as 3-74, indicating

TABLE 21

Refined cell parameters and compositions of olivines present at completion of the bracketing experiments.

Run	a (A)	b (A)	c (A)	V (A^3)	Composition mole % Fo	Δ, mole % Fo*
3-101	4.759(1)	10.222(1)	5.988(1)	291.27(8)	94	+1
3-100	4.758(1)	10.218(2)	5.987(1)	291.12(6)	94	+1
3-99	4.762(1)	10.221(2)	5.988(1)	291.44(7)	93	0
3-76	4.760(1)	10.210(3)	5.987(3)	291.04(11)	89	-4
3-74	4.760(1)	10.217(2)	5.985(1)	291.07(9)	95	+2
3-72	4.761(1)	10.218(2)	5.981(1)	290.97(7)	93	0
3-86	4.761(1)	10.218(2)	5.990(1)	291.40(6)	93	0
3-87	4.759(1)	10.214(2)	5.989(1)	291.12(6)	93	0
3-85	4.759(1)	10.216(1)	5.987(1)	291.31(5)	97	+4
3-84	4.759(1)	10.215(2)	5.990(1)	291.16(7)	98	+5
3-71	4.759(1)	10.216(2)	5.987(1)	291.06(8)	95	+2
3-70	4.760(1)	10.215(3)	5.985(2)	291.04(10)	95	+2
3-98	4.759(1)	10.219(1)	5.987(1)	291.18(6)	95	+2
3-97	4.760(1)	10.212(1)	5.989(1)	291.15(5)	93	0

Table 21 cont'd

Refinement and composition as specified in Table 6

*difference between the starting material and product

TABLE 22

Amounts of magnetite observed in bracketing experiments as estimated optically and determined directly from magnetic measurements.

Material	Js, emu/g*	eq. M, wt. %	Net increase M, wt. %	Relative Amount M**
equil mix	0.23	0.25		
3-71	3.3	3.5	3.25	3-71 > 3-76
3-84	+8.85	9.5(5)	9.25	
3-76	+0.64	0.69(1)	0.44	
				3-71 ≅ 3-70
				3-72 ≅ 3-74
				3-75 > 3-76
				3-99 > 3-76
				3-68 > 3-97
				3-68 > 3-69

*courtesy of R.B. Hargraves, Princeton University

**amount of magnetite estimated from optical examination of run products (see Appendix 4)

+average of two measurements, esd calculated from error in measurement

that the rate of magnetite production in 3-74 was greater than in 3-72. Both Run 3-75 and 3-76 at 2.0 kbar were relatively short runs compared to Run 3-99; it is difficult to separate time and temperature effects. From the data in Table 22, the maximum relative amount of magnetite at each pressure and temperature is:

Run	T(^{o}C)	P(kbar)	Run Duration hrs
3-68	322	0.56	868
3-84	341	1.01	568
3-99	361	2.01	793

This evaluation suggests that within the serpentine-brucite-magnetite stability field, more magnetite was produced at the highest temperature for a given pressure.

Dehydration Reactions

The dehydration experiments were conducted with a natural olivine (Fo_{94}) to demonstrate the similarity in products between the synthetic and natural olivines and to try to nucleate olivine in its stability field from a mix which was predominately serpentine, brucite and magnetite with traces of olivine. Runs 3-106 and 3-103 were run in the stability field of olivine + water, the other experiments were in the stability field of the breakdown products (see Figure 4 and Appendix 2).

Table 23 presents the X-ray data for olivine, serpentine and brucite. Within their stability field the olivines did not show any

TABLE 23

Refined cell parameters and compositions for olivine, brucite and serpentine formed in dehydration reactions.

Run	a (A)	b (A)	c (A)	V (A^3)	Composition mole % Fo	Δ mole % Fo*
Olivine						
3-106	4.757(3)	10.233(6)	5.993(6)	291.71(18)	93	0
3-105	4.763(1)	10.221(2)	5.988(1)	291.60(7)	88	-5
3-103	4.757(2)	10.225(2)	5.988(1)	291.21(10)	91	-2
3-104	4.760(3)	10.223(4)	5.991(2)	291.54(19)	84	-9
Brucite					mole % $Mg(OH)_2$	
3-105			+4.759(4)		93(2)	
3-103			+4.762(11)		95(5)	
3-104			+4.760(4)		94(2)	
Serpentine					β	d(002) (A)
3-106 (L)	5.320(3)	9.196(5)	7.301(7)	357.24(40)		3.653
3-105 (L)	5.311(8)	9.197(3)	7.306(7)	356.91(42)		3.653

Table 23 cont'd

Run	a (A)	b (A)	c (A)	V (A^3)	β	d(002) (A)
3-105 (C)	5.377(14)	9.213(7)	14.677(65)	719.97(363)	94° 5'(20')	
3-103 (L)	5.322(5)	9.205(5)	7.288(13)	357.09(65)		3.649
3-102 (L)	5.309(12)	9.209(3)	7.301(10)	357.05(58)		3.649
3-104 (L)	5.316(3)	9.187(4)	7.300(6)	356.56(35)		3.655

Refinement and composition as specified in Tables 6, 9 and 11

*difference between starting material and product

+only c refined

change in iron content, whereas the olivines 3-105 and 3-104 outside their stability field (i.e., at lower temperatures) increased in iron content compared to the starting olivine. Olivine in Run 3-104 was considerably enriched in iron (from Fo_{93} to Fo_{84}). Brucite had approximately the same amount of iron for all runs. Unfortunately, it was not possible to determine the iron content of brucite in Run 3-77, therefore a comparison of the brucite before and after the experiment could not be made.

Table 24 summarizes the SEM results for the serpentine minerals in these experiments. Run 3-105 showed significant development of chrysotile that allowed refinement of X-ray pattern for both lizardite and chrysotile, though chrysotile was also strongly developed in Run 3-103. Lizardite occurred as both massive plates and as laths in the 2 kbar runs. The X-ray results for lizardite show even less variation in cell edge and volume than the bracketing experiments (see Table 23):

		range of values minimum		maximum	difference
a (A)	=	5.309	-	5.322	0.013
b (A)	=	9.187	-	9.209	0.022
c (A)	=	7.288	-	7.306	0.018
V (A^3)	=	356.56	-	357.24	0.68

The samples contained a large amount of magnetite produced as finely disseminated grains to very large aggregates greater than 50 μm in size (Run 3-105, Plates 8A, 8B, 8C). The relative amounts of magnetite observed

TABLE 24

SEM results on serpentine habit for the dehydration experiments.

Run	T(°C)	P(kbar)	Run Duration hrs	Massive Platy L	Lath L	Fibers C	Fiber Bundles	Relative Amount
3-106	370	2.01	1014	x	x	x		C ≅ L
3-105	355	2.01	1014	x	x	x	+	C ≅ L
3-103	355	1.01	1035	x		x	x	C ≅ L

+present in minor amounts

from optical examination of the products were Run 3-105 > 3-102 > 3-104. The results for dehydration experiments are similar to magnetite productions in the equilibrium runs, i.e., greater magnetite production at higher temperatures.

Runs 3-106 and 3-103 were conducted in the stability field of olivine + water. The SEM results for Run 3-106 did not show nucleation of olivine, but the run products did exhibit some of the features that showed a decrease in the serpentine-brucite phases discussed earlier for the bracketing experiments: (1) shortening of chrysotile fibers; (2) rounding of the hexagonal brucite platelets; and (3) solution of lizardite grains. These features were not as well developed in Run 3-103, though some etching of brucite and lizardite platelets was observed. An SEM study of Run 3-105, conducted in the stability field of serpentine-brucite-magnetite, showed well crystallized lizardite, chrysotile and brucite.

Reactions Involving Brucite

Attempts to synthesize an iron-bearing brucite with and without the IM buffer from starting materials MgO, native iron and water were unsuccessful. Both iron filings and iron sponge were used. This failure can be attributed to the ease of nucleation of magnetite under the conditions of the experiment. A gel technique would probably be successful in overcoming nucleation barriers and would also insure homogeneity in the product.

Hostetler (1963) and Wicks (1969) have postulated the formation of serpentine from brucite, which could be expressed by the following reaction:

$$3Mg(OH)_2 + 2H_4SiO_4 = Mg_3Si_2O_5(OH)_4 + 5H_2O \qquad (15)$$

Reaction (15) was investigated in Runs 3-16, 3-17 and 3-28 with excess dissolved silica. The reaction yielded lizardite, chrysotile, $\pm$ brucite $\pm$ quartz. Table 25 presents the X-ray and SEM results for the serpentine minerals produced. X-ray least squares refinement attempted for Run 3-17 did not give a solution for either lizardite or chrysotile. The habits determined from the SEM were typical: lizardite plates and a mat of chrysotile fibers.

Fluid Analysis

pH Measurements

Table 26 presents the quench pH[a] measurements of fluid remaining at the end of the experiment with the data relevant to each of the runs. The measured fluids were very alkaline and the pH was relatively constant with a total variation of only 0.6 pH units regardless of temperature, pressure, product phases or run duration.

---

[a] The quench pH is the pH of the fluid at room temperature and pressure measured as fast as possible after the run was quenched from the temperature and pressure of the experiment.

TABLE 25

X-ray and SEM results for serpentine formed from reaction of brucite with sodium metasilicate solutions.

Run	a (A)	b (A)	c (A)	V (A^3)	β	d(002) (A)
3-16 (C)	5.351(20)	9.197(11)	14.172(454)	696.583(2012)	93° 8'(17')	
3-28 (L)	5.303(80)	9.206(16)	7.348(32)	358.77(548)		3.670

Run	T($^{\circ}$C)	P(kbar)	Run Duration hrs	Massive Platy L	Fiber C	Relative Amount
3-17	351	1.94	889	x	x	L > C
3-16	304	1.94	893	x	x	C ≅ L

TABLE 26

Quench pH measurements of fluids after reaction of olivine with water.

Run	Starting Material	T(°C)	P(kbar)	Run Duration hrs	Fluid	Products*	pH**
3-30	OP194	331	1.47	764	H_2O	O (L,C,B,M)	11.55
3-32	GSC	307	1.47	911	H_2O	L,B,M (O)	10.93
3-23	2-17	323	0.54	1606	H_2O	O (L,C,M)	10.95
3-22	2-17	304	0.54	1606	H_2O	L,C,B,M	11.10

*phases in parenthesis are present in minor amounts

**measurement of undiluted fluid at room temperature and pressure immediately after quench, measurement ±0.1 pH units

Chemical Analyses

Appendix 5 lists the Mg, Si and Fe concentrations of the fluids collected from the hydrothermal runs. Iron was probably present in most of the fluids, but was only detected by atomic absorption analysis in the acidified samples. The majority (79%) of the Mg analyses fell in the range of 0.5-7.0 ppm. However, in several runs Mg values up to 20 ppm were found, with one sample as high as 76 ppm. Si was on the average higher than Mg with the majority (73%) of the samples between 2 and 16 ppm, with one sample as high as 82 ppm. Iron was also high in the fluid, ranging from 8.5 to 458 ppm, but these concentrations of iron were probably caused by the dissolution of the IM buffer and not of the silicate charge.

Figure 5 shows the variation of fluid composition for the different experiments expressed as a function of molality vs temperature. There is a change in the amount of dissolved constituents with temperature and fluid composition. The NaCl fluid had greater concentrations of Mg when compared to the pure-water experiments, whereas Si was approximately the same in both fluids.

Figure 6 demonstrates that the dissolution of olivine may not be congruent. The mole ratio of Mg/Si in solution (0.03 to 0.77) does not reflect the mole ratio in the solid (1.6 to 1.9 in olivines studied). Si is enriched in the fluid in comparison to Mg for most (90%) of the experiments. Table 27 shows the effect of fluid composition and solid phases on the molar ratio of Mg/Si in the solution for the hydration experiments. At constant

Figure 5:A. Mg and Si molalities (X 10^5) vs temperature at 1.0 kbar P_{total} for the hydration experiments with a synthetic olivine (2-17) and NaCl in the fluid phase (Runs 3-62, 3-56, 3-57 and 3-55).

B. Mg molality (X 10^5) vs temperature at 1.0 kbar P_{total} for the hydration experiments with a synthetic olivine (2-17) and the bracketing experiments with pure water (Runs 3-1 through 3-5, and 3-87, 3-86, 3-85, 3-84, and 3-70).

The triangles indicate the Mg concentrations and Si is noted by filled circles.

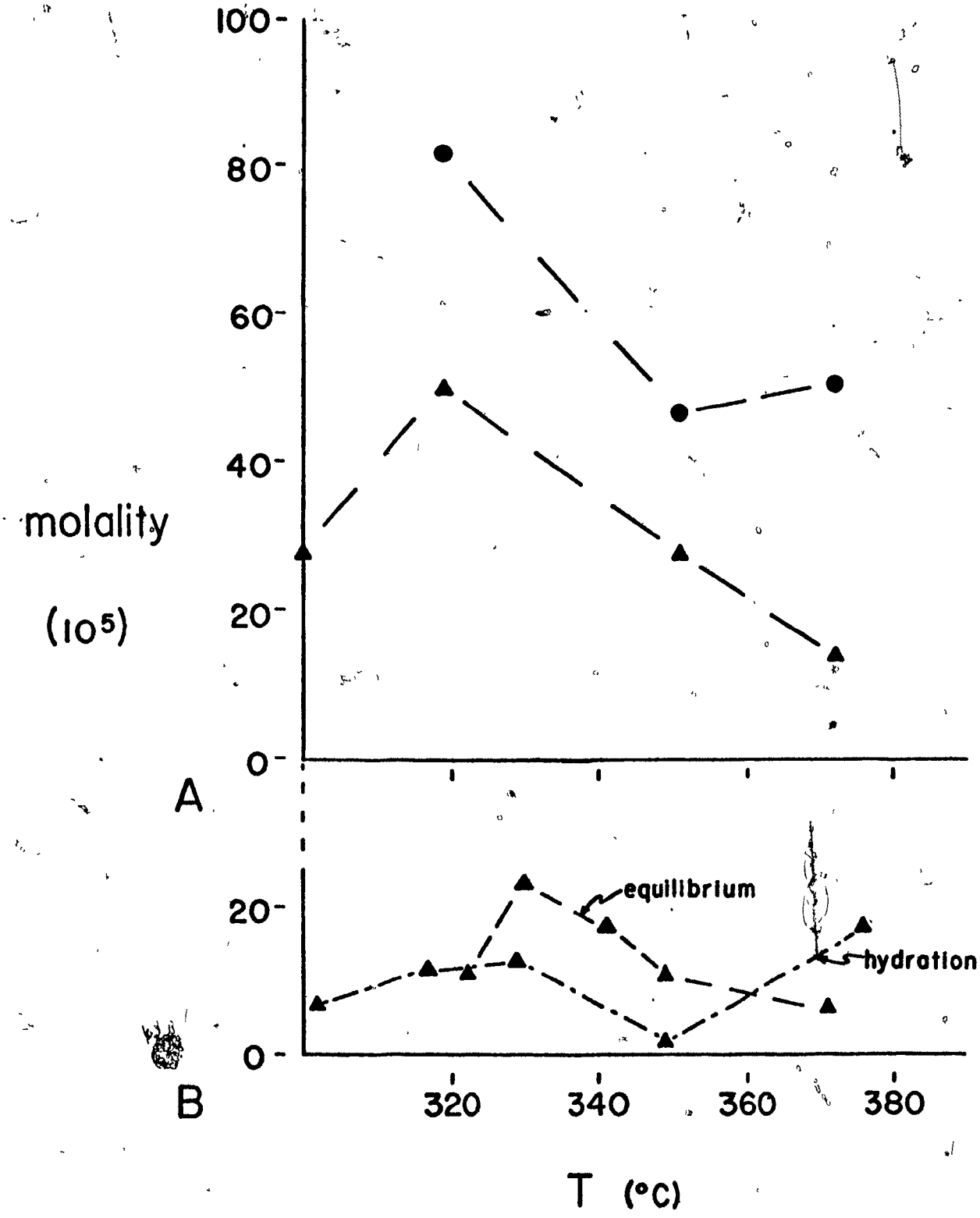
100
80
60
40
20
0
molality
(10⁵)
A
20
0
B
equilibrium
hydration
320
340
360
380
T (°C)

Figure 6: The molar ratio Mg/Si in solution vs temperature for the fluid compositions from some of the experimental runs. The x's indicate those runs done with pure water, the filled circles NaOH fluid, squares NaCl, and the triangles the alkaline chloride fluid.

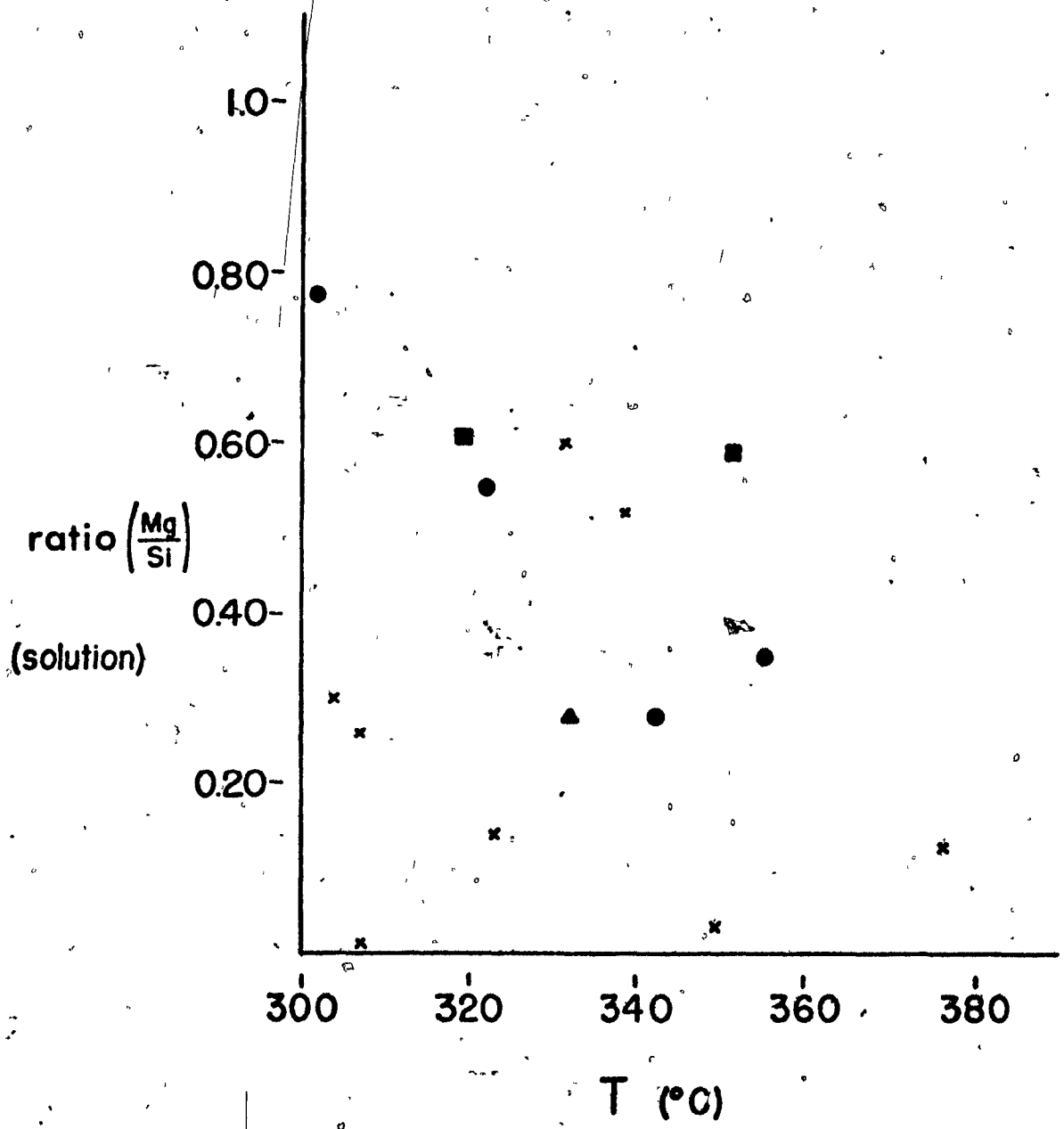
1.0
0.80
0.60
0.40
0.20
ratio (Mg/Si)
(solution)
300
320
340
360
380
T (°C)

TABLE 27

Effect of fluid composition and solid product assemblages present on the molar ratio of Mg/Si in solution during the hydration experiments with a synthetic olivine Fo_{95}.

Run	Products	T, °C	P, kbar	Run Duration hrs	Fluid	Molar Ratio Mg/Si
3-3	O	349	1.0	1559	H_2O	0.034 (1)*
3-45	O	355	0.99	524	0.01 M NaOH	0.35 (9)
3-56	O	351	1.0	481	0.14 M NaCl	0.59 (4)
3-22	L,C,B,M	304	0.54	1605	H_2O	0.30 (7)
3-54	L,C,B,M	302	1.0	550	0.01 M NaOH	0.77 (20)

*numbers in parenthesis are esd for the molar ratio as calculated from the error in the Mg and Si determination

T,P for the same starting material and product assemblage, there is an increase in the molar ratio Mg/Si for NaOH and NaCl fluids compared to the pure water experiments, even though the run duration in the water experiments was three times longer than the experiments with the other fluids.

Data in Table 28 demonstrate the effect of different starting materials on the measured amounts of Mg and Si in fluid and presents two sets of runs (Run 3-70, 3-78 and 3-47, 2-107) which most closely represent duplicate fluid samples, i.e., fluids collected from two experiments conducted at the same temperature, pressure, starting material and run duration. The variability in the measured fluid composition may be due to: (1) starting material, (2) pressure, (3) run duration, or (4) product phases. Runs 3-70 and 3-78 have time as the only variable in the experiment, and the difference between the samples could be explained by the longer run duration for 3-70. Runs 3-47 and 2-107 have starting material and temperature constant, but product phases and time vary. Trends observed in other data would indicate that the difference between Runs 3-47 and 2-107 is most probably due to the longer run duration and product phases in Run 3-47 that gave a slightly greater amount of Mg in the fluid.

TABLE 28

Possible variation in measured amounts of Mg and Si in final fluid as a function of solid assemblage, temperature, pressure and run duration.

Run	Starting Material	Products*	T(°C)	P(kbar)	Run Duration hrs	Molality Mg X 10^5	Molality Si X 10^5
3-1	2-17(Fo_{95})	L,C,B,M	302	1.01	1660	7.4	n.d.
3-32	GSC (Fo_{93})	L,B,M(O)	307	1.47	911	1.6	21.7
3-77	2-BU-66(Fo_{94})	L,C,B,M	307	1.93	999	9.9	37.4
3-30	OP194(Fo_{80})	O(L,C,B,M)	331	1.47	764	n.d.	17.8
3-47	M7863(Fo_{88})	L,B,M(O)	331	1.00	1127	9.9	292.0
2-107	M7863(Fo_{88})	O(L,C,B,M)	328	1.47	819	6.3	+
3-70	equil mix	L,C,B,M	322	1.00	837	2.7	n.d.
3-78	equil mix	L,C,B,M	321	1.01	384	1.9	n.d.

n.d. = not detected

*phases present in parenthesis are present in minor amounts

+not determined

Plate 1: Scanning Electron Microphotographs

A. Anhedral olivine grains (GSC olivine, Fo_{93}). Note angularity and lack of crystal outlines in grains; starting material for bracketing experiments with an equal weight of run products 3-48.

B. GSC olivine, Fo_{93}, higher magnification of plate 1A.

C. Euhedral lizardite plate with a few very short chrysotile needles on the plate (Run 3-1, hydration experiment).

D. Lizardite, higher magnification of Plate 1C (Run 3-1).

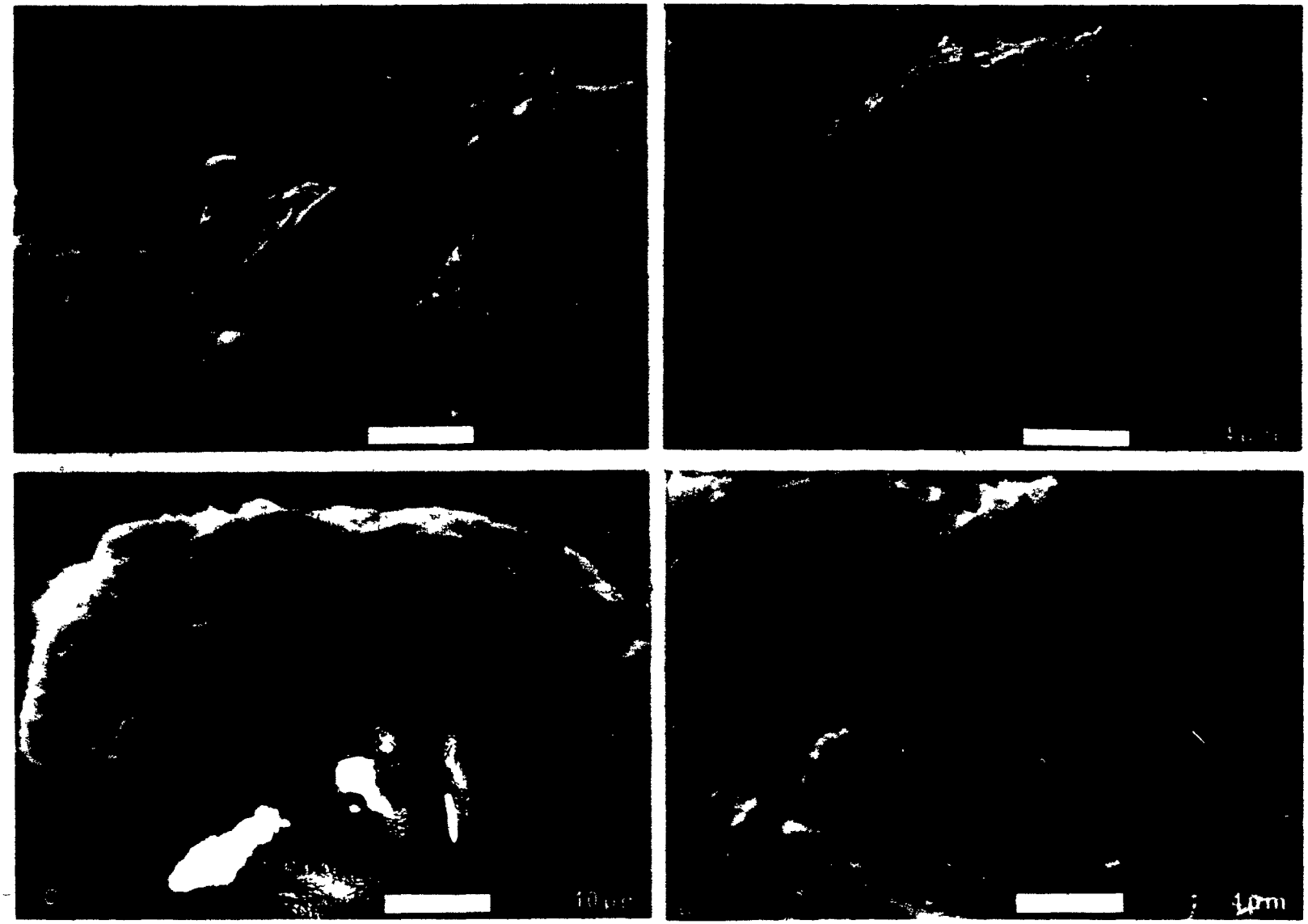
10μm
1μm

Plate 2: Scanning Electron Microphotographs

A. Thick brucite platelet surrounded by chrysotile fibers (Run 3-76, bracketing experiment in L + C + B + M stability field).

B. Chrysotile and lizardite. Note the chrysotile fiber on the right shows "tube-in-tube" structure, which may indicate development of parachrysotile, only observed in this sample (Run 3-12, hydration experiment).

C. Thin brucite platelet completely surrounded by well-developed chrysotile fibers (Run 3-76).

D. Large aggregate of brucite plates, maximum width observed in the sample was 80 μm (Run 3-76).

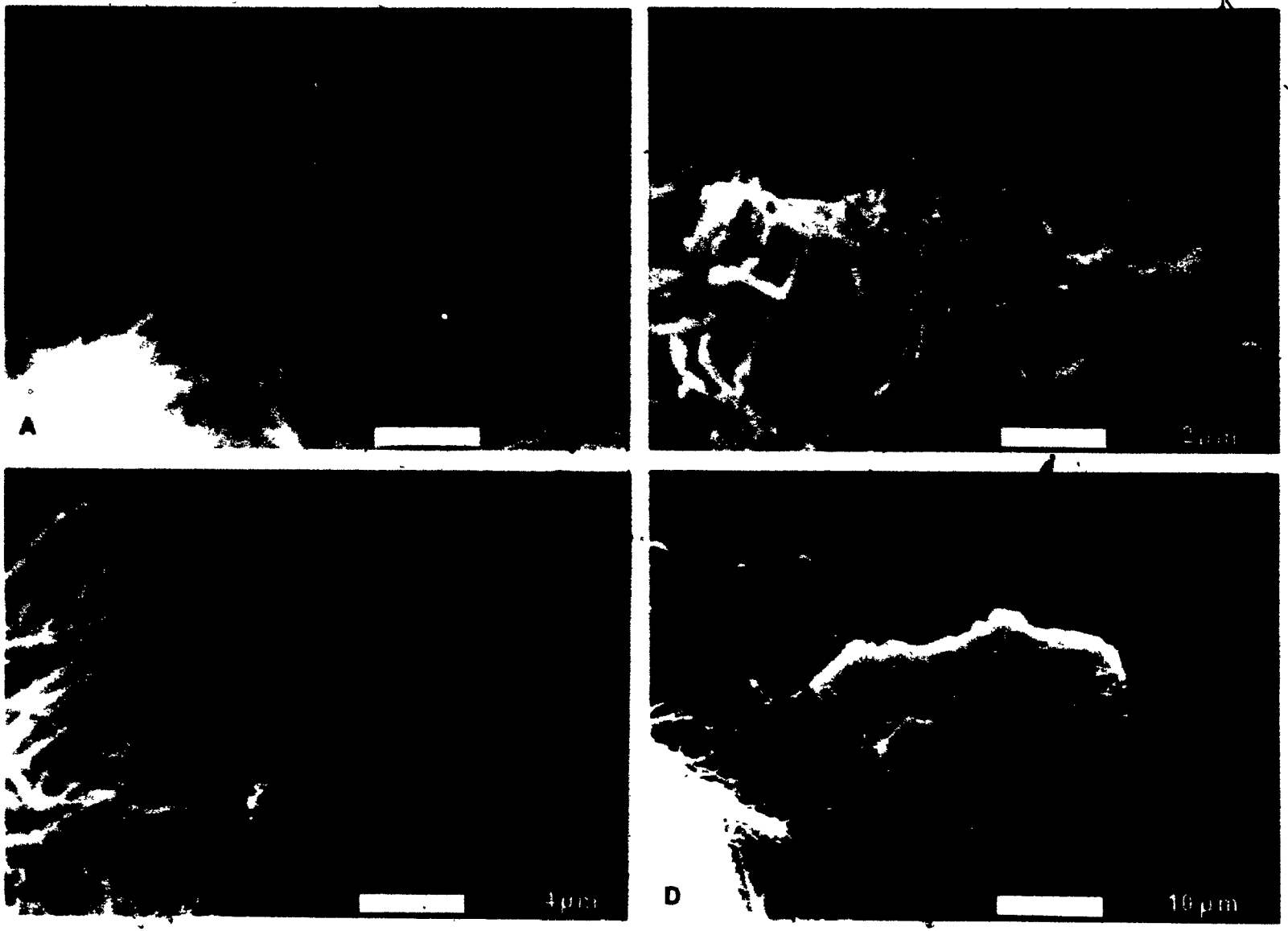
A
D
10 μm

Figure 3: Scanning Electron Microphotographs

A. Euhedral, stubby lizardite crystals with a coating of chrysotile fibers (Run 3-76).

B. Euhedral lizardite, higher magnification of Plate 3A (Run 3-76).

C. Large euhedral lizardite plate, appears also to be a substrate for chrysotile fibers (Run 3-75, bracketing experiment in L + C + B + M stability field).

D. Lizardite laths, length about 60 μm (Run 3-99, bracketing experiment in L + C + B + M stability field).

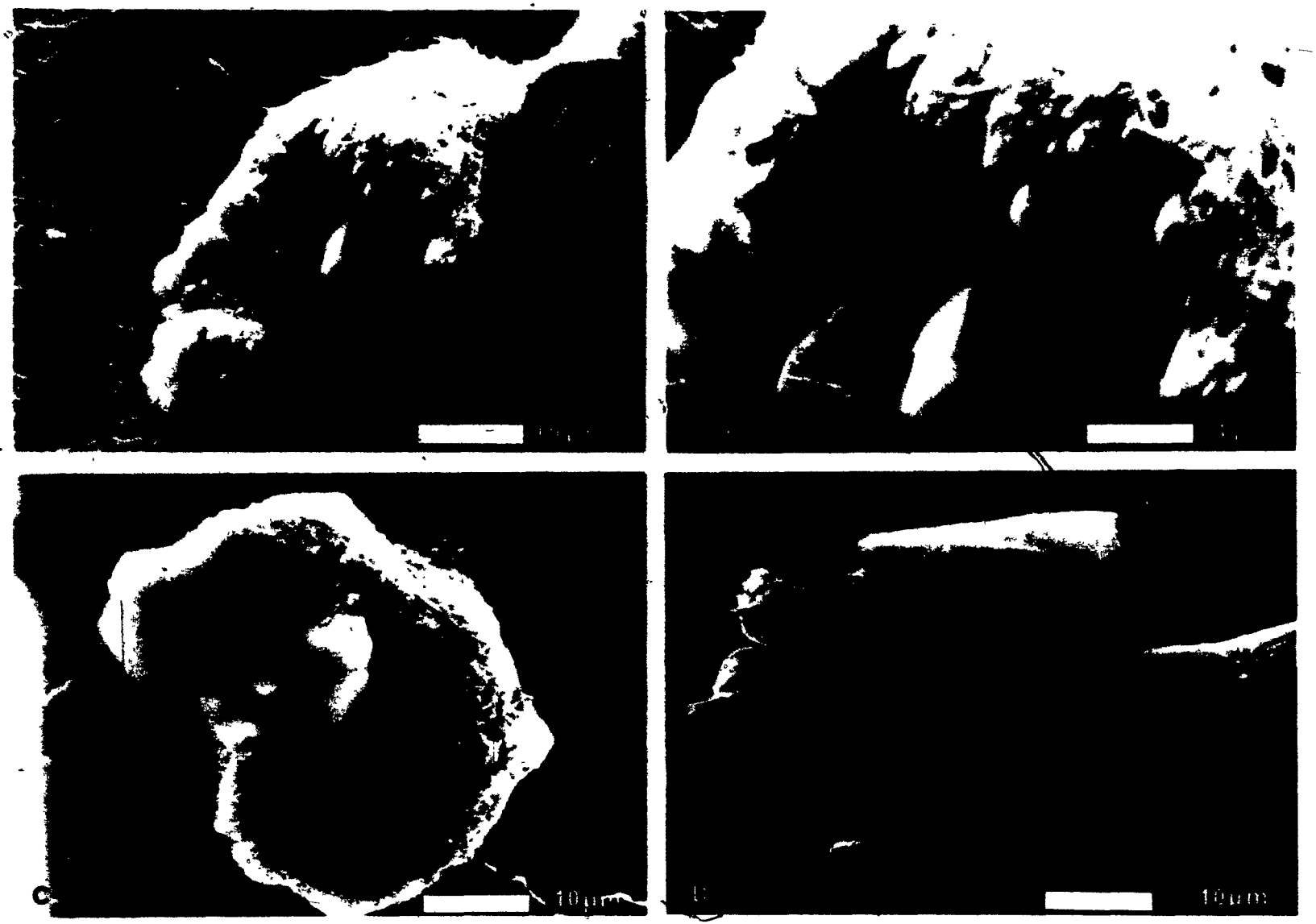
10μm
10μm

Plate 4: Scanning Electron Microphotographs

A. Very short chrysotile fibers at early stages of development (Run 3-75).

B. Lizardite lath, chrysotile fibers, and brucite platelets. The white area around the edge of the hexagonal brucite platelets is due to charging (Run 3-71, bracketing experiment in L + C + B + M stability field).

C. Lengthening of chrysotile fibers as temperature is increased, compare to plate 4A, conducted at a lower temperature (Run 3-76).

D. Maximum development of chrysotile into fiber bundles up to 100 μm in length (Run 3-76).

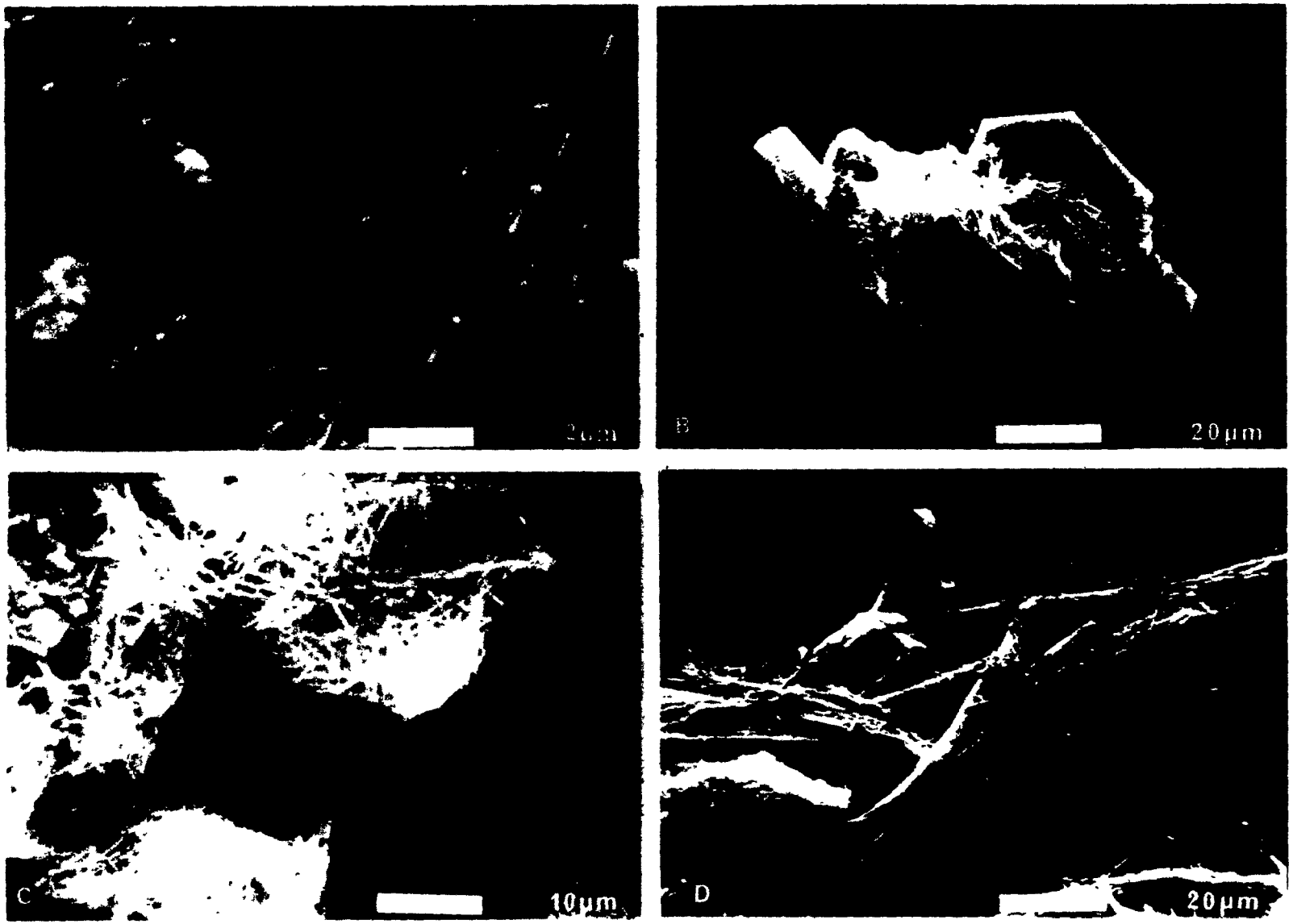
B
20μm
C
10μm
D
20μm

Plate 5: Scanning Electron Microphotographs

A. Mat of interwoven chrysotile fibers, probably forming on an olivine substrate (Run 3-99).

B. Aggregation of chrysotile fibers to form bundles, not as well-developed as in Plate 4D (Run 3-99).

C. Shortened chrysotile fibers on an olivine substrate (Run 3-100, bracketing experiment in 0 stability field).

D. Shortened chrysotile fibers, compare to Plate 5B to note decrease in development (Run 3-100).

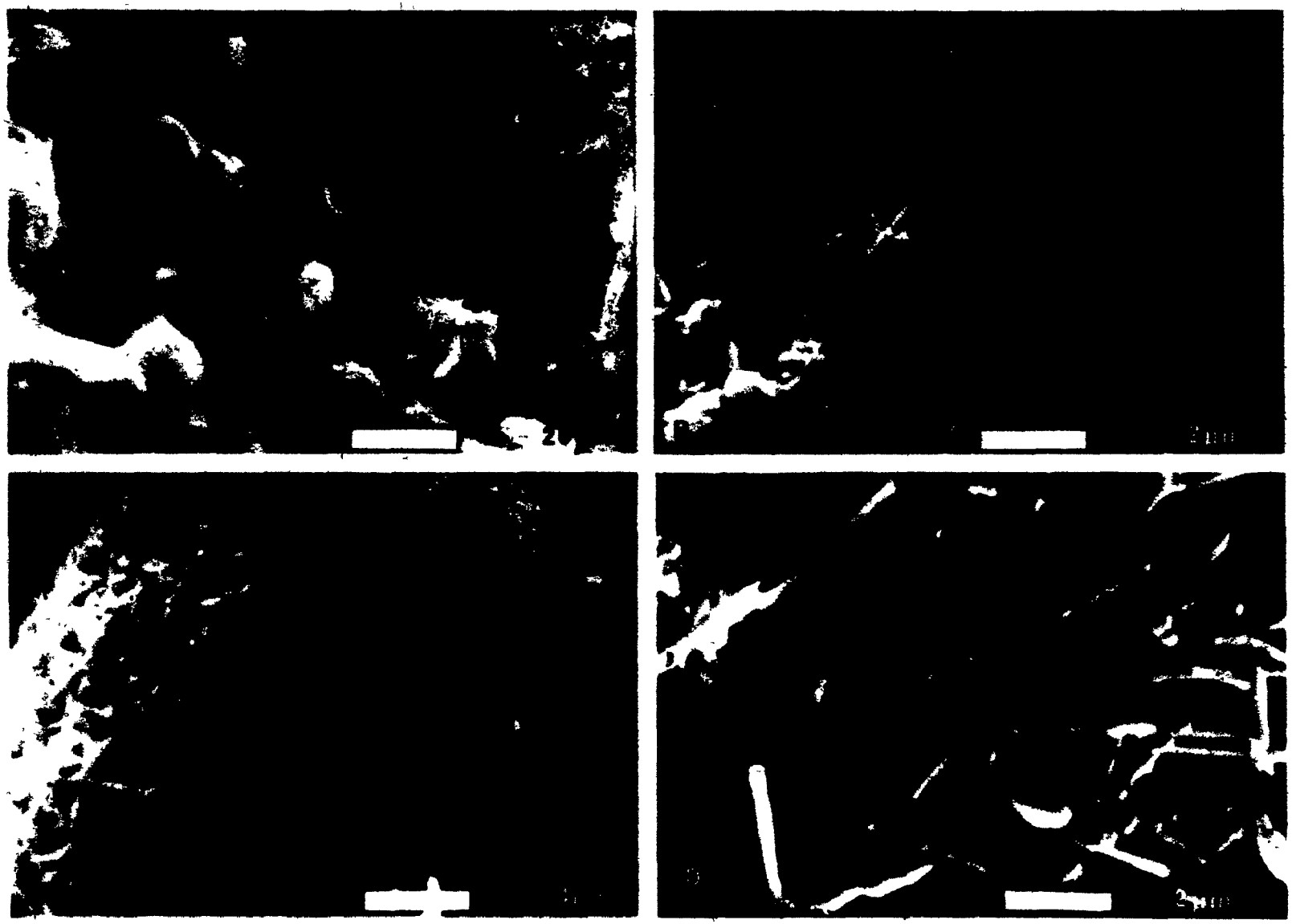

Plate 6: Scanning Electron Microphotographs

A. Etch and solution pits in lizardite (Run 3-100).

B. Development of euhedral olivine crystals from the former angular grains, compare to Plates 1A and 1B (Run 3-101, bracketing experiment in 0 stability field).

C. Euhedral olivine crystals developing on a pre-existing lizardite (?) substrate (Run 3-101).

D. Small euhedral olivine crystals, similar to Plate 6C (Run 3-101).

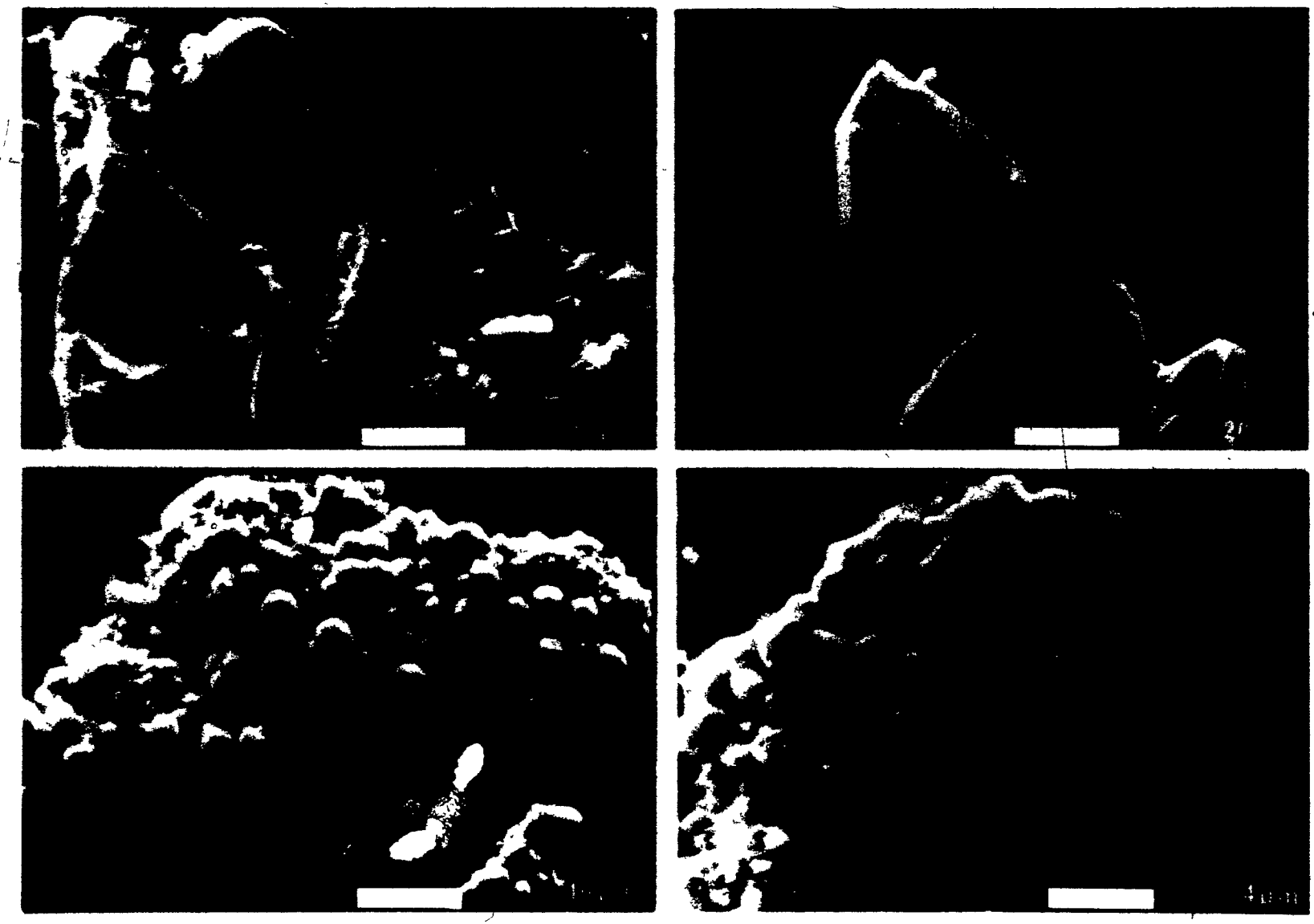

Plate 7:

A. Fine "dusty" magnetite outlining brucite platelets in a serpentine-brucite-magnetite aggregate. Transmitted light, in oil (Run 3-85, bracketing experiment, in O stability field, suggestion of solution etching of the larger brucite plate).

B. A magnetite + brucite + serpentine aggregate. Transmitted light, in oil (Run 3-64, hydration experiment with a synthetic olivine and alkaline chloride fluid).

C. "Dusty" magnetite in irregular patches in serpentine. Transmitted light, in oil (Run 3-84, bracketing experiment in L + C + B + M stability field).

D. A magnetite + brucite + serpentine aggregate. Transmitted light, in oil (Run 3-61, hydration experiment with synthetic olivine and pure water).

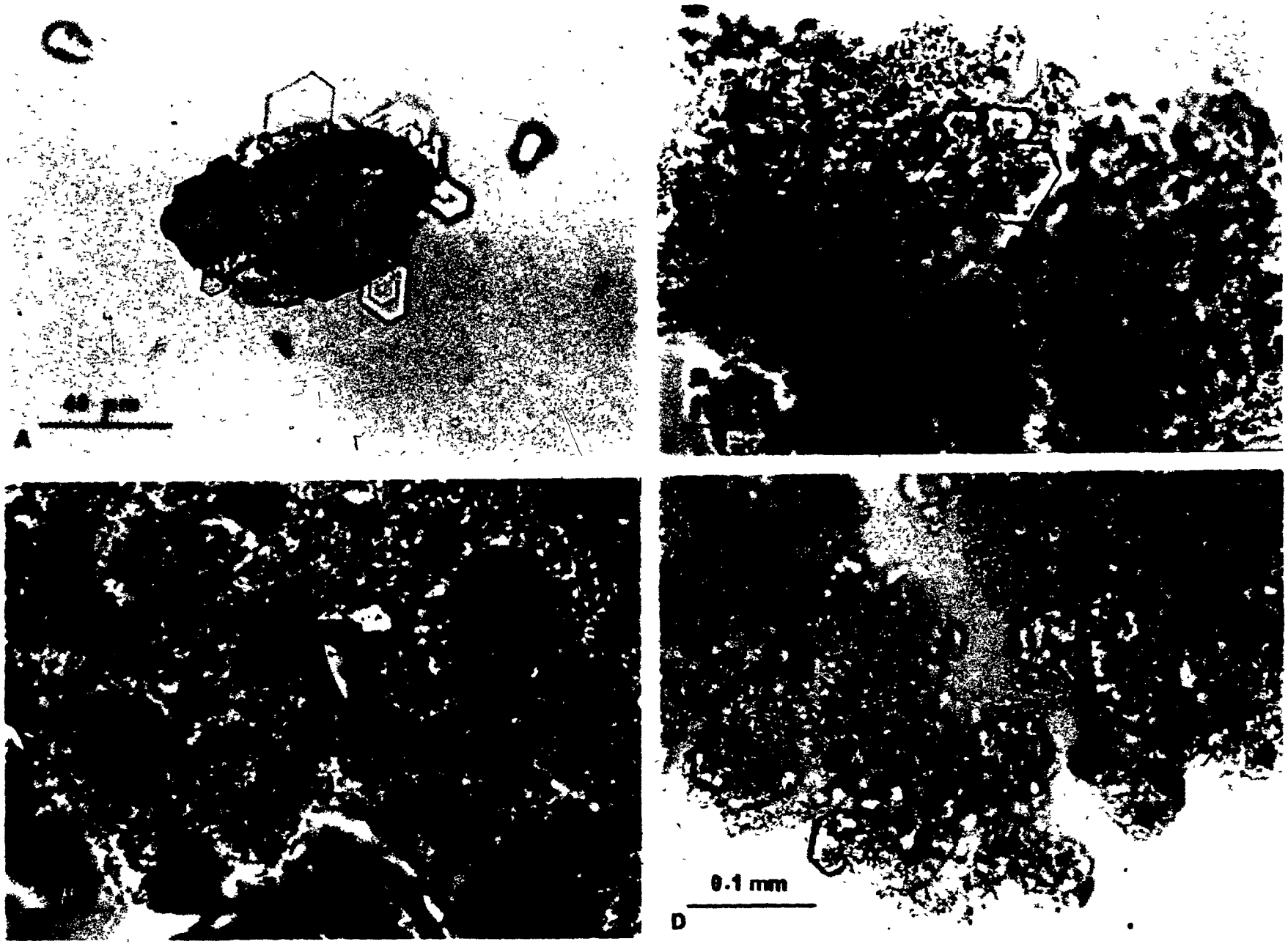
A
0.1 mm
D

Figure 8:

A. Large magnetite aggregate in serpentine, enlargement of Plate 8B. Transmitted light, in oil (Run 3-105, dehydration experiment in serpentine-brucite-magnetite stability field, natural olivine starting material).

B. Magnetite-serpentine aggregate. Transmitted light in oil (Run 3-105).

C. Magnetite, same area and magnification as Plate 8A. Reflected light, in oil (Run 3-105).

D. Chrysotile growing on a larger mass of lizardite. Note fine, long hairs of chrysotile. Transmitted light, in oil (Run 3-69, bracketing experiment in the stability field of L + C + B + M).

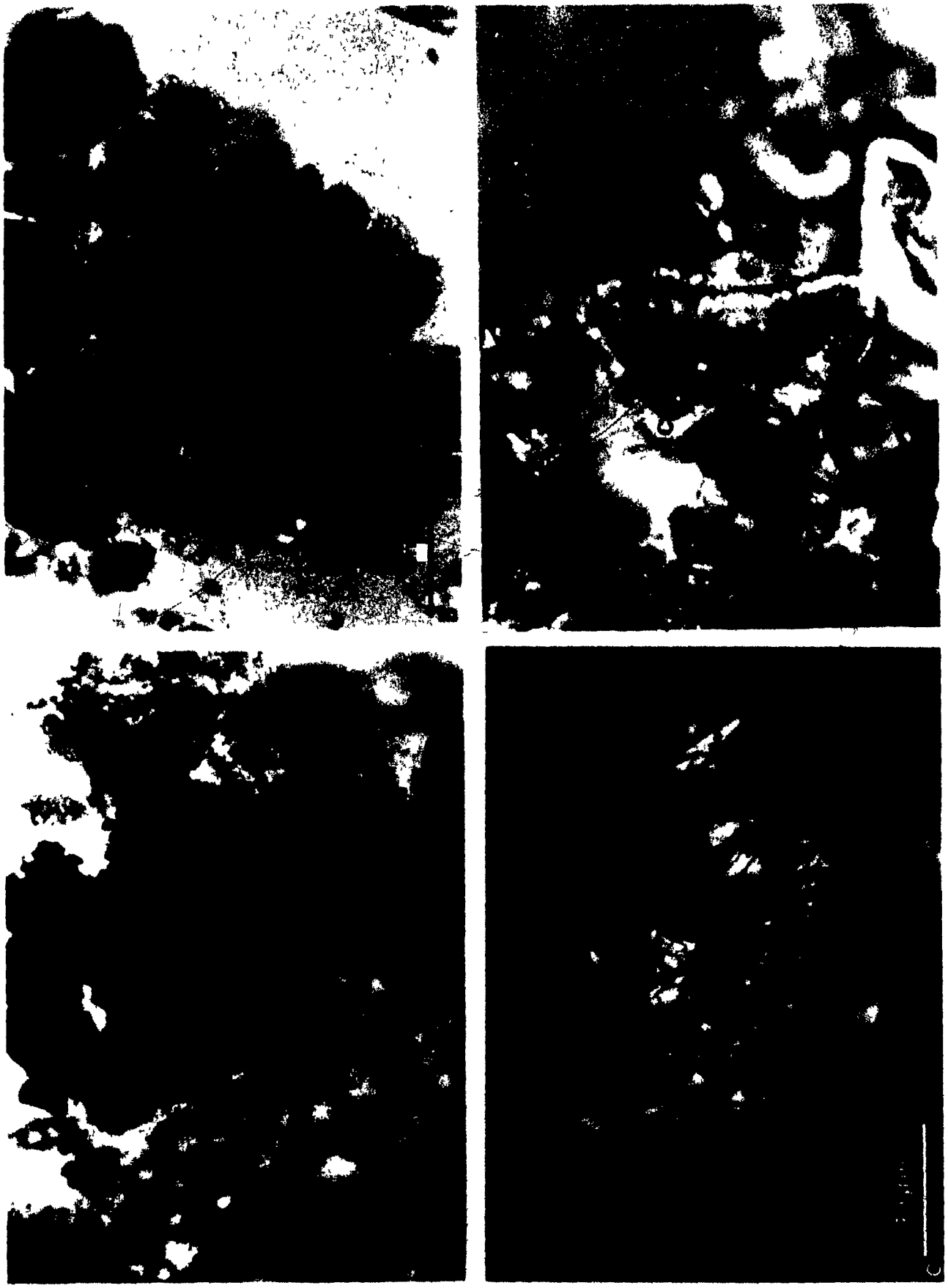

DISCUSSION OF RESULTS

Oxygen Fugacity

Two lines of evidence suggest a reducing environment during serpentinization: (1) presence of native metals (native Fe, native Cu, and most commonly awaruite, Ni_3Fe) in serpentinized ultramafic rocks (Nickel, 1959; Chamberlain et al., 1965; Ramdohr, 1967; Eckstrand, 1972) and (2) hydrogen gas released by serpentinites (Hahn-Weinheimer and Rost, 1961; Thayer, 1966; Coveney, 1972). A question arises as to the difference between the oxygen fugacity defined by the IM buffer in the experimental work and the oxygen fugacity existing at the time of serpentinization of ultramafic rocks. The oxygen fugacity in the natural environment can be inferred from the metallic phases observed. The assemblage iron-magnetite reported by Chamberlain et al. (1965) in the Muskox Intrusion is identical to the synthetic IM buffer. The common assemblage magnetite-awaruite (M-A) represents a slightly higher oxygen fugacity than native iron-magnetite because the activity of iron is decreased in the solid solution. There is some compositional variation in natural awaruites co-existing with magnetite; they may contain between 65 and 78 wt. % Ni, i.e., Ni_2Fe to Ni_3Fe (Hultin, 1968). Misra and Fleet (1973) have shown in the low-temperature phase relations in the system Fe-Ni-S that the composition of awaruite co-existing

with sulfides in serpentinites have slightly different extreme compositions: awaruite co-existing with hazelwoodite has a composition 81 wt. % Ni, whereas with troilite and pentandlite it contains 63 wt. % Ni.

The value of the oxygen fugacity defined by the assemblage Fe_3O_4-Ni_3Fe and Fe_3O_4-Ni_2Fe can be calculated in the manner described previously for the IM buffer. The reactions are:

$$1.5Ni_3Fe + O_2 = 0.5Fe_3O_4 + 4.5Ni \quad (16)$$

or

$$1.5Ni_2Fe + O_2 = 0.5Fe_3O_4 + 3.0Ni \quad (17)$$

and

$$\Delta G^o_r (T) = 0.5\,\Delta G^o_{f,M} (T) - 1.5\,\Delta G^o_{f,A}(T) \quad (18)$$

The $\Delta G^o_{f,A}(T)$ was obtained from Kubaschewski and Goldbeck (1949) and the volume data from Robie and Waldbaum (1968) assuming ideal solid solution for Fe and Ni to obtain the molar volume for Ni_3Fe and Ni_2Fe. Figure 7 presents the calculated values f_{H_2} and f_{H_2O} for the assemblages IM, Fe_3O_4-Ni_3Fe and Fe_3O_4-Ni_2Fe for the P,T range of interest for the experimental work done in this study (see Appendix 1c for actual values). The change in oxygen fugacity from IM to the assemblage M-A is not large. However, the amount of water in the gas phase is greater for M-A than for IM, although in both cases the vapor phase is definitely hydrogen-rich. Hahn-Weinheimer and Rost (1961) stated that Ni_2Fe represents a more reducing environment than Ni_3Fe, as suggested by these calculations. The vapor becomes more hydrogen-rich with decreasing temperature at constant pressure. With decreasing pressure at constant temperature the amount of hydrogen increases in proportion to the total pressure.

Figure 7: Log f_{H_2}/f_{H_2O} vs temperature for the assemblages iron-magnetite (IM), magnetite-awaruite (Ni_2Fe-Fe_3O_4 and Ni_3Fe-Fe_3O_4) for P_{total} = 500 and 2000 bars. Calculations are described in text. At 500 bars, the difference between the log f_{H_2}/f_{H_2O} for M-Ni_2Fe and M-Ni_3Fe is too small to be meaningful within the error of the thermodynamic data and assumptions necessary for the calculations (see Appendix 1c).

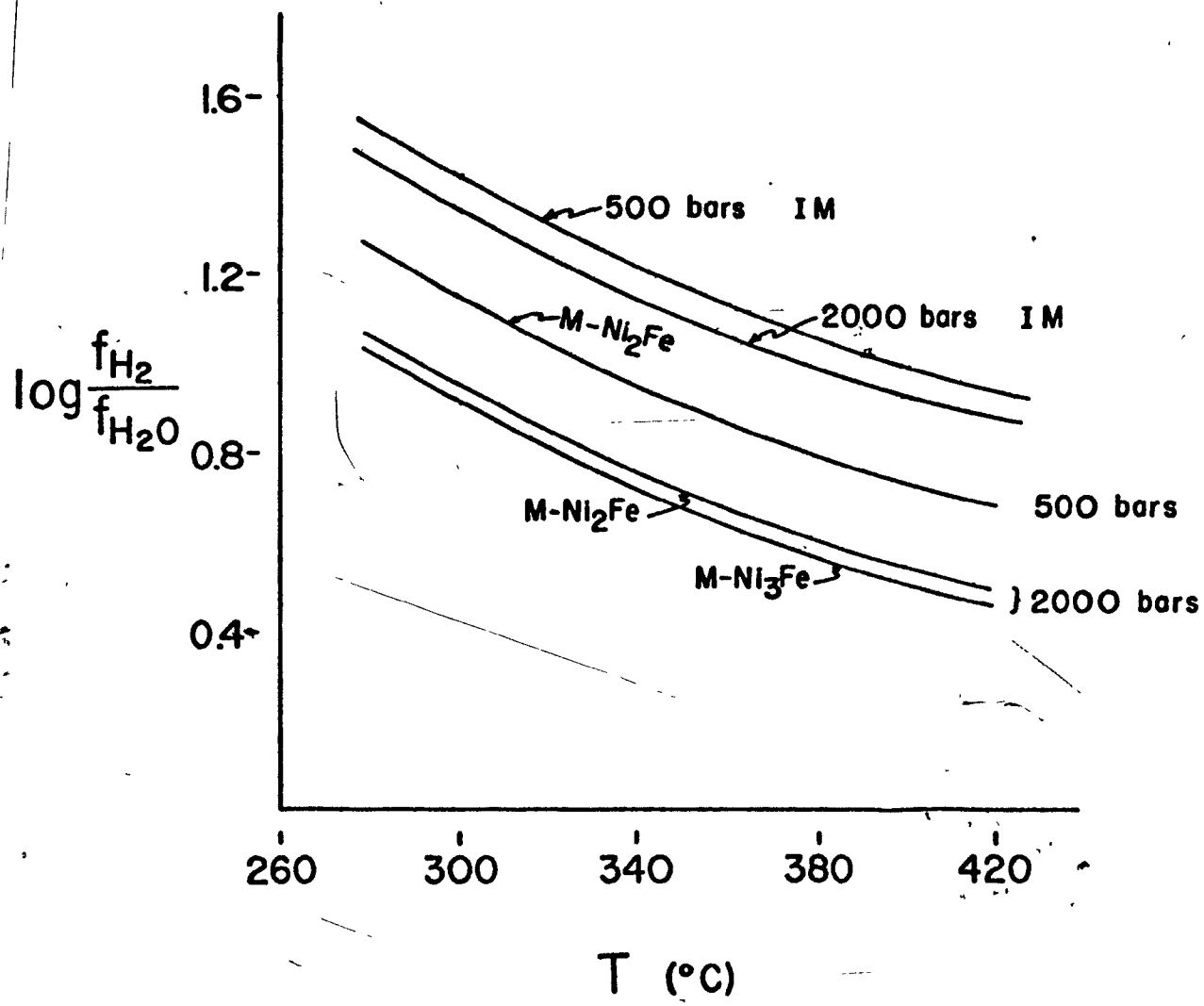
1.6
1.2
0.8
0.4
$\log \frac{f_{H_2}}{f_{H_2O}}$
500 bars IM
2000 bars IM
M-Ni_2Fe
500 bars
M-Ni_2Fe
M-Ni_3Fe
2000 bars
260
300
340
380
420
T (°C)

The above calculations indicate that the difference in f_{O_2} between IM and M-A is not geologically significant in the P,T range in which serpentinization occurs. The difference is not significant because with an oxygen fugacity less than 10^{-23} bars (Eugster, 1972), oxygen does not exist in the gas phase but participates in the formation of magnetite. The two assemblages do differ significantly in the amounts of hydrogen and water in the gas phase, and hydrogen makes up a larger proportion of the gas phase for IM than M-A at a given T and P.

It should be re-emphasized that IM and M-A assemblages define an extremely reducing and hydrogen-rich vapor phase. These conditions are unusual in the normal crustal environment, commonly thought to have an oxygen fugacity defined by QFM or HM buffers. The gas phase buffered by QFM at 300°C consists essentially of water plus a small amount of hydrogen with $\log f_{H_2}/f_{H_2O} = -2.04$ for $P_{total} = 1000$ bars (Eugster, 1972) versus 1.391 for IM and 1.066 for M-Ni_3Fe at the same T and P. The difference between QFM buffer and IM or M-A becomes immediately apparent: QFM has a vapor containing water and traces of hydrogen, and IM and M-A have a vapor rich in hydrogen containing minor amounts of water. Thus, it is not surprising that hydrogen has been reported to be escaping from serpentinized ultramafic rocks.

The composition of awaruite should be considered in terms of the Fe-Ni binary. Heumann and Karsten (1963) found a eutectoid reaction at 345°C in which α-Fe comes into equilibrium with γ-Ni_3Fe (Figure 8).

Figure 8: The Fe-Ni system from Shunk (1969); the dashed lines indicate extrapolation. α = α-Fe and γ = γ-(Fe,Ni). The shaded area indicates the range of compositions of awaruites found co-existing with magnetite in serpentinites. The awaruite compositions co-existing with sulfides have slightly different extremes in composition (see text).

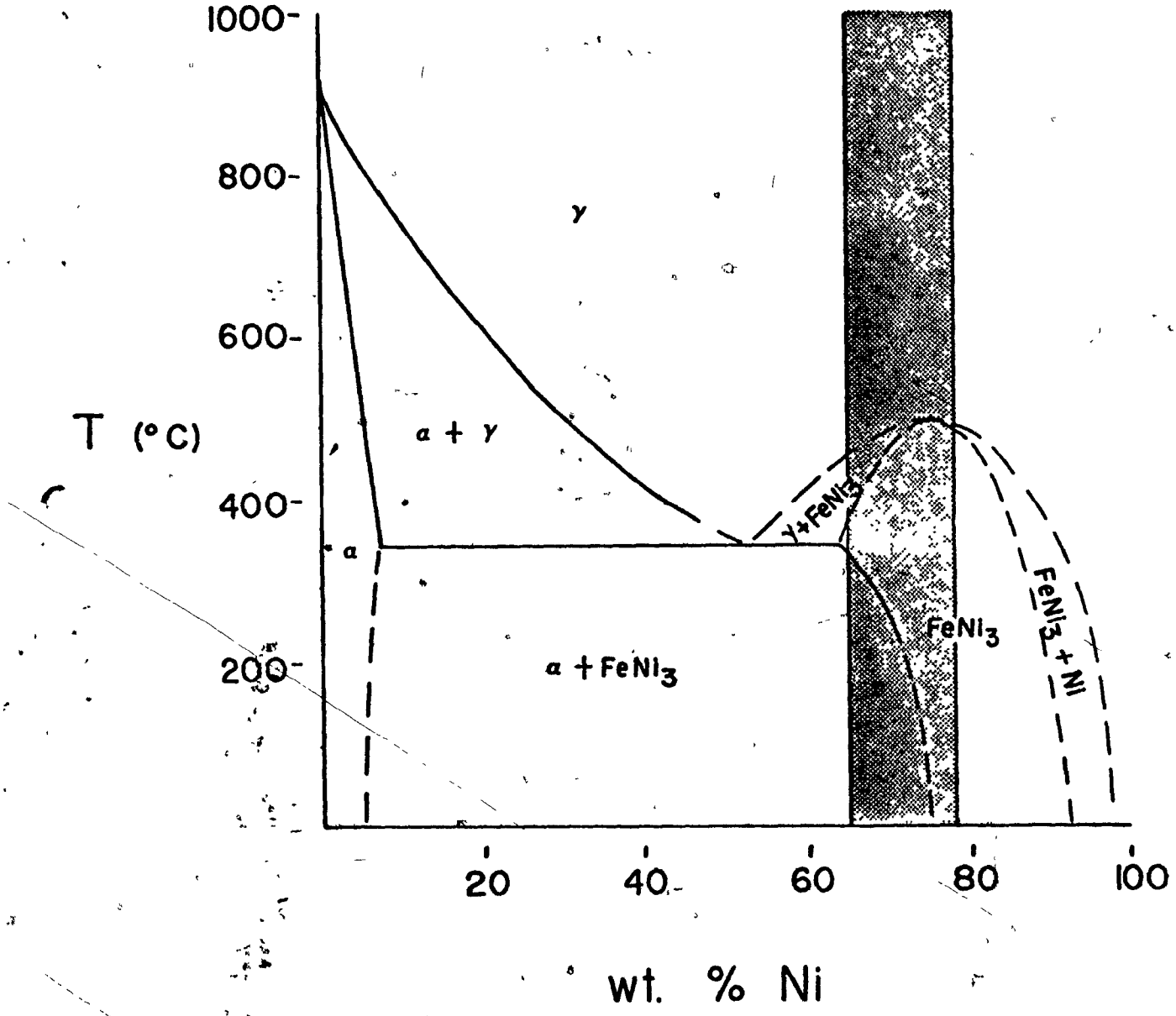
1000
800
600
400
200
T (°C)
γ
α + γ
α
α + FeNi3
γ+FeNi3
FeNi3
FeNi3 + Ni
20
40
60
80
100
wt. % Ni

The lower temperature region was extrapolated by Shunk (1969) to show the edge of the α-Fe + Ni_3Fe region at 25°C to be 76 wt. % Ni (Ni_3Fe), which shows that Ni_3Fe is most probably the stable composition at 25°C, 1 atm.

Serpentine Mineralogy

Lizardite has not been reported previously as a reaction product in an experimental study of the reaction of olivine with water, though it is a common serpentine mineral in natural serpentinites. Johannes (1968) used chrysotile as the serpentine component in the starting mixture for the equilibrium determination of the brucite reaction (Reaction (1), p. 4) as did Chernosky (1973) for the equilibrium determination of the higher temperature talc reaction (Reaction (2), p. 4). Scarfe and Wyllie (1967) did not identify the serpentine mineral formed in their experiments.

The influence of iron on the formation of lizardite is difficult to evaluate. Whittaker and Wicks (1970) investigated the chemical differences among natural serpentine minerals and have demonstrated that the lizardite structure tolerates more iron and aluminum substitution than does chrysotile. The limited chemical substitution in chrysotile is easily understood in terms of the constraints imposed by its common but peculiar cylindrical structure (Whittaker, 1956; Wicks, 1969). Iishi and Saito (1973) synthesized all three serpentine minerals (lizardite, chrysotile and antigorite) by

variations of molar ratios of $Mg(OH)_2$, SiO_2 and H_2O. It would appear that the conclusions of Iishi and Saito with respect to antigorite formation may also hold for lizardite: the presence of Fe^{2+}, Fe^{3+} and Al^{3+} are incidental to the formation of lizardite.

X-ray Results

Variations in cell dimensions of lizardite were certainly largest for lizardite formed during the reaction of olivine with water and fluids of varying composition. The reduction in variation of these parameters (homogenization) in the bracketing and dehydration experiments was most probably due to increased run duration, which allows the lizardite to crystallize and become structurally more perfect with time. This conclusion is verified by the work of Ross (1968) and Forbes (1969). Ross showed that the basal spacings of layer silicates (muscovite, biotite, etc.) will deviate from their true values when the crystals are several unit cells thick. Forbes demonstrated that the anomalous basal spacings of synthetic talc became normal with longer run durations and/or higher run temperatures and pressures. The formation of euhedral lizardite crystals in the longer hydration experiments and in the bracketing experiments as observed in SEM work provides additional evidence that crystallization is occurring with time.

Aumento (1969) observed a similar degree of cell edge variation in natural lizardites from a variety of serpentinized ultramafic rocks. He suggested that these variations may be due to differences in temperature of formation or compositional differences. Variation in the cell dimensions could also be caused by mismatch between the octahedral and tetrahedral layers of the mineral (influenced by composition) or for different stacking sequences (Radoslovich, 1962; Wicks, 1969).

Table 29 presents data on the chemical composition and cell edges of lizardite as collated from the literature. The variation in cell edge with significant differences (7-20 mole %) in Al and Fe is small (less than 1%), the greatest variation is in a and d (002). Chernosky (1973) has measured cell edge changes as a function of Al content for synthetic serpentine minerals. For low Al contents (0.5 to 10.5 mole %) such as those observed for lizardites listed in Table 29, Chernosky observed a two-phase field of lizardite + chrysotile. The cell edge differences exhibited by Chernosky's synthetic lizardite + chrysotile mixtures were small (less than 1%) and by themselves do not accurately reflect the variation in Al content, coupled with the fact that cell edges measured were for a mixture of two phases, not a single phase.

The effect of iron on cell edge of lizardite can only be inferred from natural specimens and by calculation as no experimental data are available. Table 30 presents X-ray and cell edge data for iron-bearing serpentine minerals. In Table 31 calculated values of a and b cell parameters of serpentine from observation of the end member compositions

TABLE 29

X-ray and composition data on naturally occurring lizardites. The structural formulae were recalculated for major constituents* only on the basis of the 14 oxygen method as described by Whittaker and Wicks (1970). Aumento's (1970) lizardites are reported as single phase, though the detection limit for chrysotile from the X-ray work was about 20% in a mixture of both minerals. Aumento did not specify the esd for his X-ray refinements of cell edges.

Sample	a (A)	b (A)	c (A)	d(002) (A)	d(201) (A)	Reference
108-3	5.333	9.218	7.302	3.639	2.501	Aumento (1970)
165-1	5.327	9.208	7.305	3.652	2.498	Aumento (1970)
6-1	5.312	9.207	7.304	3.645	2.496	Aumento (1970)
6-5	5.306	9.204	7.301	3.649	2.497	Aumento (1970)
19-NI-63A	5.339(3)	9.226(2)	7.315(6)	3.660	2.504	Page & Coleman (1967)
Radusa lizardite	5.301(3)	9.186(6)	7.281(5)	3.64	2.494	Krstanovic (1968)

108-3 $(Mg^{2+}_{5.4}Fe^{2+}_{0.01}Fe^{3+}_{0.5})(Si^{4+}_{3.6}Al^{3+}_{0.4})O_{10}(OH)_8$, Mid-Atlantic Ridge, 45°N

165-1 $(Mg_{5.4}Fe_{0.02}Fe_{0.58})(Si_{3.7}Al_{0.08}Fe_{0.12})O_{10}(OH)_8$, Mid-Atlantic Ridge, 45°N

6-1 $(Mg_{5.4}Fe_{0.07}Fe_{0.53})(Si_{3.7}Al_{0.3})O_{10}(OH)_8$, Mid-Atlantic Ridge, 45°N

6-5 $(Mg_{5.3}Fe_{0.03}Fe_{0.57})(Si_{3.7}Al_{0.3})O_{10}(OH)_8$, Mid-Atlantic Ridge, 45°N

19-NI-63A $(Mg_{5.98}Fe^{2+}_{0.02})(Si_{3.6}Al_{0.1}Fe^{3+}_{0.2})O_{10}(OH)_8$, New Idria, Joe 5 Pit, Calif.

Radusa lizardite $Mg_6Si_4O_{10}(OH)_8$, Radusa, Chromite Mine, Yugoslavia; electron microprobe analysis of the mineral indicated that total amount of cations other than Mg and Si was less than 1.0 wt. %

Table 29 cont'd

*recalculated under the assumption that SiO_2, Al_2O_3, Fe_2O_3, FeO and MgO make up the ideal serpentine composition of $Mg_6Si_4O_{10}(OH)$; Al distributes between octahedral and tetrahedral sites in serpentine structure indicating a coupled substitution of $Mg^{2+} + Si^{4+} = Al^{3+}(oct) + Al^{3+}(tetr)$, the same substitution holds for Fe^{3+} and is reflected in Sample 165-1

TABLE 30

X-ray and cell edge data on some iron-bearing members of the serpentine group.

Mineral	a (A)	b (A)	c (A)	d(002) (A)	d(201) (A)	Reference
greenalite						
*$(Mg_{3.0}Fe_{2.6}Al_{0.4})Si_4O_{10}(OH)$	5.539(3)	9.589(2)	7.216	3.61	2.586	Dietrich(1972)
greenalite						
$Fe_6Si_4O_{10}(OH)_8$	5.56	9.60	7.21	3.60	2.59	ASTM 11-265
cronstedtite						
$(Fe_4^{2+}Fe_2^{3+})(Fe_2^{3+}Si_2)O_{10}(OH)_8$	5.49	9.51	7.32	3.54	2.305	Steadman & Nuttal (1964) ASTM 17-470

*composition recalculated from microprobe analysis, Fe^{2+}/Fe^{3+} not determined, therefore all iron was allocated as Fe^{2+}

TABLE 31

Comparison of some observed a and b cell parameters and some calculated values taken as the average for ideal tetrahedral and octahedral sheets. An ideal 1:1 layer silicate structure assumes hexagonal symmetry in the tetrahedral sheets, no mismatch between sheets (i.e. no distortion of the octahedral sheet) and no ordering of Si and Al or Si and Fe^{3+}.

Phase	Calculated Values (A)				Average (A)		Observed Values (A)	
	tetrahedral		octahedral					
	a*	b**	a*	b***	a	b	a	b
$Mg_6Si_4O_{10}(OH)_8$	5.28	9.15	5.40+	9.36+	5.34	9.26	5.28-5.32	9.18-9.22
$Mg_{3.0}Fe_{2.6}Al_{0.4}Si_4O_{10}(OH)_8$	5.28	9.15	5.73	9.92	5.51	9.54	5.54	9.59
$Fe_6Si_4O_{10}(OH)_8$	5.28	9.15	5.95	10.30	5.62	9.72	5.56	9.60
$Fe_4Fe_4Si_2O_{10}(OH)_8$	5.53	9.59	5.77	10.00	5.65	9.79	5.49	9.51
$Mg_6FeSi_3O_{10}(OH)_8$	5.41	9.37	5.40	9.36	5.40	9.36		
$Mg_{5.8}Al_{0.2}Si_{3.8}Al_{0.2}O_{10}(OH)_8$	5.31	9.20	5.39	5.34	5.35	9.27	5.32++	9.22++

Table 31 cont'd

*$\underline{a} = b/(3)^{1/2}$ (Brindley, 1967)

**$\underline{b}_{tetra} = 9.15 + 0.87x$, where x equals the Fe^{3+} in tetrahedral site, $Si_{1-x}Fe_x$ (Brindley, 1967) in A

***$\underline{b}_{oct} = 8.923 + 0.125\ Mg^{2+} + 0.299\ Fe^{2+} + 0.079\ Fe^{3+}$ (Rodoslovich, 1962) in A

+measured, brucite layer

++Chernosky (1973)

are presented. The effect of small amounts of iron on cell edge of lizardite are difficult to evaluate from these data because lizardites often contain some Al (Table 29). The calculations show, however, that it would be difficult to detect small amounts of iron in the lizardite from cell edge measurements. The relationship between iron content and cell edge has been determined for minerals structurally related to serpentine: biotite (Wones, 1963) and talc (Forbes, 1969). There, variation in b and c cell edge was a function of iron content and oxygen fugacity. For example, Forbes (1969) observed that iron substitution produced an increase in c dimension of talc, with the amount of increase greatest for HM and lowest for IM buffers. Out of the four oxygen buffers (HM, NNO, QFM, IM) investigated by Forbes, two factors specifically characterized the IM (or WM) buffer: (1) longer run times (up to 480 hours) were needed to produce a talc with a stable d (003) spacing, and (2) a systematic correlation between d (060) and iron content was found only for talcs synthesized with IM buffer. Variation of c or d(003) for talc with increasing iron content was very small for all buffers, though c was more systematic and better correlated than the Al content of lizardites was with d (002) as determined by Chernosky (1973). The increase in basal spacing of talc with increasing iron content and oxygen fugacity suggested tetrahedral Fe^{3+} substitution even for the low oxygen fugacitites defined by IM buffer.

From the above considerations, the iron contents of the lizardites synthesized in this study are apparently small. The differences in the

cell parameters of the synthetic lizardite are within the variation observed for their natural analogues. Besides the cell dimensions, the d (060) for lizardites produced in this study was constant at 1.535 (1) A, not showing any change as might be suggested from Forbes' work on talc with the IM buffer. Without direct analysis of the lizardite, it is impossible to determine whether the cell edge variation is due to composition or other structural effects. Evaluation of structural effects such as those due to polytypism is not possible without single crystal work, an approach precluded by the fine grain size of all the synthetic lizardites produced experimentally.

Pressure and temperature of formation do not appear to affect the cell dimensions of lizardite. For example, there is as much variation in cell edges and volume between lizardites in experiments 3-25 and 3-26 (Table 9), conducted at the same T and P, as between the lizardites from experiments 3-47 and 3-77 run at different T and P.

Chrysotile gave poor refinements of cell dimensions in all cases except for Runs 3-22 and 3-26. These poor results were most probably caused by the fact that chrysotile was mixed in with lizardite as a predominant phase. Also, a poor degree of crystallinity is reflected by diffuse powder diffraction lines that are difficult to read accurately.

Habit

Table 32 presents details of habit and size of serpentine minerals based chiefly on transmission electron microscope studies. Lizardite laths (Plate 3D) have been observed in natural specimens (Wicks, pers. comm., 1974). The euhedral, hexagonal prismatic crystals of lizardite observed in the SEM work (Plates 3A and 3B) have not been described from natural assemblages. However, natural lizardites have not been as well characterized as chrysotiles. The distinction of chrysotile laths in SEM work was made on size only (thinner and shorter crystals). Whittaker and Zussman (1971) suggest that an unambiguous classification of chrysotile laths lies in electron diffraction patterns which show a minimum of two zones of reflections (hk0 and either h0l or 0kl). Chrysotile from four runs (3-77, 3-61, 3-22, 3-54) was classified as laths on the basis of SEM habit. Without electron diffraction, however, the identification can be questioned. The only other candidate is lizardite. The division between the two lath-shaped minerals is based in the final analysis on width alone, the smaller width ($< 3\ \mu m$) being attributed to chrysotile. The identification of larger laths as lizardite is unambiguous because the constraints of the cylindrical structure of chrysotile would not allow it to form such a wide lath (Whittaker, 1956). "Tube-in-tube" formation was observed in chrysotile from Run 3-12 (Plate 2B).

The common habits observed in all experiments were: massive platy lizardite with or without crystal faces, chrysotile fibers, and in

TABLE 32

Habit of natural lizardite and chrysotile observed from both transmission electron and transmitted light microscopy, as compiled from the literature.

Mineral	Habit	Size (μm)+	Reference
lizardite	plates	50*	Zussman et al.(1957)
lizardite	plates	0.1-1.0	Iishi & Saito (1973)
lizardite	hexagonal plates	100-400	Krstanovic (1964)
lizardite	anhedral grains	< 1.0*	Zussman et al. (1957)
chrysotile	fibers	0.026	Whittaker (1957)
chrysotile	fibers	0.032-0.04	Kheiker et al. (1967)
chrysotile	fibers	0.018-0.2**	Yada (1967, 1971)
chrysotile	fibers	0.02 (length, 0.04-0.8)	Iishi & Saito (1973)
chrysotile	laths maximum	0.2	Zussman et al. (1957)

+for chrysotile fibers, the outer diameter of fiber

*estimated from published photographs

**statistically significant, an average of 170 measurements of individual fibers on natural chrysotile from 5 different localities and on one synthetic chrysotile

longer runs within the chrysotile stability field, chrysotile fiber bundles. The following observations were also made:

(1) lizardite forms laths at temperatures above 315°C at all pressures investigated, and persists in runs up to 2500 hours in duration

(2) euhedral, hexagonal crystals of lizardite existed at temperatures less than 345°C at all pressures with run durations greater than 1100 hours, except in the sodium metasilicate fluid experiments where euhedral lizardite formed after only 573 hours.

(3) "chrysotile" laths formed at lower temperatures (< 310°C) at all pressures but did not persist with longer run durations (> 1660 hours) except at the lowest pressure of 0.5 kbar.

Thus, temperature may control the formation of lizardite laths, but not necessarily any of the other crystal forms within the stability field of serpentine.

Temperature, Pressure and Compositional Effects on Formation of Serpentine Minerals

Figure 9 summarizes all known synthesis data and equilibrium phase boundaries determined for the serpentine minerals. The synthesis temperatures and pressures clearly bear no relationship to the determined phase boundaries for the reactions of interest. Iishi and Saito's (1973) work demonstrates that Al or Fe are not necessary for the formation of either lizardite or antigorite. The T,P fields of lizardite, chrysotile and antigorite determined by Iishi and Saito for a fixed $Mg(OH)_2:SiO_2:H_2O$ reflect

Figure 9: Compilation of the synthesis and phase equilibrium data on the serpentine minerals as a function of temperature and pressure. For the composition data: x = Iishi and Saito (1973) composition fixed at $5.46Mg(OH)_2:4.0SiO_2:10.92H_2O$; ● = Chernosky (1973), no Al, excess water; ■ = Chernosky (1973), Al contents vary $0.0 \leq x \leq 0.25$, where x is defined by $(Mg_{6-x}Al_x)(Si_{4-x}Al_x)O_{10}(OH)_8$; ▲ = Chernosky (1973), Al contents vary $0.25 \leq x \leq 2.0$; + = Page (1966), fixed composition $5.6MgO:4.0SiO_2$ with excess water. Curve 1 determined by Chernosky (1973) for the phase assemblage chrysotile, talc, forsterite, water; Curve 2 determined by Johannes (1968) for the assemblage chrysotile, brucite, forsterite, water; Curve 3 determined in this study for the assemblage lizardite, chrysotile, brucite, magnetite, olivine (Fo_{93}), water, with oxygen fugacity defined by IM buffer.

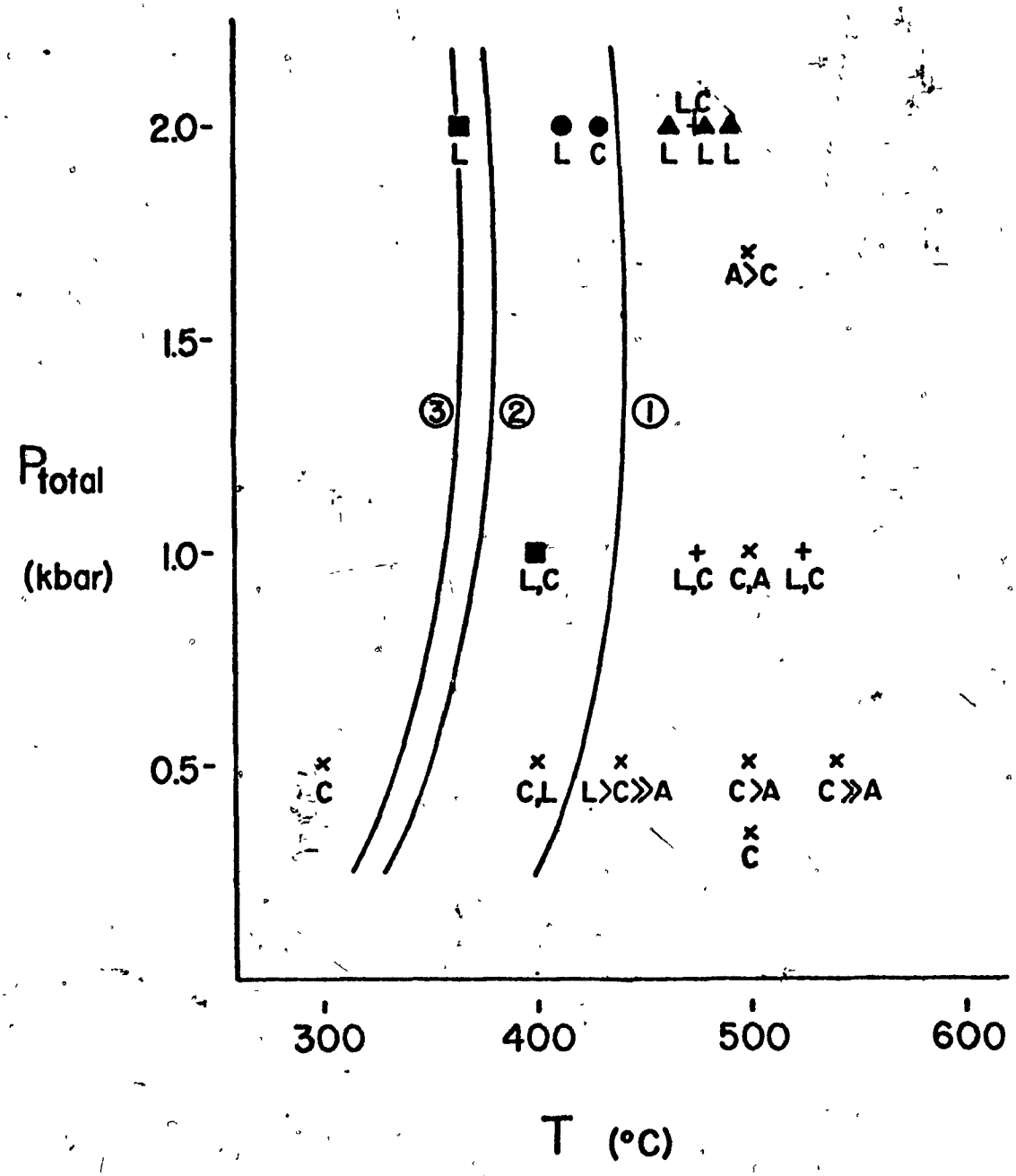
2.0
1.5
1.0
0.5
P_{total}
(kbar)
300
400
500
600
T (°C)
L
L C
L L L
L C
A>C
③
②
①
L,C
L,C
C,A
L,C
C
C,L
L>C≫A
C>A
C≫A
C

disequilibrium relationships, not surprising for runs lasting only five days.

Lizardite and chrysotile are believed to form a stable two-phase assemblage in the determination of the lower temperature brucite reaction by bracketing experiments (Curve 3, Figure 9). Experiment agrees with observations on natural assemblages because the occurrence of lizardite and chrysotile together is common in serpentinized dunites. All experiments relate to cases where water is in excess. The exact inter-relationship of lizardite, chrysotile, and antigorite in a composition and temperature diagram needs further study.

Brucite and Magnetite

Iron Content of Brucite

The iron content of brucites from partially and completely serpentinized ultramafic rocks are summarized in Table 33. It varies widely from 0 to 70 mole % $Fe(OH)_2$, with an average of about 15 mole % $Fe(OH)_2$. Hostetler et al. (1966), Page (1967a), Wicks (1969), Shteynberg and Chashchuklin (1969), and Evans and Trommsdorff (1972) have shown that: (1) brucite is enriched in iron compared to co-existing lizardite; (2) brucite usually has more iron than the parent olivine; and (3) lizardite has either more or less iron than the parent olivine.

TABLE 33

Summary of the iron content of brucite in serpentinites as determined from X-ray method of Mumpton and Evans (1965) and electron microprobe analysis. All examples are serpentinized dunites and have co-existing magnetite with brucite.

Serpentinite	mole % Fa*	% Serpentinized	Serpentine Mineralogy	Average Brucite mole % $Fe(OH)_2$
Dun Mountain,(1) New Zealand	8.5	58	L, minor C	16 (10.5-19.0)+
Hat Island,(1) Wash.	6	98	L, minor C	16.5 (5.9-24.7)
New Idria,(1),(2) Calif.		100	L + C	15 (11.4-17.7) 17
Twin Sisters,(1) Wash.	9.0	56	L	14 (11.4-16.0)
Burro Mountain,(1),(3) Calif.	7.5	54	L	13 (10.5-18.2) 18-32 (0-50)
Mount Albert,(4) Quebec	8-10	70	L	6-12 (6-42)
Muskox,(4) N.W.T.	20-15	70	L	60-70

*original composition of olivine, mole % fayalite

+numbers in parenthesis indicate the range of values found for brucite composition

(1) Hostetler et al. (1966), brucite composition determined by microprobe and chemical analysis

(2) Mumpton and Evans (1966), X-ray determination

(3) Page (1967a), X-ray and microprobe analysis

(4) Wicks (1969), X-ray analysis

The iron content of synthetic brucite in this study varies between 0-18 mole % $Fe(OH)_2$. In all types of experiments performed, more iron enters brucite at lower temperatures at constant pressure (e.g., Runs 3-12, 3-61 and 3-4, 3-1, Table 11). Iron enrichment may occur with increased run duration at constant T and P (Runs 3-25, 3-12, Table 11). Decreasing pressure at constant temperature may be correlated with a decrease in amount of iron in brucite (Runs 3-76, 3-74, 3-84 and 3-72, 3-71, Table 20). Iron-free brucite is formed in runs with an alkaline chloride fluid, but iron is present in brucite at lower temperatures ($< 330^{o}C$) in the NaOH fluid runs (Runs 3-46, 3-54, Table 13). Table 34 collates all the data on iron contents of phases and the production of magnetite. These data indicate that: (1) at constant pressure, the higher the temperature the greater the amount of magnetite produced; (2) the greater magnetite production correlates with lower iron content of co-existing olivine and brucite; (3) brucite has the highest iron content in the lowest temperature runs for the bracketing experiments at each pressure (3-76, 3-72, 3-78, and 3-70); and (4) in longer-duration hydration experiments small variations in iron content of brucite (5-10 mole % $Fe(OH)_2$)can be correlated with major amounts of magnetite formed (Runs 3-48, 3-1, 3-4 and 3-22).

Wicks (1969) noted that the absence of magnetite in some serpentinized dunites may be related to the production of an iron-rich brucite (e.g. Mayaguez Intrusion, Puerto Rico; Glen Urquhart Intrusion, Scotland).

TABLE 34

Correlation of iron content of olivine and brucite with magnetite production in the bracketing and hydration experiments.

Run	T(°C)	P(kbar)	Mole % Fa*	Δ**	Mole % Fe(OH)	Δ***	Amount of Magnetite
3-99	361	2.01	7	0	6(1)°	+2	major
3-76	344	2.01	11°°	-4	11(1)	-3	minor
3-74	341	1.48	5°°	+2	9(9)	-1	minor
3-72	332	1.48	7°°	0	11(1)	-3	minor
3-84	341	1.01	2	+5	4(4)	+4	major
3-71	330	1.00	5°°	+2	2(2)	+6	major
3-78	321	1.01			15(9)	-7	minor
3-70	322	1.00			13(1)	-5	major
3-97	336	0.54	7	0	7(2)	+1	major
3-68	322	0.56			0	+8	major
3-25	323	1.94	7	-2	2(2)		trace
3-12	321	1.99			7(7)		trace
3-61	302	1.93			18(1)		major
3-48	309	1.48			8(1)		major
3-1	302	1.01			10(1)		major
3-4	317	1.01			5(2)		major
3-22	304	0.54			6(2)		major
3-105	355	2.01	12°°	-5	7(2)		major
3-103	355	1.01	9°°	-2	5(5)		major
3-104	330	1.01	16°°	-9	6(2)		major

Table 34 cont'd

*composition of olivine at end of run, mole % fayalite

**change in the composition of olivine from the starting material olivine

***change in the composition of the brucite from starting material brucite

°error in the iron determination calculated from the error in d(001) of brucite determined from the least squares refinement

°°trace amounts of olivine remaining at the end of run

However, Wicks, Hostetler et al. (1966) and Page (1967a) have observed iron-bearing brucite co-existing with magnetite. Wicks suggested that the iron content of brucite may be related to the original iron content of the olivine (see Table 33); e.g., in the original dunite of the Muskox Intrusion, the olivine was iron-rich and then produced an iron-rich brucite upon serpentinization. If the iron content of the brucite depends on the original composition of the olivine, it provides an explanation for the limited range of iron content of the synthesized brucites: they may reflect the limited compositional range of the original olivines.

Page (1967a) related the brucite compositions at Burro Mountain, Calif., to the degree of serpentinization: (1) brucite in core rocks (least serpentinized) had the largest variation in iron content; the margin rocks (highly serpentinized) had the least variation (Table 33), and (2) the most iron-rich brucites occurred in moderately serpentinized rocks and in the late chrysotile-lizardite veins with a large production of magnetite. Page found no correlation between the primary rock type (dunite vs peridotite) and the iron content of the brucite.

Stability of $Fe(OH)_2$

Page (1966, 1967a) attempted to calculate thermodynamically the influence of Fe^{2+} on the brucite stability by assuming an ideal mixing model for the $Mg(OH)_2$-$Fe(OH)_2$ solid solution series. He considered the equation:

$$Mg_xFe_{1-x}(OH)_2 = xMg(OH)_2 + (1-x)FeO + (1-x)H_2O \quad (19)$$

to define his model. However, there is ample evidence in the literature (Shipko and Douglas, 1956; Linnenbom, 1958; Pritchard and Moull, 1971; Pritchard et al., 1971) from experiments performed in an oxygen deficient environment that the breakdown of ferrous hydroxide at temperatures below 560°C occurs by a different reaction:

$$3Fe(OH)_2 = Fe_3O_4 + 2H_2O + H_2 \quad (20)$$

Shipko and Douglas determined the following points about reaction (20): (1) $Fe(OH)_2$ was stable at room temperature and pressure in an oxygen-deficient environment; however the addition of small amounts of Ni^{2+} or Cu^{2+} "catalyzed" the reaction in the direction of the formation of magnetite even at room temperature; (2) at temperatures above 220°C, the reaction went to completion too rapidly to measure the amount of hydrogen evolved; (3) the reaction was inhibited at all temperatures by the presence of excess Fe^{2+}, OH^-, and dissolved silica; however at 316°C, excess Fe^{2+} had no effect on the decomposition of $Fe(OH)_2$; (4) minor α-Fe was found in the reaction products for the experiments above 178°C and this was attributed to the breakdown of initially-produced minor amounts of ferric hydroxide. Linnenbom (1958) reported similar results at 25°C, 1 atm for $Fe(OH)_2$ in an oxygen-deficient environment, but stated that it was converted to magnetite at 60°C and 300°C. Interestingly, Linnenbom reported

that leakage of air into the 25°C experiment caused the formation of magnetite. Pritchard et al. (1971) confirmed the results of the other studies on the decomposition of $Fe(OH)_2$ and found that magnetite produced from a solution of pH 10.5 at 200°C was different in grain size and stoichiometry (slightly deficient in Fe^{2+}) when compared to the magnetite produced at pH 13 at 230°C.

The stability of the brucite solid solution compared to its breakdown products (pure brucite, magnetite, water and hydrogen) is analogous to the annite-phlogopite stability reactions as determined by Eugster and Wones (1962) and Wones and Eugster (1965). Reaction (20) defines the breakdown of pure ferrous hydroxide and the equilibrium constant for that reaction is given by:

$$K_{20} = \frac{a_{Fe_3O_4} \quad (a_{H_2O})^2 \quad a_{H_2}}{(a_{Fe(OH)_2})^3}$$

With reference states as defined earlier, the equilibrium constant becomes:

$$K_{20} = \frac{(f_{H_2O})^2 \quad f_{H_2}}{(a_{Fe(OH)_2})^3}$$

The activity of ferrous hydroxide in the solid solution could be defined as:

$$a_{Fe(OH)_2} = \frac{\left[(f_{H_2O})^2 \quad f_{H_2}\right]^{1/3}}{\left[(f^*_{H_2O})^2 \quad f^*_{H_2}\right]^{1/3}}$$

where f_{H_2O} and f_{H_2} are the fugacities of hydrogen and water in equilibrium with the brucite solid solution and $f^*_{H_2O}$ and $f^*_{H_2}$ are the fugacities of hydrogen and water in equilibrium with the pure ferrous hydroxide at the same temperature and P_{total}. From the equilibrium constant, reaction (20) is driven to the right (towards magnetite, etc.) by decreasing either $[(f_{H_2O})^2 f_{H_2}]$ or by decreasing $a_{Fe(OH)_2}$ with f_{H_2O} and f_{H_2} constant. Experimental data are needed for reaction (20) as a function of temperature and fugacities of water and hydrogen, i.e., a study of the breakdown of pure ferrous hydroxide and brucite solid solution at different temperatures with various oxygen/hydrogen buffers. Thermochemical data are also needed on the brucite solid solutions. The difference between this formulation and that of Page (1966, 1967a) is that the brucite solid solution is defined here as a single phase consisting of two components ($Mg(OH)_2$ and $Fe(OH)_2$), and only one component need be considered thermodynamically to define the solid solution. However, from Page's treatment and considerations given above, the effect of increasing the $Mg(OH)_2$ component of the solid solution is to decrease the activity of $Fe(OH)_2$. Also, the thermal stability of end member component $Mg(OH)_2$ is much greater than $Fe(OH)_2$. Therefore, for the same values of f_{H_2O} and f_{H_2}, the assemblage Mg-rich brucite + magnetite is stabilized relative to the iron-rich brucite at higher temperatures.

A general trend of iron contents of brucite in the experimental results may be explained. A correlation exists between the amount of magnetite produced and the iron content of brucite: a smaller amount of magnetite

is associated with more iron in brucite; furthermore, the amount of magnetite increases with increasing temperature. These observations fit the experimental results and thermodynamic arguments on the stability of the brucite solid solution with respect to brucite + magnetite: Runs 3-76, 3-72, 3-78 and 3-70 of the bracketing experiments had a higher iron content in brucite and less magnetite than Runs 3-99, 3-74, 3-84, and 3-68, which were held at higher temperatures for each pressure and had more magnetite and less iron in the brucite. The iron content of the brucite may not only be an indication of the initial iron content of the olivine, but also an indication of the temperature at which serpentinization took place.

Martin and Fyfe (1970) reported that they did not observe the formation of magnetite in unbuffered experiments with a natural olivine (Fo_{85}) in temperature range of 200-300°C at 1.39 kbar and their X-ray cell edge data on brucite suggest that iron entered the brucite structure. Martin and Fyfe's experiments were done to determine the temperature of the maximum rate of reaction of olivine + water; they were conducted 50-75° C lower than those done in this study. The lack of production of magnetite follows the trend reported here.

The iron content of brucites formed during experiments with NaOH fluids (Table 13) follow the same trend as defined in the runs with olivine + water: the lower the temperature, the more iron-rich the brucite. No iron was found in the brucites formed from the reaction of olivine with alkaline chloride solutions (Run 3-95, 3-92), most probably due to the

solubility of ferrous iron in chloride solutions by the formation of a ferrous chloride complex.

Further Observations on Magnetite Occurrence

Wicks (1969) stated that most of the secondary magnetite produced during serpentinization is derived from reaction of olivine + water and only rarely from pyroxenes or amphiboles. He also noted from his detailed textural studies that magnetite has a high degree of mobility, causing a variation in textures, from the fine "dusty" particles formed in the initial stages of serpentinization to the formation of clots and stringers of magnetite in mesh textures, then to the concentration of magnetite at grain boundaries of the original olivine crystals. Wicks observed a possible parallel between the migration of the magnetite and the chemical homogeneity of lizardite in the mesh textures. Magnetite also rims primary spinels in serpentinites (Wicks, 1969; Bliss, 1972). Wenner and Taylor (1971) further recognized magnetite veinlets and euhedral magnetite grains in addition to the types described by Wicks (1969). The mode of occurrence of magnetite can be related to the type of serpentinite. Antigorite serpentinites have the largest amount of magnetite (Wenner and Taylor, 1971) and euhedral grains are very common besides clots and dusty magnetite. The lizardite-chrysotile serpentinites have a variety of different textural occurrences of magnetite generally with a much smaller amount of magnetite

(< 1-3%). The larger amount of magnetite in antigorite serpentinites is related to the higher temperatures considered to be necessary for the formation of antigorite compared to lizardite and chrysotile. Iron is probably lost from the brucite (and lizardite) to form magnetite as the serpentinite recrystallizes. Whether the recrystallization and the formation of antigorite takes place at constant or increasing temperature is conjectural, though petrologic observations and stable isotope data (Wenner and Taylor, 1971) indicate that antigorite forms at higher temperatures than lizardite or chrysotile.

Magnetite occurs in all run products as either fine micron size particles ("dusty") or as larger euhedral grains. The experimental results resemble the natural states of magnetite aggregation. Runs 3-32 and 3-48 used the same starting material and were held at the same temperature and pressure, however, Run 3-48 lasted almost twice as long as Run 3-32. The magnetite in Run 3-32 was very fine grained (< 1 μm), evenly disseminated through the serpentine, whereas magnetite in Runs 3-48 had begun to aggregate and form larger euhedral crystals. Besides longer run duration at a given temperature and pressure, higher temperatures can promote the formation of larger grains of magnetite and euhedral crystal forms.

The Bracketing Experiments - Equilibrium Determination

Evaluation of Influence of Iron on Lower Thermal Stability of Olivine

Table 35 summarizes the experimental data on reactions involving

TABLE 35

Equilibrium temperatures and pressures determined from reversed experiments for reactions involving serpentine. Curves as shown in Figure 9.

Johannes (1968) $2Mg_2SiO_4 + 3H_2O = Mg_3Si_2O_5(OH)_4 + Mg(OH)_2$ (1)

forsterite; clinochrysotile; brucite

	T(°C)	P(kbar)	T(°C)*	P(kbar)*
lower stability limit for forsterite	350 (10)**	0.5		
	365	1.0	390	1.0
	380	2.0	420	2.0
	400	3.5		
	420	5.0		

this study $10(Mg_{1.86}Fe_{0.14})SiO_4 + 14.20H_2O = 5Mg_3Si_2O_5(OH)_4 + 3.8Mg_{0.95}Fe_{0.05}(OH)_2 + 0.40\ Fe_3O_4 + 0.4H_2$ (21)

olivine; lizardite, clinochrysotile; brucite; magnetite

lower stability limit of Fo_{93}	335 (5)**	0.5		
	348	1.0	365	1.0
	366	2.0	410	2.0

Chernosky (1973) $6Mg_2SiO_4 + Mg_3Si_4O_{10}(OH)_2 + 9H_2O = 5Mg_3Si_2O_5(OH)_4$

forsterite; talc; clinochrysotile

upper stability limit for chrysotile (and probably lizardite)	420 (10)**	0.5		
	427	1.0	470	1.0
	441	2.0	510	2.0
	466	4.0		
	478	5.0		

Table 35 cont'd

*temperatures calculated for a given pressure from thermodynamic data (Olsen, 1963) for comparison with the experimentally determined temperatures and pressures on the left

**uncertainty in the temperature determination as quoted by the authors

olivine (Fo_{100} and Fo_{93}). The forsterite + talc + serpentine + water reaction (Reaction (2)) defines the upper stability limit for chrysotile (and probably lizardite) because an iron-bearing olivine + talc would shift the curve to lower temperatures as has been demonstrated for Reactions (2) and (21) (Table 35). The equilibrium curve for this reaction for an olivine Fo_{93} is shifted 15°C downwards (to lower temperatures) from the curve for pure forsterite as determined by Johannes (1968). Olsen (1963) calculated curves for the reactions of interest from thermochemical data; the curves plot at higher temperatures for a given pressure when compared to the experimentally determined curves. The error between the calculated and experimental curves is directly related to the quality of thermochemical data, especially data for chrysotile and talc (Chernosky, 1973). Note that Bowen and Tuttle's (1949) original unbuffered experiments with a natural olivine (Fo_{90}) agree with the determined equilibrium curve for Reaction (21):

T(°C)	P(kbar)	Run Duration hrs	Products
365	1.02	336	olivine
340	1.02	336	serpentine, brucite, magnetite

This does not imply, however, that a higher oxygen fugacity does not influence the reaction.

Evans and Trommsdorff (1972) and Trommsdorff and Evans (1972) have measured the Mg/Fe ratios of co-existing minerals in antigorite schist of

the southern Bergell Alps. From the Mg/Fe ratio of co-existing brucite and antigorite, Evans and Trommsdorff (1972) calculated a shift of 1-2°C at a standard state pressure of 2000 bars from the univariant curve for the reaction forsterite + water to an olivine of composition Fo_{90} in equilibrium with an antigorite of composition $Mg_{5.78}Fe_{0.22}Si_4O_{10}(OH)_8$ and a brucite of composition $Mg_{0.91}Fe_{0.09}(OH)_2$. The uncertainty in their analysis lies in the assumptions: (1) the activity of water was calculated as if pure water were the gas phase; (2) the activity coefficients for Mg in the solid solutions (brucite, antigorite, and olivine) are equal to one; (3) iron contents of the three minerals are equilibrium distributions; and (4) the conditions (P, T, f_{H_2}, etc.) for formation of the antigorite serpentines are similar to those involved in the formation of lizardite-chrysotile serpentinites. The experimental work and calculated f_{H_2} and f_{H_2O} have shown that the gas phase defined by the IM buffer or by the assemblage M-A is a hydrogen-rich, water-deficient vapor i.e. $f_{H_2} > f_{H_2O}$. Evans and Trommsdorff stated that the plot of log a_{H_2O} vs 1/T (Arrhenius plot) was somewhat curved. According to Orville and Greenwood (1965) a curved plot of log f vs 1/T is an indication that enthalpy for the reaction is not constant or alternatively that the P_s (pressure on the solid phases) is not constant. Observations discussed previously showed that magnetite is always present as a run product. The amount of magnetite produced increases with temperature as the equilibrium curve is approached and correlates with a decrease in the amount of iron in brucite. The composition

of brucite immediately adjacent to the equilibrium curve showed an average composition of $Mg_{0.95}Fe_{0.05}(OH)_2$ and a loss of iron compared to the starting brucite composition at all temperatures and pressures investigated. The iron analyses of co-existing lizardite, chrysotile and antigorite from natural occurrences indicate that the amount of iron in the brucite is much greater than the amount of iron tied up in the serpentine. This may also be true in the synthetic lizardites, though direct confirmation is lacking. In summary, the introduction of iron into the system $MgO-SiO_2-H_2O$ (even a small amount such as 7.6 wt. % FeO in Fo_{90}) may lead to a change in the gas phase (production of H_2) and consideration not only of iron partitioning among serpentine and brucite, but its appearance as magnetite. The simplified equation (serpentine + brucite = 2 forsterite + 3 water) used by Evans and Trommsdorff (1972) does not accurately describe the iron-bearing system.

Tentative Thermodynamic Data Derived from the Equilibrium Curve

Zen (1969, 1971, 1972) and Gordon (1973) have developed methods of deriving thermochemical data from reversed equilibrium curves. Zen (1973) extended his previous analysis to include redox reactions controlled by oxygen buffers. In attempting to use Zen's (1973) analysis to derive a ΔG_f^o (25°C, 1 atm) for serpentine, several problems were found to seriously affect the validity of the calculation except to prove the internal consistency of the experimental data:

(1) the non-ideal H_2-H_2O mixing model proposed by Shaw (1963, 1967) and extrapolated by Zen (1973) cannot easily be applied to hydrogen-rich gas mixtures such as defined by IM buffer at low P and T of reaction studied;

(2) the serpentine mineralogy is not single-phase: both lizardite and chrysotile appear to co-exist stably as products of the reaction and ΔG_f^o of a two-phase assemblage has little rigorous thermodynamic application;

(3) there are major discrepancies in available thermochemical data necessary for the calculation, e.g., 1.38 kcal/gfw difference in ΔG_f^o (25°C, 1 atm) for forsterite (King et al., 1967; Robie and Waldbaum, 1968);

(4) the iron content of the serpentine minerals is small but unknown; the iron content of brucite is known, but no thermochemical data are available on brucite solid solution or the olivine solid solution, only on the end members.

Therefore, the reaction investigated will not be used to derive thermochemical data, though preliminary calculations done ignoring these problems show that the experimental data are internally consistent. However, the difficulties in defining the gas mixture for the IM buffer will be outlined.

Table 36 presents data and calculations for the IM buffer for the equilibrium temperatures at P_{total} equal to 1000 and 2000 bars. The parameter Ψ is a measure of the departure of the gas mixture from ideality

TABLE 36

Results of calculations based on a large extrapolation of the equation of state for hydrogen-water mixtures of Shaw (1963, 1967) as modified by Zen (1973). Note that the values are given only to illustrate the method and to show the extremely high implied values of hydrogen fugacity. The results are qualitatively consistent with experimental observations but the numerical values of hydrogen and water fugacities may be subject to large and unknown errors (Shaw, 1974, pers. comm.).

T_e = 621^oK		T_e = 639^oK
P_e = 1000 bars		P_e = 2000
K_w = 8.15×10^{17}		2.14×10^{17}
f_{O_2} = 7.42×10^{-39} bars		4.69×10^{-37} bars
$f^o_{H_2}$ = 1326 bars		3642 bars
f^o_w = 172.4 bars		310 bars
Y = 0.54		1.719
Ψ = 0.098		0.095
$\frac{P\Psi}{RT}$ = 1.888		3.580

as is given by the approximation (Shaw, 1967):

$$\Psi = 0.0098 + 54.4/T \qquad (T, {}^{o}K; \quad \Psi, \text{ liters/mole}).$$

Shaw stated that the accuracy of the expression for Ψ falls off rapidly at temperatures below 500°C. The parameters Y and A were defined by Zen (1973) to recast the results of Shaw (1963, 1967) in different graphical form more readily applied to thermochemical calculations:

$$Y = a_{H_2O}/a_{H_2} = \frac{K_w \, f^{o}_{H_2} \, (f_{O_2})^{1/2}}{f_{H_2O}}$$

and

$$A = \frac{P\Psi}{RT} \qquad \text{(for an ideal gas A = 0).}$$

The values for Y are 0.54 and 1.72 and for A are 1.89 and 3.58 at 1 and 2 kbar, respectively (Table 36). Zen (1973, p. 71, Fig. 1) did not plot values of Y less than 1.0 and values of A greater than 2.2 on his a_{H_2} vs a_{H_2O} diagram. Shaw (1967) does not consider value of A greater than 1.4 and Zen (1973) warns further that the equation of mixing proposed by Shaw is only valid within limited values of A. Phase separation is predicted for mixtures obeying the equation defined by A with critical mixing reached at A = 2.0. Prediction of the activity of hydrogen and water in the hydrogen gas mixtures defined by the IM buffer in the temperature range below 500°C awaits further theoretical and experimental work (E. Zen and H.R. Shaw, pers. comm., 1973) well beyond the scope of this present study.

Rate of Reaction

Martin and Fyfe (1970) studied the rate of reaction of forsterite + water to form serpentine + brucite. They found that the maximum conversion of forsterite (60-75%) occurred at 260°C with run durations of up to 6 days. The temperature of maximum conversion is 100°C lower than the equilibrium temperature determined by Johannes (1968) at that pressure. The rate of reaction falls off rapidly away from the maximum as the univariant curve is approached. Their results on an iron-bearing natural olivine (Fo_{85}) were comparable to the synthetic forsterite with a decrease in reaction rate attributed by Martin and Fyfe to the increase in grain size of olivine rather than to change in composition. Their conclusion that the rate of reaction increases with increased amounts of water is not strictly valid as the equilibrium temperature at a given pressure is approached. All of the experimental work on determination of serpentine stability curves have shown the reactions to be very sluggish close to the equilibrium curve even in the presence of excess water.

Martin and Fyfe postulate that the mechanism of the forsterite + water reaction involves surface nucleation and growth at certain active sites on a reactant surface (brucite). There is no evidence from the SEM work that serpentine nucleates on a brucite substrate as they postulate, at least in the T,P range investigated here.

Reaction of Olivine with Fluids Other Than Water

There is essentially no difference in the mineralogy of serpentine or the nature of the other phases obtained from the reaction of olivine with the fluids other than water investigated in this work, except that NaCl fluids caused increased dissolution of olivine, but little formation of reaction products. In contrast, Korytkova and Makarova (1971) and Korytkova et al. (1972) reported the formation of antigorite by reaction of olivine (Fo_{85}) with alkaline (NaOH) and silica-bearing fluids at 250-300°C, 0.5-0.9 kbar in unbuffered experiments. Korytkova et al. (1972) observed formation of lizardite and chrysotile in the same T,P range as antigorite for the reaction of olivine with water and weak acid; these results agree with those obtained in this study at higher temperatures and pressures. Increase in the rate of reaction of olivine was also noted by Korytkova et al. (1972) for alkaline fluids compared to water and acid solutions. However, only 30% of their olivine was converted to lizardite (+ minor chrysotile) at 300°C, 0.5 kbar with pure water after 720 hours, much less than observed in this study at the same T,P (see Appendix 2, Run 3-22). Korytkova et al. (1972) reported magnetite as a product of the reactions with alkaline fluids. The products from the reaction of olivine with water were stated to consist of a dark-grey material, from which the presence of magnetite can be inferred. Nothing was stated by Korytkova et al. (1972) about the product from acid treatment to indicate the presence or absence of magnetite. Brucite was not mentioned as a product of any of the reactions, though the

distinctly well-developed hexagonal platelets co-existing with antigorite and chrysotile (Korytkova et al., 1972, Fig. 1b) may be brucite.

Korytkova et al. (1972) state that the pH of the fluid is the principal factor in the formation of lizardite vs antigorite. The experimental fluids in the present study are alkaline, as are natural waters that co-exist with lizardite as well as antigorite (Barnes and O'Neil, 1969; Barnes et al., 1972). However, it is quite possible that the formation of antigorite is enhanced by silica-bearing fluids at low temperatures and pressures as observed by Korytkova et al. (1972) because the composition of natural antigorites commonly have a greater wt. % SiO_2 compared to the ideal serpentine composition of $Mg_6Si_4O_{10}(OH)_8$ (Whittaker and Wicks, 1970); silica in the fluid may be stabilizing antigorite. Korytkova and Makarova (1971, 1972) and Korytkova et al. (1972) do not give the concentration of silica in fluid used in their experiments, which prevents comparison of their results with this work where antigorite was not observed. If the above postulate is correct, it is probable that the silica concentrations in their fluids were higher than those used in this study. Their experiments were conducted at a higher oxygen fugacity than those buffered by IM, probably promoting magnetite formation rather than iron for magnesium substitution in serpentine minerals and brucite. It has been observed that chrysotile forms after lizardite both in experiments (Korytkova et al., 1972; this study) and in textural observations of natural minerals (Wicks, 1969). Whether chrysotile is replacing lizardite is difficult to assess, though its later formation compared to lizardite perhaps indicates a nucleation barrier.

Composition of Serpentinizing Fluids

Compositions of fluids co-existing with serpentine minerals have been measured at a variety of temperatures, pressures, and run durations (see Table 37). Factors that must be considered in evaluating the measured concentrations of Mg and Si in solutions co-existing with serpentine and forsterite are:

(1) a difference has been shown for measured Mg and Si concentrations in solution depending on whether the mineral-fluid system was open or closed to the atmosphere; Wildman et al. (1968) and Luce (1969) have determined differences in measured Mg and Si as a function of CO_2 concentration in fluid;

(2) run duration was critical because Luce (1969) and Luce et al. (1972) have demonstrated that the dissolution of serpentine (lizardite and chrysotile) and forsterite are controlled by short-term incongruency and long-term congruency;

(3) differences in starting materials influence the short-term dissolution of magnesium silicates; synthetic material may be highly soluble due to incomplete reaction during the synthesis of the phase (Bricker et al., 1973) or due to its fine-grained, poorly crystalline nature; minerals can also present problems in solubility determinations due to small amounts of impurities (Hostetler and Christ, 1968) e.g. an "amorphous" material has been found filling the hollow tubes of chrysotile (Martinez and Comer, 1964), which would influence the short-term solubility and thus the measured amounts of Mg and Si in solution;

(4) with lizardite or chrysotile + distilled water, the pH of the fluid reaches a steady state value of 9.4 in a nitrogen atmosphere, whereas the pH of the fluid open to the atmosphere is buffered at 7.7, and the pH of the fluid does control the short-term incongruent dissolution of these minerals (Luce, 1969);

(5) Wildman et al. (1968, 1971) have defined the co-existence of brucite and serpentine as a function of dissolved Mg, SiO_2 and pH at 25°C, 1 atm and concluded from their measurements of the fluid co-existing with serpentinite in a nitrogen atmosphere that the composition of fluid is controlled by serpentine solubility rather than by brucite solubility.

TABLE 37

Measured molality of fluids co-existing with natural and synthetic serpentine and olivine at a variety of temperatures and pressures.

Phase	T(°C)	P(bars)	Run Duration hrs	pH	Molality Mg (10^5)	Molality SiO_2 (10^5)	Ratio Mg/Si	Reference
syn. C	90	1	1615	7.69	15.2	4.4	3.5	Hostetler & Christ (1968)
+C (S-2)	90	1	1227	7.70	14.0	3.8	3.7	Hostetler & Christ (1968)
*nat. C	260	1000	2160	7.12	15.0	1.9	7.9	Moiseyev (1974)
*nat. C	260	1000	1176	6.48	5.4	4.4	1.2	Moiseyev (1974)
L,C (3-69)	311	560	895		17.7	n.d.		this study
L,C (3-71)	330	1000	792		23.4	46.6	0.5	this study
++nat. L	25	1	119	8.57	3.7	4.2	0.9	Luce et al. (1972)
++nat. C	25	1	6480	9.02	8.3	8.2	1.0	Luce (1969)
++nat. O(Fo_{91})	25	1	118	9.99	15.0	0.7	21.0	Luce et al. (1972)

syn. = synthetic, nat. = natural

+locality, New Idria, Calif.

++lizardite, Morgan Hill, Calif., chrysotile, 19N16313, Thetford Mines, Quebec

*locality not given

The major factors controlling the composition of the fluid in contact with these minerals are: pH, presence or absence of dissolved CO_2, the phase and its composition, surface area of the phase in contact with the fluid, and duration of the experiment until a steady state is reached. Luce (1969) and Luce et al. (1972) showed the importance of time as incongruent dissolution becomes congruent dissolution after a minimum of 60 days, because Luce accepted Hostetler and Christ's (1968) two month experiment as congruent dissolution of chrysotile. Moiseyev's (1974) experiments may indicate that the dissolved CO_2 initially present in the distilled water or the starting material (a natural chrysotile) influenced the larger observed measured solubility of Mg and Si than would be predicted by an equilibrium calculation. Any equation written for the dissolution of chrysotile (or lizardite) contains a pH term which is then raised to some power in the equilibrium constant:

$$Mg_3Si_2O_5(OH)_4 + 5H_2O = 3Mg^{2+} + 6OH^- + 2H_4SiO_4 \qquad (22)$$

(Hostetler and Christ, 1968)

where

$$K_{22} = (a_{Mg^{2+}})^3 (a_{OH^-})^6 (a_{H_4SiO_4})^{2+},$$

with activity of water equal to one. Therefore, in calculation of the equilibrium constant for the reaction from measured Mg, Si and pH of the fluid phase, the fluid must reach a steady state pH (equilibrium pH) with the mineral. The OH^- term in the equilibrium constant for the above reaction is raised to the 6th power, introducing an appreciable error in the calculated K_{22} if the steady state pH has not been attained.

In analyzing the problems that others have had with the determination of solubility of chrysotile and lizardite, it is not surprising that the measured Mg and Si concentrations in this study are also difficult to interpret. As an additional complication, the small volume of the sample solution requires dilution. This introduces an appreciable error in some of the results due to detection limit problems, especially with regard to silica. The variables stated above for the dissolution of the Mg silicates are applicable to the fluid compositions determined in this study: pH, mineral phases present (starting material and products), run duration, temperature, pressure and initial fluid composition. The only possibility of interpretation without more detailed, systematic work is to indicate some of the trends shown by the data.

In all of the runs with pure water in which silica was detected in the fluid, the molar ratio Mg/Si was less than 1.0. This may indicate incongruent dissolution but factor (3) discussed above should be considered as well as the unknown effect of brucite on the measured amount of Mg (measurement of Mg should consider equilibrium with both Mg phases serpentine and brucite). In the experiments of Luce (1969) and Luce et al. (1972) on the incongruent dissolution of these minerals, Mg was found to enter the aqueous phase faster than Si. In the present study, the very alkaline nature of the fluid (pH > 10) influenced the initial leaching and exchange of Si between the solid and fluid, to a greater extent than with

Mg. However, there were many experiments in which Si was not detected in the fluid phase, most probably due to detection limit problems. Greater amounts of Mg were detected at all temperatures and pressures with fluids other than pure water, attesting to the fact that the alkaline and alkaline chloride solutions had greater solvent properties for Mg than pure water.

Only preliminary calculations of fluid compositions in equilibrium with the solid phases of reaction (21) can be attempted because of the complexity and multiplicity of possible reactions and the paucity of thermodynamic data at higher temperatures. A new set of calculations are clearly required because Helgeson's (1969) dissolution data for higher temperatures pertain to acid chloride solutions. Alkaline solutions without chloride appreciably affect the type and distribution of aqueous species in the fluid.

Preliminary calculations of fluid compositions show that $Mg(OH)^+$ predominates over Mg^{2+} and that $H_3SiO_4^-$ is probably more important than H_4SiO_4 at the high pH of these fluids. The available data do not allow calculation of aqueous silica species at 300°C or above (W. Nesbitt, pers. comm., 1974). The effect of pressure on species distribution in these dilute solutions is also difficult to evaluate. The preliminary calculations show that the Mg content of the fluid is too high to be controlled by equilibrium with brucite. Calculation of possible fluid compositions in equilibrium with chrysotile or lizardite is not feasible without data on aqueous silica species at these elevated T and P.

The measured composition of the fluids does not differ appreciably from compositions of waters co-existing with serpentinized or partially serpentinized ultramafic rocks. The pH is the same (i.e., the fluid is very alkaline) though the dissolved Mg is higher in the experiments than in natural waters. From thermodynamic data at 25°C, 1 atm, Barnes and O'Neil (1969) and Barnes et al. (1972) calculated the fluid composition expected if equilibrium with chrysotile and brucite is attained. They found the natural waters to be supersaturated with respect to both phases. Brucite, in fact, was observed to precipitate at the orifice of Complexion Spring (Luce, 1971). For both the natural waters and the fluids from the experiments, a large degree of supersaturation may be needed before serpentine or brucite will nucleate from solution.

Application of Experimental Results

Martin (1971) has written an excellent review paper concerning the processes of serpentinization based on experimental work and observations of serpentinites. The purpose of this section is to bring Martin's analysis up to date in light of this study and other investigations done since the late 1960's.

Evidence on Serpentinization from Equilibrium Determinations and Mineralogy of Phases

The equilibrium temperatures and pressures for the following assemblages have been determined in the presence of pure water (Table 35):

chrysotile-brucite-forsterite	(to 6.5 kbar)	(Johannes, 1968)
lizardite-chrysotile-brucite-magnetite-olivine (Fo_{93})/IM	(to 2.0 kbar)	(this study)
chrysotile-talc-forsterite	(to 7.0 kbar)	(Chernosky, 1973)

The presence of iron in the assemblage forsterite + water shifts the pertinent curve to lower temperatures. The mineralogy of the phase assemblages is equivalent to that observed in serpentinized dunite. The inter-relationship of chrysotile and lizardite cannot be determined from the work done in the forsterite + water system because both reactions (Johannes, 1968; Chernosky, 1973) were determined from a starting mix composed of chrysotile only. Work in the iron-bearing system demonstrates the co-existence of both serpentine minerals within the duration of the experiments; however, the detailed textural observations of Wicks (1969) on natural occurrences of the two minerals suggest the replacement of lizardite by chrysotile in the later stages of serpentinization. The large majority of serpentinized rocks are composed of lizardite only or of lizardite + chrysotile (Wicks, 1969; Aumento, 1970; Wenner and Taylor, 1971, 1973). With a geothermal gradient of 30°C/km, olivine would be transformed to serpentine + brucite + magnetite above depths of about 12 km. With less steep geothermal gradients, the phase assemblage serpentine + brucite + magnetite could persist to greater depths.

The relationship between serpentine mineralogy and bulk composition is not yet entirely clear. The composition of serpentine minerals show distinct

substitutions of iron (Fe^{2+} and Fe^{3+}) and aluminum in all three serpentine minerals with the largest substitutions of Fe and Al in lizardite and antigorite (Whittaker and Wicks, 1970). The iron and aluminum in the minerals may be a reflection of the bulk composition of the parent rock rather than being essential constituents in the formation of lizardite or antigorite as has been suggested by many authors. Chernosky (1973) has documented the effect of Al on serpentine mineralogy: most natural serpentine compositions are Al-poor, well within Chernosky's two-phase field of lizardite + chrysotile. The work of Iishi and Saito (1973) was critical in demonstrating that lizardite, chrysotile and antigorite can be produced simply by varying the ratio of the major component oxides: $MgO:SiO_2:H_2O$. Thus, the bulk iron content of the olivines used in this study, should not affect the formation of lizardite + chrysotile.

The stability of antigorite versus lizardite and chrysotile has not been evaluated experimentally. Field evidence indicates that antigorite may be stable to higher temperatures in a regional metamorphic environment. Appearance of antigorite may reflect a water-deficient environment. Korytkova and Makarova (1971) and Korytkova et al. (1972) showed further that antigorite did form from the action of alkaline silica-bearing fluids on olivine at low temperatures and pressures. Their studies point to a chemical control of the formation of antigorite. Certainly high pressure is not required, though increased pressure or directed pressure may cause partial dehydration of lizardite or chrysotile, aiding in formation of antigorite.

The iron content of brucite does not influence the position of the equilibrium curve determined for the phase assemblage lizardite-chrysotile-brucite-magnetite-olivine(Fo_{93})/IM. The iron content of the brucite at an oxygen fugacity defined by the IM buffer or the natural assemblage M-A appears to indicate temperatures of reaction below the equilibrium curve. Magnetite + brucite form at the expense of iron-bearing brucite as temperatures are increased to the equilibrium curve. At oxygen fugacities higher than IM or M-A at the same T,P, the iron would probably not enter brucite, but would form magnetite, though further work with different oxygen fugacity buffers is needed to clarify this point. The ubiquitous occurrence of magnetite-awaruite is important with respect to defining the oxygen-deficient conditions during serpentinization.

Evidence on the Nature of the Fluid Phase

The fugacity of water is less than P_{total} if the fluid phase contains additional components. The experimental work and calculations done in this study show that the gas phase was made up of H_2 and H_2O with $f_{H_2} > f_{H_2O}$, though water was still present in excess compared to the amount needed to convert all the olivine to serpentine + brucite + magnetite. There may not always be an excess of water in the natural environment, and in a closed system H_2 may build up to the point of having a major effect on the activity of water in the fluid phase. For other dissolved constituents

(except CO_2) the comparative decrease in activity of water is not likely to affect serpentinization to an appreciable extent. For example, Helgeson (1969) has calculated that the activity of water decreases to 0.919 for a 3 M NaCl solution at 270°C, 1 atm indicating that a large concentration of dissolved inorganic material may not lead to a substantial decrease in the activity of water in the fluid.

Present experimental evidence and observations on natural waters indicate that the fluids reacting with olivine to form serpentine or fluids in contact with serpentinite are very alkaline (pH > 9). Such fluids are reactive and have the possibility of carrying significant quantities of dissolved silica. The fluid phase is also likely to be extremely reducing (H_2 rich) if serpentinization is taking place at other than surface conditions in a closed or partly closed environment where H_2 cannot readily escape. However, the CO_2 content of the fluid phase must be very low because serpentine is not stable with respect to talc in CO_2-bearing fluids due to the decrease in the activity of water (Johannes, 1969). Dilute fluids resembling those used in the experiments with pure water do not carry appreciable amounts of dissolved constituents (av. 4.8 ppm Mg and av. 10.4 ppm Si). However, the NaCl, NaOH, and alkaline chloride solutions carried increased quantities of Mg, but Si was similar to pure water experiments (av. 11.0 Mg and 9.6 ppm Si). The silica concentration in fluids from the experiments is controlled by pH; the pH of both the pure water and other fluids was alkaline (pH > 10). Note that the experiments

done with NaCl (without NaOH) showed a large dissolution effect, but did not favor reaction to serpentine during the experiment. The concentration of present day sea water is about 0.47 M NaCl (Stumm and Morgan, 1971), approximately twice as concentrated as the NaCl fluids used in the experiments. Sea water is still a possible fluid for serpentinization given longer reaction times and lower temperatures; experimentally the alkaline chloride fluid (NaOH + NaCl) was effective in reaction of olivine to form serpentine.

The ability of the fluid to carry dissolved constituents has an important bearing on the constant volume versus constant chemical composition arguments presented in the INTRODUCTION. The fluid properties, such as pH, presence or absence of Cl^-, determine which elements may be leached and possibly transported by the fluid. The composition of dissolved constituents in the pure water experiments would not indicate widespread removal of Mg or Si. However, the alkaline chloride and NaCl fluids are capable of removing larger amounts of Mg. Barnes et al. (1972) have found spring waters in contact with partially serpentinized ultramafic rocks to have variable contents of dissolved silica, though the amount of dissolved Mg was always lower compared to that in fluids from completely serpentinized rocks. The complexity of the interrelated factors that control the composition of the fluid phase, coupled with the difficulties of calculation of the composition of the fluid in equilibrium with serpentine + brucite + magnetite, do not allow more than the above general statements to be made about the fluid phase.

The kinetic studies of Martin and Fyfe (1970) showed that the reaction of olivine to form serpentine + brucite was initially surface- and solution-controlled until the olivine becomes surrounded by serpentine + brucite after which it becomes controlled by the rate of diffusion of fluid to the olivine-serpentine interface. The accessibility of water to the olivine can be increased by shearing, fracturing, and faulting of the ultramafic body; this increases surface area and thus the rate of serpentinization. The volume of fluid is important with respect to possible metasomatic effects; these will be minor if a fixed volume of fluid remains in a closed environment, without significant removal, but could be major if fresh fluid has continuous access to the rock body in an open, highly sheared environment. The experimental work in this study gives limited insight to this particular problem because the experiments were done in a water-excess environment and in a closed system geometry.

SUMMARY

Oxygen Fugacity

Evaluation of the efficiency of the iron-magnetite (IM) buffer by examination of the buffer material, and the presence of a gas and fluid phase at the end of the experimental runs, indicates that the oxygen fugacity can be defined by IM buffer to temperatures as low as 300°C at 0.5 kbar total pressure. Thermodynamic calculations of the fugacities of oxygen, hydrogen and water show that the gas phase in the presence of IM is oxygen-deficient, hydrogen-rich and water-poor: $f_{H_2} > f_{H_2O}$, with $f_{O_2} < f_{H_2O}$. Similar calculations for the assemblage magnetite-awaruite (M-A) demonstrated that the gas phase is similar in f_{O_2} to that co-existing with IM: the gas phase is also oxygen deficient and is hydrogen-rich, but contains more water than was the case with IM. The fugacities of hydrogen and water presented for the assemblages IM and M-A were calculated assuming an ideal mixing model (Eugster and Wones, 1962) and the calculations yield extremely high values for f_{H_2}.

Application of the H_2-H_2O mixing model of Shaw (1963, 1967) as extrapolated by Zen (1973) does not yield satisfactory results on the prediction of the activity of hydrogen and water in these mixtures. Therefore, though the calculated values of f_{H_2} and f_{H_2O} are qualitatively consistent with

experimental observations, the actual numerical values of f_{H_2} and f_{H_2O} presented in Appendices 1b and 1c (Figures 3 and 7) may be subject to large and unknown errors.

The conditions that lead to the formation of the assemblage IM or M-A during serpentinization are quite different than what is commonly thought to be the normal crustal f_{O_2} environment, closer to the f_{O_2} defined by the QFM or HM buffers (Eugster, 1972). The ubiquitous assemblage M-A in natural serpentinites thus provides a definite indicator of a locally extremely reducing, hydrogen-rich environment.

Serpentine Mineralogy

Lizardite and chrysotile are the serpentine minerals observed in all experiments: no evidence for antigorite was found in the X-ray, optical or SEM work. The range in the unit cell parameters of lizardite, from results of least squares refinements of Guinier powder patterns, are:

a (A)	=	5.278	-	5.380
b (A)	=	9.143	-	9.211
c (A)	=	7.290	-	7.329
V (A^3)	=	355.08	-	361.73

The bracketing and dehydration experiments feature much smaller variation of the lizardite cell dimensions than noted above for the hydration and variable fluid composition experiments. With time, the lizardite became

better formed structurally as inferred by development of euhedral crystals and demonstrated by the cell dimensions. Theoretical considerations of the effect of composition on cell edge of lizardite lead to the conclusion that small amounts of iron (< 10 wt. % FeO) would be difficult to detect by variations in cell edges; this conclusion also has been demonstrated experimentally for small amounts of Al in serpentine in the two-phase, lizardite + chrysotile, compositional field. The temperature and pressure of formation cannot be correlated with observed cell edge variations in lizardite. Chrysotile, though present in almost all runs, did not in most cases yield a satisfactory least squares refinement of the X-ray powder diffraction data, probably due to the fact that lizardite was usually present in amounts greater than chrysotile.

From the Scanning Electron Microscope (SEM) data the following crystal forms of serpentine were observed:

lizardite - massive plates, laths, and euhedral, hexagonal crystal forms

chrysotile - fibers, laths and fiber bundles

All the crystal forms have been observed in natural specimens with the exception of the hexagonal stubby crystals of lizardite. The most common forms were massive, platy lizardite and chrysotile fibers. There may be a temperature control on the formation of lizardite laths in that they were only observed in runs conducted at temperatures greater than 315°C; no such control was noted for any of the other morphological forms of lizardite or chrysotile. "Chrysotile" laths do not appear to persist with increased run duration.

Lizardite and chrysotile appear to form a stable two-phase assemblage that has been observed commonly in natural serpentinites. Iishi and Saito (1973) have shown that Fe^{3+}, Fe^{2+}, and Al^{3+} are not necessary for the formation of lizardite or antigorite by synthesizing all three serpentine minerals (lizardite, chrysotile and antigorite) by varying the ratio of the major component oxides of serpentine ($MgO:SiO_2:H_2O$) in a water-deficient environment. The effect of bulk composition was further emphasized by the work of Korytkova and Makarova (1971), who produced antigorite from the reaction of olivine with silica-bearing fluids at 250-300°C, at less than 1.0 kbar. It appears doubtful then that the iron content of the olivine influenced the formation of lizardite in this experimental work.

Brucite and Magnetite

Brucite and magnetite were observed in all experimental runs. The iron content of brucite was shown to be related to the amount of magnetite produced: the smaller the amount of magnetite, the larger the iron content of the brucite. The iron content of the brucite varies between 0-18 mole % $Fe(OH)_2$, though the variation observed in natural brucites is much larger attaining 70 mole % $Fe(OH)_2$. Furthermore, the amount of magnetite produced increases with temperature. Experiments in an oxygen-deficient atmosphere have documented that the breakdown of ferrous hydroxide occurs by the following reaction:

$$3Fe(OH)_2 = Fe_3O_4 + 2H_2O + H_2. \qquad (20)$$

The stability of brucite solid solution with respect to brucite + magnetite can be defined by Reaction (20) if $Fe(OH)_2$ is considered to be the mole fraction of ferrous hydroxide in the solid solution. The equilibrium constant for Reaction (20) is:

$$K_{20} = \frac{(f_{H_2O})^2 \quad f_{H_2}}{(a_{Fe(OH)_2})^3}$$

where the $a_{Fe(OH)_2}$ can be formulated by analogy with expressions defining annite-phologopite stability relationships determined by Eugster and Wones (1962) and Wones and Eugster (1965):

$$a_{Fe(OH)_2} = \frac{\left[(f_{H_2O})^2 \; f_{H_2}\right]^{1/3}}{\left[(f^*_{H_2O})^2 \; f^*_{H_2}\right]^{1/3}}$$

f_{H_2} and f_{H_2O} are the fugacities of hydrogen and water in equilibrium with brucite solid solution assemblage and $f^*_{H_2}$ and $f^*_{H_2O}$ are the fugacities of hydrogen and water in the analogous assemblage containing pure ferrous hydroxide at the same temperature and P_{total}. Experimental or thermochemical data are not available on $Fe(OH)_2$ or $(Mg,Fe)(OH)_2$, so that $a_{Fe(OH)_2}$ cannot be rigorously evaluated as a function of temperature at this time. However, from the preliminary calculations of Page (1966, 1967a), the low-temperature experimental studies on the breakdown of $Fe(OH)_2$ and the thermal stability

of $Mg(OH)_2$, it can be concluded that very large amounts of Mg are required to stabilize the brucite solid solutions at higher temperatures.

Considerations of the breakdown of ferrous hydroxide suggest an explanation for the experimental observations because the brucite solid solutions appear stable at lower temperatures compared to brucite + magnetite. The fact that brucite becomes more iron-rich as temperature falls below the equilibrium curve, coupled with the fact that the largest amount of magnetite was observed at temperatures close to the equilibrium curve, indicates that the brucite solid solution breaks down according to Reaction (20). The amount of iron in brucite is a function of oxygen fugacity, iron content of olivine, and the temperature at which serpentinization took place.

The distribution of magnetite closely parallels the textural observations on natural serpentinite assemblages. Run products showed two major modes of occurrence of magnetite: fine micron-size ("dusty") particles or larger euhedral grains. Increased run duration and temperature promote the aggregation of magnetite into larger, more euhedral grains.

Determination of the Reaction Boundary for Olivine (Fo_{93}) + H_2O

The reaction that defines the maximum thermal stability of the assemblage olivine (Fo_{93}) + water at an oxygen fugacity defined by IM buffer,

$$10(Mg_{1.86}Fe_{0.14})SiO_4 + 14.2H_2O = 5Mg_3Si_2O_5(OH)_4 + 3.8Mg_{0.95}Fe_{0.05}(OH)_2 + 0.4Fe_3O_4 + 0.4H_2$$

has been bracketed with reversed experiments at: 0.5 kbar, 335°C (± 5°C), 1.0 kbar, 348°C (±5°C), and 2.0 kbar, 366°C (± 5°C). This curve is shifted to a lower temperature by 15°C from the one defined by Johannes (1968) for the assemblage forsterite + brucite + clinochrysotile + water.

Fluids Involved in Serpentinization

Published studies on the solubility of serpentine and forsterite have shown that the fluid composition in equilibrium with those minerals depends on pH, presence or absence of CO_2, surface area of phase available to the fluid, starting material, and duration of experiment. Luce (1969) and Luce et al. (1972) demonstrated that the solubility of forsterite and serpentine was controlled by short-term incongruency and long-term congruency.

The molar ratio Mg/Si is less than 1.0 for all the fluid compositions measured in this study. The high pH of the fluids (~ 11.0) leads to more efficient removal of Si than Mg for the pure water experiments. The amounts of dissolved Mg and Si averaged 4.8 ppm and 10.4 ppm respectively in the experiments with pure water and Mg increases to 11 ppm and Si is 9.6 ppm in NaCl, NaOH and alkaline chloride fluids.

The high pH of the fluid, coupled with the strongly reducing environment created by the IM buffer (high f_{H_2}) does not readily lend itself to calculation of the amount of Mg and Si in solution, assuming equilibrium between fluid and solids. Helgeson's (1969) data pertain to acidic chloride solutions at elevated temperatures and are of limited use here. Alkaline solutions, with or without chloride, considerably influence the type and distribution of aqueous species. For example, $Mg(OH)^+$ probably predominates over Mg^{2+} and $H_3SiO_4^-$ over H_4SiO_4 for the high observed pH of the fluids from the experiments. The activity of water is also decreased due to the amount of H_2 present in the gas phase.

REFERENCES CITED

Anderson, G.M. and C. Wayne Burnham (1967). Reactions of quartz and corundum with aqueous chloride and hydroxide solutions at high temperatures and pressures. Am. J. Sci. 265, 12-27.

Aumento, F. (1970). Serpentine mineralogy of ultrabasic intrusions in Canada and on the Mid-Atlantic Ridge. Geol. Surv. Can. Paper 69-53.

_____ and H. Loubat (1971). The Mid-Atlantic Ridge near 45° N. XVI Serpentinized ultramafic inclusions. Can. J. Earth Sci. 8, 631-663.

Barnes, I. and J.R. O'Neil (1969). The relationship between fluids in some fresh Alpine-type ultramafics and possible modern serpentinization. Western U.S. Geol. Soc. Am. Bull. 80, 1947-1960.

_____, J.B. Rapp, and J.R. O'Neil (1972). Metamorphic assemblages and the direction of flow of metamorphic fluids in four instances of serpentinization. Contrib. Mineral. Petrol. 35, 263-276.

Bliss, N.W. (1972). A Comparative Study of Two Ultramafic Bodies at the SW End of the Manitoba Nickel Belt: With Special Reference to Chromite Mineralogy. Ph.D. Thesis, McGill University, Montreal, Que.

Bogolepov, V.G. (1969). Problem of serpentinization of ultrabasic rocks. Int. Geol. Rev. 12, 421-432.

Bottinga, Y. and M. Javoy (1973). Comments on oxygen isotope geothermometry. Earth Planet. Sci. Letters, 20, 250-265.

Bowen, N.L. and O.F. Tuttle (1949). The system $MgO-SiO_2-H_2O$. Geol. Soc. Am. Bull. 60, 439-460.

Bricker, O.P., H.W. Nesbitt and W.D. Gunter (1973). The stability of talc. Am. Mineral. 58, 64-72.

Brindley, G.W. (1967). Nomenclature, geometry of ideal layers, bonding in layer silicates. Amer. Geol. Inst. Short Course Lecture Notes, GWB 1A-25A.

Burnham, Charles W. (1962). LCLSQ, chrystallographic lattice-constant least squares refinement program. Carnegie Inst. Wash. Year Book, 61, 132-135.

Burnham, C. Wayne, J.R. Holloway, N.F. Davis (1969). Thermodynamic properties of water to 1000°C and 10,000 bars. Geol. Soc. Am. Spec. Pap. 132.

Chamberlain, J.A., C.R. McLeod, R.J. Traill and G.R. Lachance (1965). Native metals in the Muskox Intrusion. Can. J. Earth Sci. 2, 188-215.

Chernosky, J.V. (1973). An Experimental Investigation of the Serpentine and Chlorite Group Minerals in the System $MgO-Al_2O_3-SiO_2-H_2O$. Ph.D. Thesis Massachusetts Institute of Technology, Cambridge, Mass.

Christensen, N.I. (1970). Composition and evolution of the oceanic crust. Mar. Geol. 8, 139-154.

Coleman, R.G. (1971). Petrologic and geophysical nature of serpentinites. Geol. Soc. Am. Bull. 82, 897-918.

_____ and T.E. Keith (1971). A chemical study of serpentinization - Burro Mountain, Calif. J. Petrol. 12, 311-328.

Condie, K.C. and J. Madison (1969). Composition and volume change accompanying progressive serpentinization of dunites from Webster-Addie ultramafic body. N.C. Am. Mineral. 54, 1173-1179.

Coveney, R.M. (1972). Gold Mineralization at the Oriental Mine, Calif. Ph.D. Thesis, University of Michigan, Ann Arbor, Mich.

Dietrich, V. (1972). Ilvaite, ferroantigorite and greenalite as associated oxide-sulfide mineralizations in Oberhalbstein serpentinites. Schweiz. mineral. petrogr. Mitt. 52, 57-74.

_____ and T. Peters (1971). Regionale Verteilung der Mg-Phyllosilikate in den Serpentiniten des Obehalbsteins. Schweiz. mineral. petrogr. Mitt. 51, 329-35.

Eckstrand, O.R. (1972). Redox control of the formation of nickeliferous opaque mineral assemblages in a serpentinite (abstr.). 24th Int. Geol. Congr., Section 10, 25.

Eugster, H.P. (1957). Heterogeneous reactions involving oxidation and reduction at high pressures and temperatures. J. Chem. Phys. 26, 1760-1761.

_____ (1959). Reduction and oxidation in metamorphism. In P.H. Abelson, Ed., Researehes in Geochemistry. John Wiley and Sons, N.Y., pp. 397-426.

Eugster, H.P. (1972). Reduction and oxidation in metamorphism (II). 24th Int. Geol. Congr., Section 10, 3-11.

_____ and D.R. Wones (1962). Stability relations of the ferruginous biotite, annite. J. Petrol. 3, 82-125.

Evans, B.W. and V. Trommsdorff (1972). Der Einfluss des Eisens auf die Hydratisierung von Duniten. Schweiz. mineral. petrogr. Mitt. 52, 251-256.

Evans, H.T., D.E. Appleman, and D.S. Handwerker (1963). The least squares refinement of crystal unit cells with powder diffraction data by an automatic computer indexing method. Abstr. Amer. Crystallogr. Ass. Meet., Cambridge, Mass., 42-43.

Faust, G.T., K.J. Murata, and J.J. Fahey (1956). Relation of minor elements of serpentinites to their geologic origin. Geochim. Cosmochim. Acta, 10, 316-320.

Fisher, G.W. and L.G. Medaris (1969). Cell dimensions and X-ray determinative curve for synthetic Mg-Fe olivines. Am. Mineral. 54, 741-753.

Fisher, J.R. and E. Zen (1971). Thermochemical calculations from hydrothermal phase equilibrium data and the free energy of water. Am. J. Sci., 270, 297-314.

Forbes, W.C. (1969). Unit-cell parameters and optical properties of talc on the join $Mg_3Si_4O_{10}(OH)_2$ - $Fe_3Si_4O_{10}(OH)_2$. Am. Mineral. 54, 1399-1408.

Fyfe, W.S. (1973). Dehydration reactions. Am. Assoc. Pet. Geol. Bull. 57, 190-197.

Gordon, T.M. (1973). Determination of internally consistent thermodynamic data from phase equilibrium experiments. J. Geol. 81, 199-208.

Haas, J.L. and R.A. Robie (1973). Thermodynamic data for wustite $Fe_{0.947}O$, magnetite Fe_3O_4 and hematite Fe_2O_3 (abstr.). Trans. Am. Geophys. Union, 54, 483.

Hahn-Weinheimer, P. and F. Rost (1961). Adzessorische Mineralien und Elemente im Serpentinit von heupoldsgrun (Munchberger Gneismasse). Geochim. Cosmochim. Acta, 21, 165-181.

Hearle, J.W.S., J.T. Sparrow and P.M. Cross (1972). The Use of the Scanning Electron Microscope. Pergamon Press, N.Y. 278 pp.

Helgeson, H.C. (1969). Thermodynamics of hydrothermal systems at elevated temperatures and pressures. Am. J. Sci. 267, 729-804.

Heumann, T. and G. Karsten (1963). Karbonylverfahren und aufdampfverfahren zur bestimmung von geringer Berveglichkeit am beispiel der Eisen-Nickel-legierungen. Arch. Eisenhuettenw, 34, 781-785.

Hostetler, P.B. (1963). The stability and surface energy of brucite in water at 25°C. Am. J. Sci. 261, 238-258.

_____, R.G. Coleman, F.A. Mumpton and B.W. Evans (1966). Brucite in Alpine serpentinites. Am. Mineral. 51, 75-98.

_____ and C.L. Christ (1968). Studies in the system $MgO-SiO_2-CO_2-H_2O$ (I): The activity-product constant of chrysotile. Geochim. Cosmochim. Acta, 32, 485-497.

Huebner, J.S. (1971). Buffering techniques for hydrostatic systems at elevated pressures. In, G.C. Ulmer, Ed., Research Techniques for High Pressure and High Temperatures. Springer-Verlag, N.Y., pp. 123-177.

Hultin, I. (1968). Awaruite (josephinite) a new mineral for Norway. Contributions to the mineralogy of Norway #36. Norsk. Geol. Tidsskr. 48, 179-185.

Iishi, K. and M. Saito (1973). Synthesis of antigorite. Am. Mineral. 58, 915-919.

Jahns, R.H. (1967). Serpentinites of the Roxbury district, Vermont. In, P.J. Wyllie, Ed., Ultramafic and Related Rocks. John Wiley and Sons, Inc., N.Y., pp. 137-155.

Jambor, J.L. and C.H. Smith (1964). Olivine composition determination with small diameter X-ray powder cameras. Mineral. Mag. 33, 730-741.

Jasmund, K. and H.M. Sylla (1971). Synthesis of Mg- and Ni-antigorite. Contrib. Mineral. Petrol. 34, 84-86.

_____ and _____ (1972). Synthesis of Mg and Ni antigorite: a correction. Contrib. Mineral. Petrol. 34, 346.

Johannes, W. (1968). Experimental investigation of the reaction forsterite + H_2O = serpentine + brucite. Contrib. Mineral. Petrol. 19, 309-315.

_____ (1969). An experimental investigation of the system $MgO-SiO_2-H_2O-CO_2$. Am. J. Sci. 267, 1083-1104.

Kahn, H.L. (1968). Principles and practice of atomic absorption. In, Advances in Chemistry Series #73, Trace Inorganics in Water, Am. Chem. Soc., Washington, pp. 183-229.

Kheiker, D.M., I.M. Flantsbaum, and L.V. Bubeleva (1967). Determination of elementary fiber dimensions in chrysotile asbestos. Soviet Phys. Crystall. 12, 370-374.

King, E.G., R. Barany, W.W. Weller and L.B. Pankratz (1967). Thermodynamic properties of forsterite and serpentine. U.S. Bur. Mines Rept. Inv. 6962.

Kitahara, S., S. Takenouchi and G.C. Kennedy (1966). Phase relations in the system $MgO-SiO_2-H_2O$ at high temperatures and pressures. Am. J. Sci. 264, 223-233.

Korytkova, E.N. and A.D. Fedoseev (1969). Production of fibrous amphiboles by recrystallization of serpentine under hydrothermal conditions. In, N.A. Toropov, Ed., Chemistry of High Temperature Materials. Consultants Bureau, N.Y., pp. 153-155.

_____ and T.A. Makarova (1971). Experimental study of the serpentinization of olivine. Dokl. Akad. Nauk U.S.S.R. 196, 144-145.

_____ and _____ (1972). Experimental investigation of the hydrothermal alteration of olivine in connection with the formation of asbestos. Geochem. Int. 9, 957-961.

_____, _____, and G.I. Kosulina (1972). Experimental serpentinization of olivine. Int. Geol. Rev. 14, 1074-1078.

Krstanovic, I. (1968). Crystal structure of single-layer lizardite. Z. Kristallogr. 126, 163-169.

Kubaschewski, O. and O. von Goldbeck (1949). The thermodynamics of the iron nickel alloys. Trans. Faraday Soc. 45, 948-960.

Kullerud, G. (1971). Experimental techniques in dry sulfide research. In, G.C. Ulmer, Ed., Research Techniques for High Pressure and High Temperature. Springer-Verlag, N.Y. pp. 289-315.

Linnenbom, V.J. (1958). The reaction between iron and water in the absence of oxygen. J. Electrochem. Soc. 105, 322-324.

Loney, R.A., G.R. Himmelberg and R.G. Coleman (1971). Structure and petrology of the Alpine type peridotite at Burro Mountain, California, U.S.A. J. Petrol. 12, 245-309.

Luce, R.W. (1969). Dissolution of Magnesium Silicates. Ph.D. Thesis. Stanford University, Stanford, Calif.

_____ (1971). Brucite identified as crystallizing from a natural cold alkaline spring gel. Clay and Clay Miner. 19, 335-336.

_____, R.W. Bartlett and G.A. Parks (1972). Dissolution kinetics of magnesium silicates. Geochim. Cosmochim. Acta, 36, 35-50.

Martin, B. (1971). Some comments on the processes of serpentinization from experimental and other work. Spec. Publ. Geol. Soc. Aust. #3, pp. 301-310.

_____ and W.S. Fyfe (1970). Some experimental and theoretical observations on kinetics of hydration reactions with particular reference to serpentinization. Chem. Geol. 6, 185-202.

Martinez, E. and J.J. Comer (1964). The concentration and study of the interstitial material in chrysotile asbestos. Am. Mineral. 49, 153-157.

Misra, K.C. and M.E. Fleet (1973). The chemical compositions of synthetic and natural pentlandite assemblages. Econ. Geol. 68, 518-539.

Miyashiro, A. (1966). Some aspects of peridotite and serpentinite in orogenic belts. J. Geol. Geophys. Japan, 37, 45-61.

Moiseyev, A.N. (1974). Serpentinite-water interaction at 200-260°C and 1 kbar, a preliminary report (abstr.). Trans. Am. Geophys. Union, 55, 478.

Moores, E.M. (1973). Geotectonic significance of ultramafic rocks. Earth Sci. Rev. 9, 241-258.

Mumpton, F.A. and C.S. Thompson (1966). The stability of brucite in the weathering zone of the New Idria serpentinite. Clays and Clay Miner., Proc. 14th Natl. Conf., Pergamon Press, N.Y. pp. 249-257.

Nickel, E.E. (1959). The occurrence of native Ni-Fe in the serpentine rocks of the Eastern Townships of Quebec Province. Can. Mineral. 6, 307-319.

Olsen, E. (1963). Equilibrium calculations in the system Mg, Fe, Si, O, H and Ni. Am. J. Sci. 261, 943-956.

Orville, P.M. and H.J. Greenwood (1965). Determination of ΔH of reaction from experimental pressure-temperature curves. Am. J. Sci. 263, 678-683.

Page, N.J. (1966). Mineralogy and Chemistry of the Serpentine Group Minerals and the Serpentinization Process. Ph.D. Thesis, University of California, Berkeley, Calif.

_____ (1967a). Serpentinization at Burro Mountain, Calif. Contrib. Mineral. Petrol. 14, 321-342.

_____ (1967b). Serpentinization considered as a constant volume metasomatic process: a discussion. Am. Mineral. 52, 545-549.

_____ (1968). Chemical differences among the serpentine "polymorphs". Am. Mineral. 53, 201-215.

_____ and R.G. Coleman (1967). Serpentine mineral analyses and physical properties. U.S. Geol. Surv. Prof. Pap. 575-B, 103-107.

Pistorius, C.W. (1963). Some phase relations in the system $MgO-SiO_2-H_2O$ to high pressures and temperatures. Neues Jahrb. Mineral. Monatsch. 11, 283-293.

Pritchard, A.M. and B.T. Moull (1971). Mossbauer spectra of some iron compounds formed from alkaline solutions. Corr. Sci. 11, 1-10.

_____, J.R. Haddon and G.N. Walton (1971). A study of some of the products of the corrosion of iron under hydrothermal conditions using the Mossbauer effect. Corr. Sci. 11, 11-24.

Radoslovich, E.W. (1962). The cell dimensions and symmetry of layer lattice silicates II. Regression relations. Am. Mineral. 47, 617-636.

_____ (1963). The cell dimension and symmetry of later-lattice silicates VI. Serpentine and kaolinite morphology. Am. Mineral. 48, 368-378.

_____ and K. Norrish (1962). The cell dimensions and symmetry of layer-lattice silicates I. Some structural considerations. Am. Mineral. 47, 599-616.

Rainwater, F.H. and L.L. Thatcher (1960). Methods for collecting and analysis of water samples. U.S. Geol. Surv. Water Supply Pap. 1454.

Raleigh, C.B. and M.S. Paterson (1965). Experimental deformation of serpentinite and its tectonic implications. J. Geophys. Res. 70, 3965-3985.

Ramdohr, P. (1967). A widespread mineral association connected with serpentinization. Neues Jahrb. Mineral. Abh. 107, 241-265.

Robie, R.A. and D.R. Waldbaum (1968). Thermodynamic properties of minerals and related substances at 298.15°K (25.0°C) and one atmosphere (1.013 bars) pressure and at higher temperatures. U.S. Geol. Surv. Bull. 1259.

Ross, M. (1968). X-ray diffraction effects by non-ideal crystals of biotite, muscovite, montmorillonite, mixed-layer clays, graphite and periclase. Z. Kristallogr. 126, 80-97.

Scarfe, C.M. and P.J. Wyllie (1967). Serpentine dehydration curves and their bearing on serpentine deformation in orogenesis. Nature, 215, 945-946.

Seitz, M.G. and S.R. Hart (1972). Uranium and boron distributions in some oceanic ultramafic rocks. Earth Planet. Sci. Letters, 21, 97-107.

Shaw, H.R. (1963). Hydrogen-water vapor mixtures: control of hydrothermal atmospheres by hydrogen osmosis. Science, 139, 1220-1222.

_____ (1967). Hydrogen osmosis in hydrothermal experiments. In P.H. Abselson, Ed., Researches in Geochemistry, Vol. 2, John Wiley and Sons, N.Y. pp. 521-541.

_____ and D.R. Wones (1964). Fugacity coefficients for hydrogen gas between 0°C and 1000°C for pressures to 3000 atm. Am. J. Sci. 262, 918-929.

Shipko, F.J. and D.L. Douglas (1956). Stability of ferrous hydroxide precipitates. J. Phys. Chem. 60, 1519-1523.

Shteynberg, D.S. and I.S. Chashchuklin (1969). Composition of brucite in serpentinites and the procedure for identifying it. U.S.S.R. Acad. Sci. Dokl. Earth. Sci. 186, 115-118.

Shunk, F.A. (1969). Constitution of Binary Alloys, Second Supplement, McGraw Hill Book Co., N.Y. 720 pp.

Speakman, K. (1970). Reactions in the system $CaO-MgO-SiO_2-H_2O$. Hydrothermal treatment of some compositions on the joins $Ca_3Si_2O_7$-$Mg_3Si_2O_7$ and Ca_2SiO_4-Mg_2SiO_4. Mineral. Mag. 37, 578-587.

Steadman, R. and P.M. Nuttal (1964). Further polymorphism in cronstedtite. Acta Crystallogr. 17, 404-407.

Stumm, W. and J.J. Morgan (1970). Aquatic Chemistry. Wiley-Interscience, N.Y. 583 pp.

Thayer, T. (1966). Serpentinization considered as a constant volume metasomatic process. Am. Mineral. 51, 685-710.

Thayer, T. (1967). Serpentinization considered as a constant volume metasomatic process: a reply. Am. Mineral. 52, 549-553.

Thompson, G. and W.G. Melson (1970). Boron contents of serpentinites and metabasalts in the oceanic crust: implications for the boron cycle in the oceans. Earth Planet. Sci. Letters, 8, 61-65.

Trommsdorff, V. and B.W. Evans (1972). Progressive metamorphism of antigorite schist in the Bergell tonalite aureole (Italy). Am. J. Sci. 272, 423-437.

Tuttle, O.F. (1949). Two pressure vessels for silicate-water studies. Geol. Soc. Am. Bull. 60, 1727-1729.

Varlakov, A.S. and M.F. Zhuzhgova (1964). Geochemistry of boron in the ultramafic rocks of the Orenburg district. Geochem. Int. 4, 782-787.

Wenner, D.B. and H.P. Taylor (1971). Temperatures of serpentinization of ultramafic rocks based on O^{18}/O^{16} fractionation between co-existing serpentine and magnetite. Contrib. Mineral. Petrol. 32, 165-185.

_____ and _____ (1973). Oxygen and hydrogen isotope studies of the serpentinization of ultramafic rocks in oceanic environments and continental ophiolite complexes. Am, J. Sci. 273, 207-239.

Whittaker, E.J.W. (1956). The structure of chrysotile. II. Clinochrysotile. Acta Crystallogr. 9, 855-862.

_____ (1957). The structure of chrysotile. V. Diffuse reflections and fiber texture. Acta Crystallogr. 10, 149.

_____ and F.J. Wicks (1970). Chemical differences among the serpentine polymorphs: a discussion. Am. Mineral. 55, 1025-1047.

_____ and J. Zussman (1956). The characterization of the serpentine minerals by X-ray diffraction. Mineral. Mag. 31, 107-26.

_____ and _____ (1971). The serpentine minerals. In, J.A. Gard, Ed., The Electron-Optical Investigation of Clays. Mineral. Soc., London, pp. 159-191.

Wicks, F.J. (1969). X-ray and Optical Studies on Serpentine Minerals. D.Phil.Thesis, Oxford University, Oxford, England.

Wildman, W.E., M.L. Jackson and L.D. Whittig (1968). Serpentinite rock dissolution as a function of carbon dioxide pressure in aqueous solution. Am. Mineral. 53, 1252-1263.

_____, _____, and _____ (1971). Serpentine stability in relation to the formation of iron-rich montmorillonite in some California soils. Am. Mineral. 56, 587-602.

Wise, W.S. and H.P. Eugster (1964). Celadonite: synthesis, thermal stability and occurrence. Am. Mineral. 49, 1031-1083.

Wones, D.R. (1963). Physical properties of synthetic biotites on the join phologopite-annite. Am. Mineral. 48, 1300-1321.

_____ and H.P. Eugster (1965). Stability of biotite: experiment, theory and application. Am. Mineral. 50, 1228-1272.

Wyllie, P.J. (1967). Ultramafic and Related Rocks. John Wiley and Sons, Inc., N.Y. 464 pp.

Yada, K. (1967). Study of chrysotile asbestos by a high resolution electron microscope. Acta Crystallogr. 23, 704-707.

_____ (1971). Study of microstructure of chrysotile asbestos by high resolution electron microscopy. Acta Crystallogr. 27A, 659-664.

Yang, J.C. (1960). The system $MgO-SiO_2-H_2O$ below 300°C I. Low temperature phases from 100 to 300°C and their properties. J. Am. Chem. Soc. 43, 542-549.

_____ (1961). The growth of synthetic chrysotile fibers. Am. Mineral. 46, 748-752.

Yoder, H.S. (1967). Spilites and serpentinites. Carnegie Inst. Wash. Year Book, 65, 269-279.

Zen, E. (1969). Free energy of formation of pyrophyllite from hydrothermal data: values, discrepancies and implications. Am. Mineral. 54, 1592-1606.

_____ (1971). Comments on the thermodynamic constants and hydrothermal stability relations of anthophyllite. Am. J. Sci. 270, 136-150.

_____ (1972). Gibbs free energy, enthalphy, and entrophy of ten rock forming minerals: calculations, discrepancies, implications. Am. Mineral. 57, 524-553.

_____ (1973). Thermochemical parameters of minerals from oxygen-buffered hydrothermal equilibrium data, method, application to annite and almandine. Contrib. Mineral. Petrol. 39, 65-80.

Zussman, J, G.W. Brindley and J.J. Comer (1957). Electron diffraction studies of serpentine minerals. Am. Mineral. 42, 133-153.

Zvyagin, B.B. (1967). Electron-Diffraction Analysis of Clay Mineral Structures. Plenum Press, N.Y. 364 pp.

Appendix 1a: Observation of the iron-magnetite buffer for the hydrothermal runs.

Appendix 1b: Calculated fugacities of oxygen, hydrogen and water for the temperature-pressure range of interest. The hydrogen and water fugacities are tabulated in bars directly, whereas the oxygen fugacity is given in log units (bars).

Appendix 1c: Calculated oxygen, hydrogen, and water fugacities for the iron-magnetite buffer and magnetite-awaruite in temperature-pressure range of interest. The hydrogen and water fugacities are tabulated in bars, whereas the oxygen fugacity is given in log units (bars).

Note: The numerical values of f_{H_2} and f_{H_2O} in Appendices 1b and 1c were calculated assuming an ideal mixing model (Eugster and Wones, 1962), and though qualitatively consistent with experimental observations on H_2-H_2O system, they may be subject to large and unknown errors (see text for further explanation).

Appendix 1a

Run	M, %*	Amt. Fluid Remaining, %**	Additional comments***
3-106	30	<33+	capsule puffed double, gas escape on opening
3-105	25	50+	capsule puffed double, gas escape on opening
3-104	25	33+	capsule puffed double, gas escape on opening
3-103	30	50+	capsule puffed double, gas escape on opening
3-102	x	x	capsule puffed, leak on quench
3-101	50	x	capsule puffed, leak due to accidental drop of pressure in line
3-100	40	33+	capsule puffed double, large amt. gas escape on opening
3-99	30	33+	capsule puffed double, large amt. gas escape on opening
3-98	50	>50+	capsule puffed double, large amt. gas escape on opening
3-97	10	50+	capsule puffed double, gas escape
3-96	25	x	capsule puffed double, leaked on quench
3-95	15	50	capsule puffed double, large amt. gas escape
3-94	x	x	capsule puffed double, gas escape on opening
3-93	15	>33	capsule puffed double, small amt. gas escape
3-92	40	33	capsule puffed double, no gas escape

Run	M, % *	Amt. fluid Remaining, % **	Additional comments***
3-87	25	x	capsule puffed, gas escape on opening
3-86	20	50	capsule puffed, gas escape
3-85	15	25	capsule puffed double, gas escape
3-84	15	25	capsule puffed, gas escape
3-78	15	>25	capsule puffed, gas escape
3-77	x	>50	capsule puffed, gas escape
$3\text{-}76_1$	12	x	capsule puffed, gas escape
$3\text{-}76_2$	10	50	capsule puffed, large amt. gas given off
$3\text{-}75_1$	15	<10	capsule puffed, gas given off
$3\text{-}75_2$	15	x	capsule collapsed, no gas given off, small amount of fluid remaining
3-74	10	>10	capsule puffed, gas escape on opening
3-72	15	25	capsule puffed, gas given off
3-71	20	25	capsule puffed, gas given off on opening
3-70	20	>10	capsule puffed, gas escape
3-69	x	>10	capsule puffed, gas escape
3-68	10	10	capsule puffed, gas escape
3-64	15	<10	capsule puffed double, gas escape (?leak on quench)

Run	M, % *	Amt. fluid Remaining, %**	Additional Comments***
3-63	25	>25	capsule puffed double, large amt. gas escape
3-62	25	50	capsule puffed double, gas escape on opening
3-61	25	>10	capsule puffed, gas escape
3-60	25	25	capsule puffed, large amt. gas escape on opening
3-57	10	<25	capsule puffed double, gas escape
3-56	15	>50	capsule puffed double, gas escape
3-55	10	>10	capsule puffed double, gas escape
3-54	15	<10	capsule puffed double, gas escape
3-48	10	<10	capsule puffed, gas escape
3-51	20	>10	capsule puffed double, large amt. gas escape
3-50	25	x	capsule puffed, leaked on quench
3-49	20	>33	capsule puffed double,gas escape
3-47	12	<10	capsule puffed double, gas escape
3-46	25	x	capsule puffed double, large amt. gas escape
3-45	25	x	capsule puffed double, leaked on quench
3-43	45	33	capsule puffed double, large amt. gas escape

Run	M, %*	Amt. fluid Remaining, %**	Additional comments***
3-42	35	33	capsule puffed double, gas escape on opening
3-32	20	33	capsule puffed double, large amt. gas escape
3-31	20	< 25	capsule puffed double, large amt. gas escape
3-30	25	< 33	capsule puffed double, large amt. gas escape
3-26	10	< 10	capsule puffed, large amt. gas escape
3-25	10	< 10	capsule slightly puffed, small amt. gas escape
3-23	20	50	capsule puffed double, small amt. gas escape
3-22	10	< 10	capsule puffed double, large amt. gas escape
3-15	20	x	capsule puffed double, leak on quench
3-14	25	x	capsule puffed double, leak on quench
3-12	20	x	capsule puffed double, leak on quench
3-5	30	10	Fe filings + M, capsule puffed, gas escape, M reaction rims on Fe
3-4	25	< 25	Fe filings + M, capsule puffed, gas escape, M reaction rims on Fe
3-3	25	50	Fe filings + M, capsule puffed, gas escape, M reaction rims on Fe
3-2	15	25	Fe filings + M, capsule puffed, gas escape, M reaction rims on Fe

Run	M, %*	Amt. fluid Remaining, %**	Additional comments***
3-1	10	33	Fe filings + M, capsule puffed, gas escape, M reaction rims on Fe
2-110	7	50	Fe filings + M, capsule slightly puffed, no M rims
2-109	x	x	Fe filings + M (leak?)
2-108	8	> 50	Fe filings + M, capsule slightly puffed, no M rims
2-107	10	> 50	Fe filings + M, capsule not puffed, no M rims
2-106	tr.	> 30	Fe filings, capsule not puffed
2-102	15	> 50	Fe filings + M, capsule not puffed, no M rims
2-101	12	x	Fe filings + M, capsule slightly puffed, small amt. gas escape, no M rims
2-100	min.	> 50	Fe filings, capsule slightly puffed, small amt. gas escape
2-98	15	x	Fe filings + M, capsule puffed, gas escape, M reaction rims on Fe
2-95	10	10	Fe filings, capsule puffed, gas escape
2-94	20	33	Fe filings, capsule puffed, large amt. gas escape
2-99	7	33	Fe filings, capsule puffed, gas escape, M reaction rims

*% magnetite is approximate, estimated visually from polished section, native Fe always present

**wt. % fluid remaining at end of run, determined from directly weighing amount collected (minimum amount because the fluid was not removed quantitatively)

***initial buffer starting material was Fe sponge + filings, unless otherwise stated

x phase is present, amount not estimated

+ amount of fluid remaining at the end of run estimated visually upon opening capsule

Appendix 1b

T, °C	P_{total}, bars 500	1000	1500	2000
300				
$-\log f_{O_2}$	42.108	42.055	42.002	41.949
f_{H_2}	467	912	1375	1867
f_{H_2O}	18	37	59	86
320				
$-\log f_{O_2}$	40.140	40.359	40.308	40.257
f_{H_2}	464	905	1361	1846
f_{H_2O}	22	46	73	105
340				
$-\log f_{O_2}$	38.823	38.774	38.724	38.675
f_{H_2}	462	898	1346	1825
f_{H_2O}	27	56	88	127
360				
$-\log f_{O_2}$	37.336	37.288	37.240	37.192
f_{H_2}	458	888	1327	1793
f_{H_2O}	33	67	105	151
380				
$-\log f_{O_2}$	35.940	35.894	35.848	35.801
f_{H_2}	454	878	1310	1774
f_{H_2O}	39	79	124	177
400				
$-\log f_{O_2}$	34.627	34.582	34.536	34.492
f_{H_2}	447	865	1288	1740
f_{H_2O}	45	92	145	205

Appendix 1c

	P_{total} (bars)					
	IM		M-A (Ni_2Fe)		M-A (Ni_3Fe)	
T(°C)	500	2000	500	2000	500	2000
300						
$-\log f_{O_2}$	42.108	41.949	41.594	41.158	41.590	41.018
f_{H_2}	467	1867	398	1053	398	934
f_{H_2O}	18	86	27.4	120	27.5	125
400						
$-\log f_{O_2}$	34.627	34.492	34.102	33.729	34.112	33.625
f_{H_2}	447	1740	380	1014	381	930
f_{H_2O}	45	205	70.2	289	69.7	298

APPENDIX 2 Hydrothermal run table showing the nature of the starting materials, temperature, pressure, run duration, buffer, composition of the initial fluid phase and run products. The temperature variation during the run was less than 2°C, the pressure variation ± 50 bars. Run duration was measured from the time the bomb was placed in the furnace.

Run	Starting Material	T(°C)	P(kbar)	Run Duration hrs	Buffer	Fluid*	Products**
			Experiments with synthetic olivines + pure water				
3-14	0 (2-17)	376	1.94	1128	IM	H_2O	O
3-60	0 (2-17)	338	1.94	674	IM	H_2O	45% O, L, C, tr. B, M
3-25	0 (2-17)	323	1.94	742	IM	H_2O	40% O, L, tr. C, B, M
3-15	0 (2-17)	349	1.99	1107	IM	H_2O	80% O, L, M
3-26	0 (2-17)	322	1.94	739	IM	H_2O	tr. O, L, B, M
3-12	0 (2-17)	321	1.99	1150	IM	H_2O	tr. O, L, C, B, M
3-61	0 (2-17)	302	1.93	504	IM	H_2O	tr. O, L, C, B, M
2-95	0 (2-33)	375	1.47	504	IM	H_2O	O
2-92	0 (2-19)	351	1.47	576	-	H_2O	tr. O, L, C, B
2-94	0 (2-33)	339	1.47	575	IM	H_2O	40% O, L, tr. B, M
2-99	0 (2-33)	329	1.47	529	IM	H_2O	tr. O, L, C, M
3-30	0 (OP-194)	331	1.47	764	IM	H_2O	70% O, L, C, tr. B, M
3-48	0 (GSC)	309	1.48	1773	IM	H_2O	tr. O, L, C, B, M

Run	Starting Material	T(°C)	P(kbar)	Run Duration hrs	Buffer	Fluid*	Products**
3-32	O (GSC)	307	1.47	911	IM	H_2O	20% O, L, B, M
2-98	O (2-33)	302	1.47	625	IM	H_2O	tr. O, L, C, B, M
3-5	O (2-17)	376	1.00	1539	IM	H_2O	O, tr. L
3-3	O (2-17)	349	1.01	1559	IM	H_2O	O, tr. L, tr. B
3-31	O (OP-54)	321	0.99	764	IM	H_2O	?
3-2	O (2-17)	329	1.01	1637	IM	H_2O	O, tr. L
3-4	O (2-17)	317	1.01	1492	IM	H_2O	tr. O, L, C, B, M
3-1	O (2-17)	302	1.01	1660	IM	H_2O	tr. O, L, C, B, M
2-109	O (2-33)	377	0.51	720	IM	H_2O	O
2-108	O (2-33)	349	0.51	793	IM	H_2O	10% O, L, B, M
3-23	O (2-17)	323	0.54	1606	IM	H_2O	80% O, L, M, C
2-110	O (2-33)	316	0.51	743	IM	H_2O	5% O, L, C, B, M
3-22	O (2-17)	304	0.54	1605	IM	H_2O	tr. O, L, C, B, M

Run	Starting Material	T(°C)	P(kbar)	Run Duration hrs	Buffer	Fluid*	Products**
			Experiments with natural olivines + pure water				
3-77	2-BU-77	307	1.93	999	IM	H_2O	tr. O, L, C, B, M
2-101	M7863	375	1.47	504	IM	H_2O	O
2-100	M7863	347	1.47	528	IM	H_2O	70% O, L, C, B, M
2-107	M7863	328	1.47	819	IM	H_2O	10% O, L, C, B, M
2-102	M7863	317	1.47	504	IM	H_2O	40% O, L, C, B, M
2-106	M7863	303	1.47	815	IM	H_2O	50% O, L, B, M
3-47	M7863	331	1.00	1127	IM	H_2O	40% O, L, B, M
			Experiments with synthetic and natural olivines with fluids of variable composition				
3-50	0 (2-17)	352	1.48	525	IM	0.14 M $NaSi^+$	min. O, L, C, tr. M, (?)
3-51	0 (2-17)	317	1.48	525	IM	0.12 M $NaSi^+$	tr. O, L, M
3-43	0 (2-17)	331	0.99	573	IM	0.05 M $NaSi^+$	min. O, L, M
3-42	0 (2-17)	306	0.99	573	IM	0.06 M $NaSi^+$	L, C, B, M
3-62	0 (2-17)	372	1.00	517	IM	0.39 M NaCl	O, tr. L, tr. B, tr. M
3-56	0 (2-17)	351	1.00	481	IM	0.14 M NaCl	O, tr. L, M

Run	Starting Material	T(°C)	P(kbar)	Run Duration hrs	Buffer	Fluid*	Products**
3-55	0 (2-17)	319	1.00	481	IM	0.12 M NaCl	O, L, M
3-57	0 (2-17)	300	1.00	483	IM	0.25 M NaCl	O, tr. L, M
3-45	0 (2-17)	355	0.99	524	IM	0.01 M NaOH	O, tr. L, M, tr. B
3-49	0 (2-17)	342	1.48	596	IM	0.03 M NaOH	min. O, L, tr. C, M, B
3-46	0 (2-17)	322	1.48	524	IM	0.01 M NaOH	tr. O, L, B, M, tr. C
3-54	0 (2-17)	302	1.00	550	IM	0.01 M NaOH	tr. O, L, C, B, M
3-63	0 (2-17)	332	1.00	525	IM	0.19 M NaCl 0.01 M NaOH	O, tr. L, tr. B
3-64	0 (2-17)	302	1.00	524	IM	0.33 M NaCl 0.02 M NaOH	tr. O, L, C, B, M
3-96	2-BU-66	346	2.01	433	IM	0.23 M NaCl 0.01 M NaOH	O, L, C, B, M
3-95	2-BU-66	330	2.01	433	IM	0.23 M NaCl 0.01 M NaOH	min. O, L, C, B, M
3-92	2-BU-66	317	1.00	526	IM	0.12 M NaCl 0.01 M NaOH	min. O, L, C, B, M
3-93	2-BU-66	320	0.57	479	IM	0.19 M NaCl 0.01 M NaOH	tr. O, L, C, B, M
3-94	2-BU-66	310	0.57	478	IM	0.12 M NaCl 0.01 M NaOH	min. O, L, C, B, M

Run	Starting Material	T(°C)	P(kbar)	Run Duration hrs	Buffer	Fluid*	Products**
			Reversed experiments on the reaction boundary for olivine (Fo_{93}) + H_2O				
3-101	equil mix++	392	2.02	695	IM	H_2O	O, L, C, B, tr. M
3-100	equil mix	376	2.01	794	IM	H_2O	O, L, C, B, M
3-99	equil mix	361	2.01	793	IM	H_2O	O, L, C, B, M
3-76	equil mix	344	1.93	479	IM	H_2O	tr. O, L, C, B, M
3-75	equil mix	335	1.93	480	IM	H_2O	tr. O, L, C, B, M
3-74	equil mix	341	1.48	481	IM	H_2O	tr. O, L, C, B, M
3-72	equil mix	332	1.48	791	IM	H_2O	tr. O, L, C, B, M
3-86	equil mix	371	1.01	569	IM	H_2O	O, L, C, B, tr. M
3-87	equil mix	361	1.01	568	IM	H_2O	O, L, C, B, tr. M
3-85	equil mix	349	1.01	567	IM	H_2O	O, L, C, B, M
3-84	equil mix	341	1.01	568	IM	H_2O	O, L, C, B, M
3-71	equil mix	330	1.00	792	IM	H_2O	tr. O, L, C, B, M
3-78	equil mix	321	1.01	384	IM	H_2O	tr. O, L, C, B, M
3-70	equil mix	322	1.00	837	IM	H_2O	tr. O, L, C, B, M

Run	Starting Material	T(°C)	P(kbar)	Run Duration hrs	Buffer	Fluid*	Products**
3-98	equil mix	352	0.54	814	IM	H_2O	O, L, C, B, M
3-97	equil mix	336	0.54	814	IM	H_2O	O, L, C, B, M
3-68	equil mix	322	0.56	863	IM	H_2O	tr. O, L, C, B, M
3-69	equil mix	311	0.56	895	IM	H_2O	tr. O, L, C, B, M
				Dehydration reactions			
3-106	3-77	370	2.01	1014	IM	H_2O	O, L, C, B, M
3-105	3-77	355	2.01	1014	IM	H_2O	O, L, C, B, M
3-103	3-77	356	1.01	1035	IM	H_2O	O, L, C, B, M
3-102	3-77	339	1.01	1058	IM	H_2O	O, L, C, B, M
3-104	3-77	330	1.01	1035	IM	H_2O	O, L, C, B, M
				Reactions involving brucite			
3-8	MgO+Fe	605+++	1.53+++	67	IM	H_2O	B, M
3-19	MgO	599+++	1.46+++	70	-	H_2O	B
3-18	MgO+Fe+Fe_2O_3	599+++	1.46+++	70	-	H_2O	B, M, tr. Hm
2-85	MgO	400	1.47	795	IM	H_2O	B
2-70	MgO + Fe	400	1.47	169	IM	H_2O	B, M, Fe

Run	Starting Material	T(°C)	P(kbar)	Run Duration hrs	Buffer	Fluid*	Products**
2-72	MgO+Fe	399	1.50	152	IM	H_2O	B, M, min. MgO
2-71	MgO+Fe	399	1.48	170	IM	H_2O	B, M, min. MgO
2-77	MgO+Fe	398	1.51	360	IM	H_2O	B, M
2-74	MgO+Fe	302	1.51	341	IM	H_2O	B, M, Fe
2-67	MgO	300	1.47	333	IM	H_2O	B, tr. MgO
2-75	MgO+Fe	299	1.51	341	IM	H_2O	B, Fe
2-76	MgO+Fe	299	1.51	341	IM	H_2O	B, M
3-28	B (3-19)	376	1.94	744	-	0.5 M NaSi+	L, C, B, tr. Au,(?)
3-17	B (2-67)	351	1.94	889	-	0.5 M NaSi+	L, tr. C, tr. B,(?)
3-16	B (2-67)	304	1.94	893	-	0.5 M NaSi+	L, C, B, qtz
				Buffer kinetic experiments			
3-6a	Fe sponge	340 +++	1.53 +++	69		H_2O	95% M, Fe
3-6b	Fe sponge	338 +++	1.54 +++	21		H_2O	5% M, Fe
3-6c	Fe sponge	335 +++	1.53 +++	43		H_2O	30% M, Fe

Run	Starting Material	T(°C)	P(kbar)	Run Duration hrs	Buffer	Fluid*	Products**
2-78a	Fe filings	400	1.50	43		H_2O	Fe
2-78b	Fe filings	399	1.50	71		H_2O	1% M, Fe
2-78c	Fe filings	401	1.51	93		H_2O	3% M, Fe
2-80a	Fe filings	400	1.47	143		H_2O	5% M, Fe
2-80b	Fe filings	402	1.47	127		H_2O	tr.M, Fe

qtz = quartz
Fe = native Fe
Hm = hematite
tr. = trace amount present 2%
min. = minor amount present 2-40%

*initial fluid composition

**% olivine is an approximate volume estimate from optical and X-ray results, % magnetite is estimated from polished section

+sodium metasilicate, $Na_2SiO_3.9H_2O$

++a mixture composed of equal weights of products of Run 3-48 + GSC olivine

+++uncalibrated temperature, pressure equipment utilized

APPENDIX 3: Detailed description of the samples examined by the Scanning Electron Microscope, including phase distribution, habit and grain size.

Run	O	L	C	B	M	Remarks concerning grain size and habit *
2-94	x	x			x	lizardite is massive grains, plates, and laths, some of the plates have curled edges, O - irregular pitted grains, M - cubes
2-102		x	x			L - massive, plates and laths (20 μm in width), C laths of width of 0.8 - 1.1 μm
3-4		x	x			L - plates, C - bundle of lath of width ~1 μm
3-12		x	x	x	(?)	L - massive, plates, some development of euhedral faces in L; interlocking mat of C fiber of max length of 10-15 μm, fibers appear to coat lizardite platelets, parachrysotile possible (cone-in-cone structure observed in some fibers); B - hex. platelet
3-16		x	x			very fine mat of C needles coating irregular, thin, curved plates of L; irregular. Massive grains of Qtz or sodium metasilicate
3-17		x	x			platy and massive L, some plates curled; minor C - fibers
3-42		x	x	x		platy, massive (60 μm) L; subhedral to euhedral crystal development in L; 1 μm , B - hex. platelet; C - needles of 0.2 - 0.3 μm width, needles form a mat on surface of L and grow in vapor cavities, fibers less than 10 μm in length
3-48		x	x	x	(?)	massive, irregular grains of L, some larger L laths, C - fine needles 0.35 μm width and 4 - 10 μm length, some L plates, B - hex. plates of 4 - 18 μm, cube M - 2 μm
3-54		x	x	x		plates of L, needles and laths C, large brucite platelets - 28 μm
3-64		x	x	x		platy and massive L, chrysotile needles, B platelets

Run	O	L	C	B	M	Remarks concerning grain size and habit *
3-69	x	x	x	x		platy, laths and some massive L, very fine, long chrysotile needles of 0.2 μm in width, needles covering L and B and filling vapor cavities, single B platelets, most L a substrate for C
3-72	x	x	x			platy and lath L, fibrous C, coating L
3-75		x	x	x		grains covered with C needles, B platelets up to 22 μm in size, some euhedral morphology developed in L, C and B as in Run 3-48
3-76		x	x	x		C - development of long fiber bundles up to 100 μm in length and 10 - 12 μm in width, euhedral morphology in L (hex. or trigonal), well crystallized brucite - 25 - 80 μm
3-99	x	x	x	x		L plates and laths (10 - 12 μm in width and 30 - 60 μm in length), long C fibers, B, angularity in O grains, some suggestion of O growth in small number of 2 μm size particles that are very irregular
3-100	x	x	x	x		O euhedral and not covered with C fibers, shortening and thickening of C fibers, some B and well crystallized L, O growth in newly precipitated grains (?) - 8 μm
3-101	x	x	x	x		definite euhedral O, growth on pre-existing substrate, shortening of C needles, some L laths, 8 μm x 3 μm smaller than in Run 3-99, increase in grain size of new O material (15 μm), etching of L grains, rounding of B platelets, minor amount of B
3-70		x	x	x	(?)	well developed B - 30 - 40 μm platelets x 4 μm thick; relatively short C needles - 4 - 5 μm length, some C laths; plates and euhedral crystals of L
3-71		x	x	x		B - 20 μm hex. platelet; L laths, plates and euhedral morphology, C fiber development and increase in length of fibers

Run	O	L	C	B	M	Remarks concerning grain size and habit *
3-84	x	x	x	x		B - 15 - 20 μm hex. platelets, C forms fiber bundles, euhedral L, minor O - large anhedral grains with some C coating
3-85	x	x	x	x		B - 10 - 18 μm hex. platelets, some rounding of B; C fibers and laths, shortening from 3-84, clear anhedral O grains, L platelets with new O growing on them
3-87	x	x	x	x		O grains are sharp anhedral, decrease in amount of B present (4 - 6 μm) hex. platelets, some lath L, development of solution or etch pits in some L, O growth in newly precipitated grains (?) - 10 μm for some grains
3-86	x	x	x	x		rounded B platelets, short C fiber, vapor cavities in L, 5 μm size of newly formed material - O (?)
3-1		x	x	x	(?)	well-developed L morphology in plates and other euhedral forms, plates 60 - 100 μm, chrysotile needles short - less than 10 μm, hex. B platelets, micron-size cubes - M
3-22		x	x	x		C needles short, thick, some lath development, hex. brucite (max. 40 μm), L - massive, thin irregular shaped platelets, and some euhedral morphology
3-23	x	x	x	x		surface of large O grains altered, fine C needles - 15 - 20 μm length, L laths and very small platelets - 4 - 10 μm; B small hex. platelets - 2 - 6 μm
3-30	x	x	x	x		C fibers are 20 - 30 μm long, covering and coating grains; L - small platelets 4 μm, some larger angular O grains - 20 μm, some very large brucite platelets 40 - 60 μm

Run	O	L	C	B	M	Remarks concerning grain size and habit *
3-61		x	x	x		C laths and fibers, lath - 1 μm x 10 μm long) about equal distribution between laths and fibers, B - hex. platelets, L - massive and platy
3-77		x	x			short, squat C laths (2 - 4 μm in length), L - massive and platy, C growing on surface of larger rounded grains of O
3-97		x	x	x		10 - 40 μm hex. B platelets; 20 - 100 μm massive and platy L, definite euhedral L morphology; C fibers well developed and form long (50 - 100 μm) fiber bundles; minor L laths
3-98	x	x	x	x		new euhedral O growing on pre-existing O grains (1 - 4 μm); shortening of C fibers, B shows rounded edges to hex. platelets, L laths have dissolution holes, newly precipitated material - O is less 2 μm
3-103		x	x	x		C needles coating larger grains (O?), C fiber bundles, 30 μm width, irregular grains of L, hex. B platelets - 20 μm, some solution etching of L and B
3-105		x	x	x		well-developed long C fibers (40 μm), L - massive, platy, and 20 μm laths, B well formed, less than 10 μm size
3-106	(?)	x	x	x		some shortening of C fibers compared to Run 3-105, C forms mat on other grains, rounding of B platelets, angularity in larger grain aggregates, solution features in L platelets

hex. = hexagonal
x - phase positively identified in SEM sample
? - phase identification tentative

*all sizes are approximate from visual comparison with scale at time of observation, or from photographs

APPENDIX 4: Magnetite distribution in run products as observed optically by binocular, transmitted and reflected light microscopy.

Run	Color Powder	Observed By X-ray	Magnetite Distribution
3-25	T		very small amount < 1%, irregularly distributed
3-12	T		very small amount < 1%, irregularly distributed
3-61	G	x	very large aggregates, moderate to large grain size
2-94	T		few small grains in silicate
2-99	T		large amount of finely disseminated grains (dusty), not evenly distributed
3-32	T		very fine-grained (< 1 μm), evenly disseminated
2-98	T	x	evenly distributed, small to moderate grain size, some euhedral grains
3-30	T		trace amounts, very fine grained
3-4	G	x	disseminated, varying grain size - small to moderate
3-1	G	x	disseminated, large to moderate grain size, some euhedral grains
2-108	T		fine to moderate size, evenly distributed
3-26	T		fine, disseminated
2-110	G	x	disseminated, moderate size
3-22	G	x	large, euhedral grains, disseminated
3-77	G		fine, disseminated throughout serpentine
2-100	G		moderate grain size, some euhedral grains, abundant
2-107	G		evenly distributed, moderate size, euhedral (cubes)

Run	Color Powder	Observed By X-ray	Magnetite Distribution
2-102	G	x	moderate size, evenly distributed
2-106	G		moderate, euhedral cubes, evenly disseminated
3-47	G		large euhedral crystals, evenly distributed
3-48	light G		very fine-grained, disseminated, few large euhedral crystals
3-50	light Gn		fine-grained, disseminated
3-51	G		very fine-grained, disseminated
3-43	T		some large discrete grains, also very fine grained, disseminated
3-42	G	x	finely disseminated, large to moderate discrete grains
3-62	dark B		traces, fine-grained
3-56	T		small amount, fine-grained
3-55	T		traces, fine-grained
3-45	T		traces, fine-grained
3-49	G		finely disseminated grains, some large euhedral grains
3-46	T		finely disseminated, some large euhedral grains
3-54	G	x	grains of all sizes, abundant, some euhedral
3-63	dark B		finely disseminated grains
3-64	G	x	moderate to large size, some aggregates of smaller grains form larger clots, abundant
3-96	G		abundant, fine to large grain size
3-95	G		finely disseminated, larger aggregates about 10 μm size

Run	Color Powder	Observed By X-ray	Magnetite Distribution
3-92	G		moderate size, euhedral grains (cubes) and finely disseminated
3-93	G		finely disseminated
3-94	G		finely disseminated
3-101	light G		minor, finely disseminated, sizable number of large aggregate grains
3-100	light G		large amount of finely disseminated grains
3-99	G		large amount of finely disseminated, larger grains in aggregates, amount greater than 3-76
3-76	light G		finely disseminated, outlines other phases
3-75	G		finely disseminated, forms irregular patches in serpentine
3-74	G		finely disseminated, irregular patches, approximately same amount as in 3-72
3-72	G		finely disseminated, irregular patches in serpentine
3-86	T		finely disseminated, irregular patches
3-87	G		finely disseminated, irregular patches, some moderate size grains
3-85	G		finely disseminated, irregular patches, some moderate size grains
3-84	G		finely disseminated, irregular patches, some very large aggregates
3-71	G		finely disseminated, irregular patches, many large grain aggregates
3-78	G		finely disseminated, irregular patches
3-70	light G		finely disseminated, irregular patches, some moderate grains, amount approximately same as 3-71

Run	Color Powder	Observed By X-ray	Magnetite Distribution
3-98	light G		finely disseminated, irregular patches
3-97	G		finely disseminated, irregular patches, more present than in 3-98
3-68	G	x	finely disseminated, some large, euhedral aggregates, amount greater than in 3-69 and 3-97
3-69	light Gn		finely disseminated
3-106	G		large amount of fine to moderate-size grains, disseminated
3-105	G		finely disseminated and very large grain aggregates (>50 μm)
3-103	G		finely disseminated, some moderate-size grains, irregular patches
3-102	G		large amount of finely disseminated
3-104	G		large amount of fine to moderate-size grains, disseminated

T	=	tan	fine	=	<1-2 μm
G	=	grey	moderate	=	2-10 μm
Gn	=	green	large	=	>10 μm
B	=	brown			

APPENDIX 5: Chemical analyses of fluids collected after the experiments. The results are presented as concentration in ppm Mg, Si and Fe and in terms of molality (moles/kg solution). The method of error calculation is presented in the description of techniques for chemical analysis in section on EXPERIMENTAL METHODS.

Run	Fluid	Mg(ppm)*	Si(ppm)*	Fe(ppm)*	Molality Mg (10^5)	Molality Si (10^5)	Molality Fe (10^5)	Ratio Mg/Si
3-1	H_2O	1.80(8)	n.d.					
3-2	H_2O	3.1 (1)	n.d.		12.8			
3-3	H_2O	0.47(2)	15.8(24)		1.93	56.3		0.034
3-4	H_2O	2.8 (1)	n.d.		11.5			
3-5	H_2O	4.2 (2)	33.4(113)		17.3	119.0		0.145
3-12	H_2O	1.8 (1)	n.d.		7.40			
3-14	H_2O	2.60(1)	n.d.		10.7			
+3-15	H_2O	°24.0 (11)	n.d.		98.7			
3-22	H_2O	16.2 (7)	62.4(210)		66.6	222.0		0.30
3-23	H_2O	0.58(3)	4.8(28)		2.39	17.1		0.14
3-26	H_2O	°17.5 (7)	n.d.		72.0			
3-30	H_2O	n.d.	5.0(41)			17.8		
3-60	H_2O	5.2 (2)	11.6(31)		21.4	41.3		0.53
3-61	H_2O	6.4 (36)	n.d.		26.3			
3-32	H_2O	0.39(2)	6.1(25)		1.6	21.7		0.074
3-47	H_2O	2.4 (1)	81.9(667)		9.87	292.0		0.034
3-77	H_2O	2.4 (1)	10.5(9)	102.7(15)	9.87	37.4	184.0	0.26
+3-50	NaSi°°	6.2 (3)			25.5			
2-107	H_2O	1.53(7)			6.29			

Run	Fluid	Mg(ppm)*	Si(ppm)*	Fe(ppm)*	Molality Mg (10^5)	Molality Si (10^5)	Molality Fe (10^5)	Ratio Mg/Si
3-51	NaSi[oo]	[o] 1.40(6)	n.d.		5.76			
3-45	NaOH	1.40(6)	4.6(18)		5.76	16.4		0.35
3-46	NaOH	3.4 (2)	7.1(57)		14.0	25.3		0.55
3-49	NaOH	2.00(9)	8.1(33)		8.23	28.8		0.29
3-54	NaOH	19.9 (9)	29.7(122)		81.9	106.0		0.77
3-55	NaCl	12.2 (5)	23.0(51)		50.2	81.9		0.61
3-56	NaCl	6.7 (3)	13.2(16)		27.6	47.0		0.59
3-57	NaCl	6.8 (3)	n.d.		28.0			
3-62	NaCl	3.5 (2)	14.3(18)		14.4	50.9		0.28
3-63	alk.Cl	2.3 (1)	9.6(30)		9.46	34.2		0.28
[+]3-64	alk.Cl	75.6 (34)	n.d.		311.0			
[+]3-92	alk.Cl	14.2 (6)	3.0(12)	8.5(5)	58.4	10.7	15.2	5.46
[+]3-93	alk.Cl	6.4 (3)	2.1(12)	45.6(27)	26.3	7.48	81.7	3.52
3-95	alk.Cl	2.4 (1)	9.7(13)	56.4(34)	9.87	34.5	101.0	0.29
3-68	H_2O	8.5 (4)	n.d.		35.0			
3-69	H_2O	4.3 (2)	n.d.		17.7			
[++]3-70	H_2O	2.7 (1)	n.d.		11.1			
3-71	H_2O	5.7 (3)	13.1(36)		23.4	46.6		0.50
3-72	H_2O	9.1 (4)	n.d.		37.4			

Run	Fluid	Mg(ppm)*	Si(ppm)*	Fe(ppm)*	Molality Mg (10^5)	Molality Si (10^5)	Molality Fe (10^5)	Ratio Mg/Si
++3-76	H_2O	2.00(9)	n.d.	458.0(67)	8.23		820.0	
3-78	H_2O	1.90(8)	n.d.		7.82			
3-84	H_2O	4.2 (2)	n.d.	115.3(70)	17.3		206.0	
3-85	H_2O	2.6 (1)	34.9(39)	-	10.7	124.0		0.09
++3-86	H_2O	1.50(7)		32.4(19)	6.17		58.0	

n.d. - not detected

molality - moles/kg solution

Figures in parentheses represent the esd at 95% confidence level calculated from the standard solutions in terms of the least units cited for the value to their immediate left, thus 15.8(24) indicates an esd of 2.4.

*concentration in undiluted solution

+possible leak during quench, i.e., minor or no gas escape on opening the capsule

++contamination suspected

°element at the detection limit in the measured (diluted) solution

°°sodium metasilicate

In Runs 3-74, 3-76, 3-77, 3-78, 3-84, 3-85, 3-86, 3-92, 3-93, and 3-95, the fluid was placed into acidified distilled water at the time of dilution.